



ScuDo

Scuola di Dottorato ~ Doctoral School
WHAT YOU ARE, TAKES YOU FAR



Doctoral Dissertation
Doctoral Program in Energy Engineering (31st Cycle)

Development of Automated Calibration Methodology for Last Generation of Diesel Automotive Powertrains

Pranav Arya

* * * * *

Supervisor

Prof. Federico Millo

Doctoral Examination Committee:

Prof. Michael Bargende, Universität Stuttgart

Prof. Nicolò Cavina, Università degli Studi di Bologna

Prof. Claudio Dongiovanni, Politecnico di Torino

Prof. Lucio Postriotti, Università degli Studi di Perugia

Prof. Bianca Maria Vaglieco, Istituto Motori - C.N.R.

Politecnico di Torino

April 30, 2019

This thesis is licensed under a Creative Commons License, Attribution - Noncommercial - NoDerivative Works 4.0 International: see www.creativecommons.org. The text may be reproduced for non-commercial purposes, provided that credit is given to the original author.

I hereby declare that, the contents and organisation of this dissertation constitute my own original work and does not compromise in any way the rights of third parties, including those relating to the security of personal data.



.....
Pranav Arya
Turin, April 30, 2019

Summary

The recent developments in automotive diesel engine subsystems, like injection systems and air management systems, allow for a much greater control and flexibility over the combustion process, thus resulting in significant reductions in emissions and fuel consumption. However, these developments also increase the complexity of the complete system leading to a much higher number of control parameters. This increase in number of control parameters makes the task of diesel engine calibration more complicated, as it requires a solution to an optimization problem of high dimensionality. The traditional optimization methods such as simple gradient method or steepest descent method are not suited for high dimensional optimization problems such as common rail diesel engine since they have a tendency of getting trapped in local optima. To complicate the matter further, the optimized calibration, stored in the form of maps inside the engine control unit, must fulfill stringent requirements in terms of smoothness, ensuring a subtle transition of control parameters between neighbor operating points. This additional requirement of smoothness often means moving away from the optimum calibration, thus resulting in penalties in terms of emissions and fuel consumption. Moreover, traditional calibration methods are often slow and dependent on the experience of the calibration team, which can lead to an increase in the development time and cost for a newly designed engine.

It is therefore necessary to develop a methodology that can reduce this loss of optima and carry out the engine calibration task in a quick and automatic way. With this aim, in this work, a one-click methodology has been developed that uses Genetic Algorithm (GA) to generate multiple optimum calibrations for each engine operating point. These multiple optimum calibrations form a Pareto front, thus providing a solution to classical multi objective optimization problem of diesel engine. Using these multiple optimum calibrations, a large number of calibration

maps are generated. These maps are evaluated on the basis of smoothness and performance over a driving cycle. Following the evaluation, some calibrations are shortlisted automatically based on a tradeoff between the required level of smoothness and minimization of emissions. These shortlisted calibrations can be finally reviewed by the calibration team to select the final calibration.

The multiple optimum calibrations generated using GA were compared with an existing calibration optimized using traditional methods for a C segment vehicle with a curb mass of 1650 kg for a Euro 6d application. Firstly, using the in house developed code for GA optimization, significantly better calibrations were obtained for all the engine operating points. Using these better calibrations and an integrated approach that reduces the loss of optima due to smoothening, a simultaneous reduction of 1% BSFC, 10 % NO_x and 5% Soot was achieved over WLTC in comparison to the existing calibration. These reductions were obtained while achieving the same level of smoothness of the calibration maps of the existing calibration. Most importantly, using the described methodology the time required for calibration can be reduced drastically. The activity that typically takes couple of weeks can be carried out in couple of days. Moreover, using a reduced version of the described methodology an existing calibration was modified within minutes to provide significant reductions in one of the emissions (15% NO_x) without deteriorating any of the other emissions, fuel consumption, combustion noise and exhaust temperature.

Acknowledgment

First and foremost I would like to express my deepest gratitude towards my dear supervisor Professor Federico Millo. Without his guidance and support this work would have been hardly possible.

I would also like to acknowledge and thanks FEV Italy for sponsoring my Ph.D. scholarship. I would also like to extend my gratitude towards Dr. Fabio Mallamo and Mr. Mauro Scassa for providing me their valuable advice and assistance.

*I would like to dedicate
this thesis to my loving
wife and Parents.*

*I would always be grateful for their support
and encouragement.*

Contents

1. Introduction.....	1
1.1 Advancements in diesel engine subsystems	1
1.1.1 Air Management System.....	2
Turbocharging System.....	2
Exhaust Gas Recirculation System.....	3
Variable Value Actuation System.....	4
1.1.2 Injection System.....	5
1.1.3 Exhaust After-Treatment System.....	6
1.2 Driving Cycles and Emission Regulations	6
2. State of the Art Engine Calibration Methods.....	10
2.1 What is Engine Calibration.....	10
2.2 Model Based Calibration	11
2.2.1 Physical Models	12
3D Models.....	12
2D Models.....	12
1D Models.....	12
2.2.2 Experimental Models	13
Polynomial Models	14
Black Box Models	15
2.3 Different Approaches for Engine Calibration.....	15
2.3.1 Local Approach for Calibration	15
2.3.2 Global Approach for Calibration	18
2.3.3 Mixed Approach for Calibration.....	19
2.4 Motivations for Improving Calibration Methodology	20
3. Engine Emission Models	21
3.1 Model Domain and Process	21
3.2 Model Quality	23
4. Optimization	27
4.1 Multi Objective Optimization.....	28
4.1.1 Dynamic Constraint Definition.....	30
4.1.2 Genetic Algorithm Optimizer	37
Initialization	38
Selection.....	38
Recombination.....	38

Mutation.....	39
Evaluation and Replacement	39
Stopping Criteria.....	39
4.1.3 Pareto Front Generation	40
4.1.4 Results	41
4.2 Single Objective Optimization with Existing Calibration	46
4.2.1 Methodology	46
4.2.2 Results	49
5. Smooth Map Generation.....	55
5.1 Time-Based Weight Calculation.....	55
5.2 Calibration Map Generation	57
5.3 Smoothness Weight Settings	60
5.4 Multiple Calibration Maps Generation	61
5.5 Calibration Evaluation	63
5.5.1 Smoothness Evaluation	63
5.5.2 Performance Evaluation	64
6. Results and discussion	65
6.1 Case Wise Comparison of Average Smoothness and Performance	65
6.2 Smoothness and Performance of Shortlisted Calibrations.....	68
6.3 Discussion.....	71
7. Conclusions.....	73
8. References.....	75

List of Tables

Table 1-1 European Emission Standards for Light Duty Diesel Vehicles	7
Table 3-1 Range of variation of each control parameter for the experiments to generate empirical models [41].....	22
Table 3-2 Different correlation coefficients used for evaluating the model quality [41].....	23
Table 4-1 Different combinations for biasing of constraints [41].....	33
Table 4-2 Reduced range of variation for generation of random calibrations in order to preserve the smoothness of the existing calibrations [41].....	48
Table 5-1 Time based weight of each key point in a decreasing order	56
Table 5-2 Different cases for smoothness weight settings of different control parameters [50]	61
Table 6-1 Values of different control parameters for three diverse calibrations each optimized with a different objective [50]	71
Table 6-2 Value of different emissions relative to BaseCal for three diverse calibrations each optimized with a different objective [50]	71

List of Figures

Figure 1-1 A layout sketch of dual stage turbocharger with a waste gate at high pressure stage [2]	3
Figure 1-2 A typical layout of dual loop EGR system [7]	4
Figure 1-3 A typical injection strategy used for modern automotive diesel engines	6
Figure 1-4 Speed profiles for NEDC and WLTC	7
Figure 1-5 Phasing of different European emission standards for light duty vehicles along with the different type approval cycles.....	9
Figure 1-6 Engine operating points for a C segment car on the WLTC and a RDE cycle	9
Figure 2-1 Engine control using the lookup tables stored in ECU.....	10
Figure 2-2 Full factorial experimental design for two parameters each having 10 levels	13
Figure 2-3 Number of experiments required for a full factorial design as a function of number of control parameters and levels of each control parameter ..	14
Figure 2-4 Output response estimation using a black box model	15
Figure 2-5 Key point definition for WLTC using a clustering algorithm.....	16
Figure 2-6 Start of Injection map creation from the optimum values at different Key Points.....	17
Figure 2-7 Manual smoothening of Start of Injection map.....	18
Figure 2-8 Modelling of the complete engine operating range using global Design of Experiment	19
Figure 3-1 BSFC model response [41].....	24
Figure 3-2 NO _x model response [41].....	24
Figure 3-3 Soot model response [41]	24
Figure 3-4 CO model response.....	25
Figure 3-5 HC model response.....	25
Figure 3-6 CN model response [41].....	25
Figure 3-7 Exhaust temperature model response	26
Figure 4-1 Flow chart describing the methodology to solve one optimization problem [41]	29
Figure 4-2 BSFC-Soot normalized scatter plot calculated from randomly generated calibrations [41].....	32
Figure 4-3 BSFC-NO _x normalized scatter plot calculated from randomly generated calibrations [41].....	32
Figure 4-4 BSFC-Soot scatter points included inside the constraint boundary [41].....	34
Figure 4-5 BSFC-NO _x scatter points included inside the constraint boundary [41].....	35

Figure 4-6 BSFC-Soot scatter for stored calibrations, i.e. calibration passing the objective function test [41]	36
Figure 4-7 BSFC-NO _x scatter for stored calibrations, i.e. calibration passing the objective function test [41]	36
Figure 4-8 Engine control parameters represented in a form of chromosome [41].....	37
Figure 4-9 Sequence of steps for optimization using genetic algorithm [41] .	38
Figure 4-10 Uniform crossover-based recombination technique [41]	39
Figure 4-11 Generation of Pareto front using systematic variation of dynamic constraints and optimization objective [41].....	40
Figure 4-12 BSFC-Soot scatter for optimized calibrations [41]	42
Figure 4-13 BSFC-NO _x scatter for optimized calibrations [41].....	42
Figure 4-14 BSFC-Soot scatter for optimized calibrations in comparison with a base calibration [41].....	43
Figure 4-15 BSFC-NO _x scatter for optimized calibrations in comparison with a base calibration [41].....	44
Figure 4-16 SOI-Air scatter of the optimized calibrations [41].....	45
Figure 4-17 Rail pressure-Boost pressure scatter of the optimized calibrations [41].....	45
Figure 4-18 Reduced work flow for the single objective optimization methodology with an existing calibration present [41]	47
Figure 4-19 SOI map from the base calibration [41]	48
Figure 4-20 Parallel surfaces around the SOI map to preserve the smoothness [41].....	49
Figure 4-21 NO _x variation in comparison to the base calibration during the complete optimization process [41].....	50
Figure 4-22 Increase of fitness over the complete optimization process [41] ..	51
Figure 4-23 CO variation in comparison to the base calibration during the complete optimization process [41].....	51
Figure 4-24 HC variation in comparison to the base calibration during the complete optimization process [41].....	52
Figure 4-25 CN variation in comparison to the base calibration during the complete optimization process [41].....	52
Figure 4-26 Soot variation in comparison to the base calibration during the complete optimization process [41].....	53
Figure 4-27 BSFC variation in comparison to the base calibration during the complete optimization process [41].....	53
Figure 4-28 Percentage NO _x reduction possible for all the selected key points using the described optimization methodology	54
Figure 5-1 Time based weight evaluation of each point using a clustering algorithm [50]	56
Figure 5-2 SOI plane shown as an example of the map generation method [50]	58
Figure 5-3 SOI value closest to the generated plane for the remaining 17 key points [50].....	59

Figure 5-4 SOI map generated using multiple optimum calibrations and SOI plane [50]	59
Figure 5-5 Iterative methodology using nested loop structure to generate a large number of calibration maps [50].....	62
Figure 6-1 Average SOI map smoothness for the five different parameter weight settings [50].....	66
Figure 6-2 Average air flow map smoothness for the five different parameter weight settings [50].....	66
Figure 6-3 Average reduction in emissions over WLTC for the five different parameter weight settings [50].....	67
Figure 6-4 Smoothness of injection pressure, SOI and air flow maps for shortlisted calibration sets in comparison with BaseCal [50].....	68
Figure 6-5 Simultaneous reductions in NO _x , Soot and BSFC for the shortlisted calibration in comparison to BaseCal over WLTC [50]	69
Figure 6-6 Injection pressure map from 3 rd shortlisted calibration set [50]....	69
Figure 6-7 SOI map from 3 rd shortlisted calibration set [50].....	70
Figure 6-8 Air flow map from 3 rd shortlisted calibration set [50].....	70

Abbreviations

1D	One Dimensional
2D	Two Dimensional
3D	Three Dimensional
AFR	Air Fuel Ratio
ASI	After start of injection
BMEP	Break Mean Effective Pressure
CFD	Computational Fluid Dynamics
CI	Compression Ignition
CO	Carbon Monoxide
CO ₂	Carbon Dioxide
DI	Direct Injection
DoE	Design of Experiments
DT	Dwell Time
EATS	After Treatment System
ECU	Engine Control Unit
EGR	Exhaust Gas Recirculation
ET	Energizing Time
EU	European Union
GA	Genetic Algorithm
GP	Gaussian Process
HC	Unburned Hydrocarbons
HRR	Heat Release Rate
ICE	Internal Combustion Engine
KP	Key Point

LoLiMoT	Local Linear Model Tree
LOO	Leave One Out
MOO	Multi Objective Optimization
NEDC	New European Driving Cycle
NO	Nitric Oxide
NO ₂	Nitrogen Dioxide
NO _x	Nitrogen Oxides
NN	Neural Network
PAH	Polycyclic Aromatic Hydrocarbons
PEMS	Portable Emission Measurement System
PM	Particulate Matter
PMP	Particulate Measurement Programme
PN	Particulate Number
RDE	Real Driving Emissions
SOI	Start of Injection
TA	Type Approval
VGT	Variable Geometry Turbine
VVA	Variable Valve Actuation
WLTC	World harmonized Light vehicles Test Cycle

Chapter 1

Introduction

For more than a century diesel engines have been an integral part of the transportation industry. Four stroke diesel engines are quite commonly used in passenger cars, light-duty vehicles, and heavy-duty vehicles. Diesel engines have always been popular because of their high efficiency and high torque. Furthermore, since their emergence in the late 19th century, diesel engines have been through a constant innovative change, thus continuously improving and maintaining their dominance in the transportation industry. These constant developments have led to very complex modern day diesel engines with much higher number of control parameters than their previous counterparts. This rising number of control parameters increase the cost and effort required for optimizing the diesel engine calibration. Moreover, with stringing emission regulations and test procedures for automotive diesel engines, it is necessary to optimize the engine in the complete operating range.

Before going into the details of engine calibration and optimization, in first section of this chapter, a short overview of the recent advancements that have taken place in various subsystems of diesel engines is provided along with the control parameters associated with these subsystems. In the second section, a brief introduction to the recent changes in diesel engine emissions regulations and testing methods is mentioned.

1.1 Advancements in diesel engine subsystems

The constant innovative development in different diesel engine subsystems have resulted in a drastic reduction in fuel consumption and pollutant emissions [1]. The different subsystems of a modern diesel engine, that can be broadly categorized in air management, injection and aftertreatment systems, have been described in brief in this section.

1.1.1 Air Management System

The amount of fuel that can be injected in an Internal Combustion Engine (ICE) is limited by the amount of air entering the cylinder. Furthermore, the emissions from ICE are very strongly linked to the amount of air and turbulence inside the cylinder. In diesel engine combustion, as there is no prior mixture formation, the air management systems play an even more important role. Due to their importance, the air management systems have gone through a tremendous technological development. Some of the components of this systems are outlined below.

Turbocharging System

For a long time, turbocharging has been used as a method for increasing the torque and power of the diesel engines. The remaining enthalpy in the exhaust gases from the engine is used to drive a turbine which in turn drives a compressor. This compressor is used to raise the intake air to a higher pressure, typically known as boost pressure, to increase the density of the air entering the cylinder, thereby increasing the mass of air trapped. Thus, more fuel can be injected into the cylinder producing more torque and power. In the last couple of decades, turbocharging has also been used as a successful method to downsize diesel engines, meaning that same torque can be generated using smaller engines. This has resulted into a significant reduction in CO₂ from the diesel engines. Furthermore, turbocharging is a very useful method to extract the enthalpy from the exhaust gases there by reducing the energy wastage.

To further exploit the potential of turbocharging, two stage turbochargers are commonly used in diesel engines now a days. A sketch of a dual stage turbocharger is shown in Figure 1-1. The layout shown in Figure 1-1 shows a fixed geometry high pressure turbine with a waste gate valve. Due to its fixed geometry, this kind of turbine has a limited operating area which has to be matched to the engine. Therefore, a waste gate valve is used to limit the torque generated by the turbine at very high loads to avoid the problem of over speeding of the turbocharger.

Instead of fixed geometry turbines with waste gate valves, Variable Geometry Turbines (VGT) are being increasingly used in modern turbocharging systems. Dual stage turbocharging systems use a complex control strategy to achieve a desired intake manifold pressure or boost pressure. The use of VGT increases the level of complexity even further.

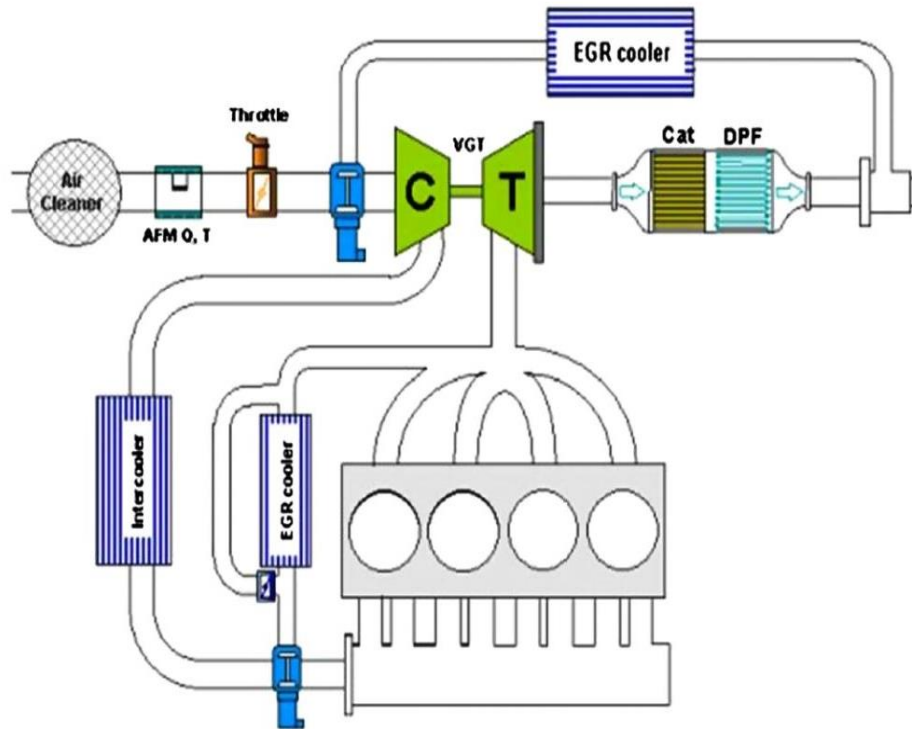


Figure 1-2 A typical layout of dual loop EGR system [7]

Long route EGR is more effective in controlling the NO_x due to lower temperatures of the exhaust gases. Furthermore, long route results typically shows more favorable trade-offs for both BSFC- NO_x and Soot- NO_x . However, long route EGR suffers from poor transient response. Transient response is the time required to achieve the desired value of any control parameter. Due to the higher volume to be filled or emptied in case of long route EGR transient response is poor. Short route EGR does not have this drawback, but it is less effective in controlling NO_x . Therefore, the best solution is a dual loop EGR, that can improve the response of the system during transients and at the same time provide advantages of lower emissions during steady state behavior [7].

However, in case of a dual loop EGR architecture is adopted, the complexity of the control is further increased, since two different paths for exhaust recirculation have to be managed. Furthermore, the control problem is made even more complicated by the need of coordinating the EGR control with the boost control, since for example, actions taken on the VGT to control the boost level will affect the pressure gradient between exhaust and intake systems, thus leading to changes in the EGR rate.

Variable Value Actuation System

Variable Valve Actuation (VVA) system works by modifying the valve timing or the valve lift or both. By modifying the timing of the valves, VVA systems can for instance allow the late closing of Exhaust Valve (EV) that can result in reduction of pumping work and internal EGR.

VVA systems are quite commonly used in gasoline engines because of their effectiveness in reducing the pumping losses due to throttling at part load. However, as there is no throttling in diesel engines, until recently the use of VVA was very limited for diesel applications. However, due to the requirement of faster warm up of the Exhaust After-Treatment System (EATS), there is a growing interest in VVA technology for diesel engines. Several research works have highlighted the potential of VVA in achieving a higher exhaust gas temperature with a marginal fuel penalty [8,9]. More recently, the potential of VVA for CO₂ reduction in light duty diesel engines has also been investigated [10]. Finally, VVA systems can also be used to generate swirl motion using an asymmetric valve lifts, thus eliminating the need for swirl control flaps in the intake ports to adapt the swirl level to different engine loads and speeds.

1.1.2 Injection System

The fuel injection has a major impact on mixture formation and thereby on emissions and combustion efficiency. Several researchers have studied the effect of optimized injection strategies for reducing the emissions [11,12]. In fact, being such a powerful method, injection parameter optimization has been used for reducing emissions from bio-diesel fed engines also [13]. Moreover, optimized injection strategy can be useful for reduction of combustion noise [14].

Being of such high importance, a short description of the injection parameters associated with a modern diesel common rail fuel injection system is provided here. The mass of the fuel injected into the cylinder of a last generation automotive diesel engine can be divided into multiple injection events using the common rail fuel injection system. Figure 1-3 shows a typical injection strategy used in modern diesel engines which consists of two pilot injections, one main injection, followed by one after and one post injection. It should also be added here that the injection strategy might and does change depending on the engine operating conditions, in terms of injection timing, injection events and injected mass for each event.

The mass of the fuel injected in each injection event is controlled by the Energizing Time (ET), which is the time duration for which the electrical command is applied to the injector to keep it open. The time interval between electrical commands of two subsequent injection events is known as Dwell Time (DT). These two parameters are associated with each injection event. Apart from these, injection pressure and Start of Injection (SOI) have to be considered to define the complete injection strategy. In this way, a modern common rail diesel engine can easily have up to a dozen of parameters just for injection system control.

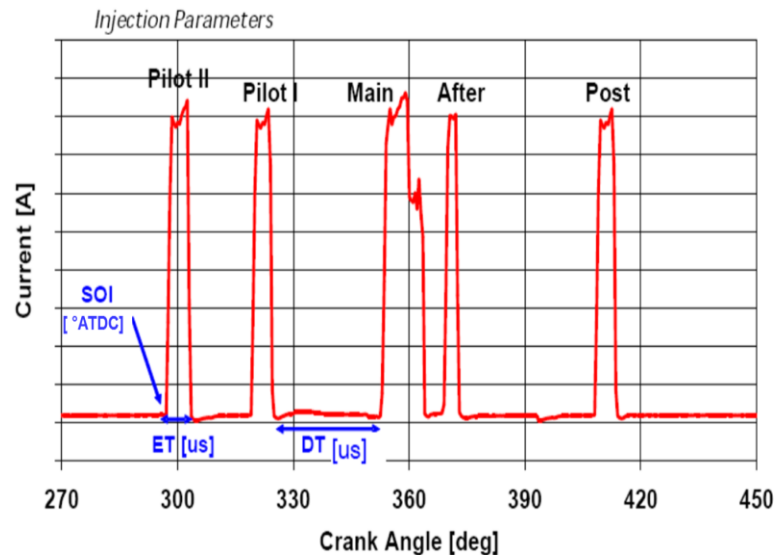


Figure 1-3 A typical injection strategy used for modern automotive diesel engines

1.1.3 Exhaust After-Treatment System

Although the recent advancements in the above described air management and fuel injection systems contributes to significantly reduced engine out emissions, the current stringent legislation requirements can be fulfilled only by means of exhaust aftertreatment systems.

Modern diesel engine EATS system typically consists of at least three components, one responsible for HC and CO control, one responsible for PM control and one for NO_x control. Furthermore, with some modern EATS architecture it is also possible to combine, for example, the functionality of PM and NO_x control in just one component. Since the present work aims at reducing the engine out emissions by optimizing the engine calibration, no further description will be provided here concerning the EATS. The references in this introduction section will therefore be limited to the need of adopting different calibration modes (e.g. normal operating mode, particulate filter regeneration mode, catalyst warm up mode etc.) to fulfill the needs of the EATS in terms of regeneration, temperature management etc. [8]. Although the optimization methodology proposed in this work has been developed, applied and assessed for the minimization of engine-out pollutant emissions in normal operating mode, the same approach could be adopted also for other calibration modes. .

1.2 Driving Cycles and Emission Regulations

The emissions from the automotive diesel engine in Europe have been controlled by European Union (EU) legislation for more than two decades now but these limits are becoming more and more strict. This can be seen from Table 1-1 that shows the legislative limits for light duty diesel vehicles in Europe. Furthermore, in the last decade (Euro 5/6), a limit has also been introduced for Particulate Number (PN) under Particulate Measurement Programme (PMP) developed by the UN/ECE.

Table 1-1 European Emission Standards for Light Duty Diesel Vehicles

Stage	Date	CO	HC	HC+NO _x		PM	PN
				g/km			
Euro 1	1992.07	2.72	-	0.97	-	0.140	-
Euro 2, IDI	1996.01	1.00	-	0.70	-	0.080	-
Euro2, DI	1996.01	1.00	-	0.90	-	0.100	-
Euro 3	2000.01	0.64	-	0.56	0.50	0.050	-
Euro 4	2005.01	0.50	-	0.30	0.25	0.025	-
Euro 5a	2009.09	0.50	-	0.23	0.18	0.005	-
Euro 5b	2011.09	0.50	-	0.23	0.18	0.005	6.0x10 ¹¹
Euro 6	2014.09	0.50	-	0.17	0.08	0.005	6.0x10 ¹¹

However, as the emissions from the vehicles are largely dependent on the operating conditions of the engine, they are certified using standard driving cycles and procedures. These standard driving cycles and testing protocols are known as type approval procedures. New European Driving Cycle (NEDC) has been used for Type Approval (TA) procedure for light duty vehicles in Europe until September 2017. NEDC, being far from a realistic driving scenario, was replaced by World harmonized Light duty Test Cycle (WLTC) [15,16], aiming to close the gap between TA and real world driving conditions. The speed profile for NEDC and WLTC is shown in Figure 1-4. It can be seen from Figure 1-4 that WLTC has higher maximum speed and higher acceleration than NEDC. WLTC also has reduced stationary time and increased transient phases, thus making it more realistic and much closer to the real driving conditions than NEDC.

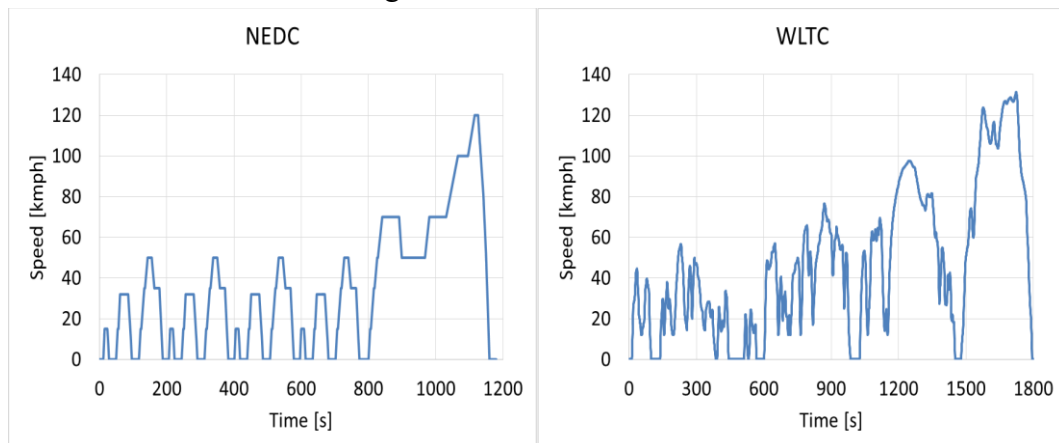


Figure 1-4 Speed profiles for NEDC and WLTC

However, even though the operating conditions over WLTC are closer to real driving conditions in comparison with NEDC, several studies demonstrated that emissions recorded on the road during the normal operation of the vehicles are typically significantly higher than those measured in during TA tests [17]. Moreover, even without violating the legislation by using so called “defeat devices” [18] (i.e. devices capable to detect the execution of a TA test and to activate specific

emission control strategies in these conditions), the definition of a given driving schedule such as the WLTC or the NEDC paves the way for the development of technologies and control strategies “tailored” to the TA procedure. These technologies and these strategies can on the contrary be only partially effective in controlling vehicle emissions on the road, in typical driving conditions, thus making the tightening of the legislation limits only partially effective in controlling the environmental impact of the new vehicles. For these reasons vehicles sold after September 2017 also need to comply with the Real Driving Emissions (RDE) type approval procedure. In RDE test procedure the emissions from the vehicles are measured on the road during normal vehicle operation using a Portable Emission Measurement System (PEMS), and emissions recorded on the road should not exceed values recorded in the lab during TA procedure by a so called “conformity factor” which should ideally be as close as possible to unity.

According to the legislations, an RDE cycle must last between 90 to 120 minutes and the route has to include one segment each of urban (<60 km/h), rural (60 to 90 km/h) and motorway (>90km/h) driving conditions. Furthermore, each segment must cover a minimum distance of 16 km [19].

Due to the introduction of the WLTC and RDE, Euro 6 emission standard for light duty diesel vehicles was introduced in multiple phases. This is shown schematically in Figure 1-5. The different phases for Euro 6 are described here briefly [20].

- Euro 6a: This phase excluded the PMP measurement procedure for PM and PN. Furthermore, this stage was only applicable to vehicles that meet Euro 6 standards ahead of regulatory deadlines and therefore it is not shown in Figure 1-5.
- Euro 6b: This phase enforced the Euro 6 emission requirements including PMP measurement procedure for PM and PN.
- Euro 6c: For this phase, Euro 6 emission requirements were enforced but with a different type approval cycle (WLTC).
- Euro 6d-TEMP: Compliance of Euro 6c emission standard along with RDE testing with temporary conformity factor. A conformity factor of 2.1 was used for initially which was reduced to 1.5 during the later stages of RDE. (A RDE test with conformity factor of 2.1 or 1.5 means that the emission measurement obtained during the RDE test trip cannot be higher 2.1 or 1.5 times the legislation limit.)
- Euro 6d: Full Euro 6 emission requirements, i.e., Euro 6c emission standard and RDE testing against final conformity factors.

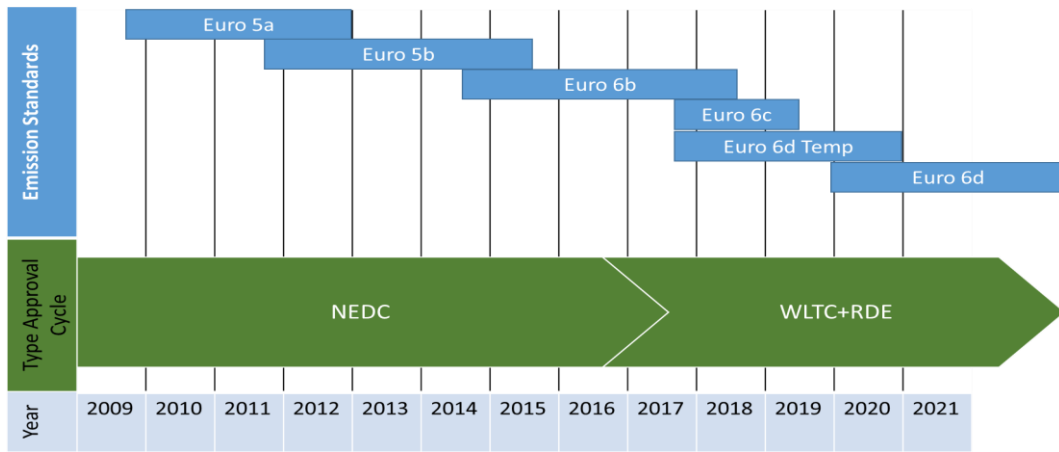


Figure 1-5 Phasing of different European emission standards for light duty vehicles along with the different type approval cycles

Due to the introduction of RDE, the engine calibration has to be optimized for the complete operating range. This is clear by looking at the engine operating points for a C segment vehicle typically encountered on the WLTC and one RDE cycle shown in Figure 1-6. The red line in the Figure 1-6 represents the full load curve. It is quite evident from the Figure 1-6 that RDE cycle is more demanding and covers almost the complete engine operating region.

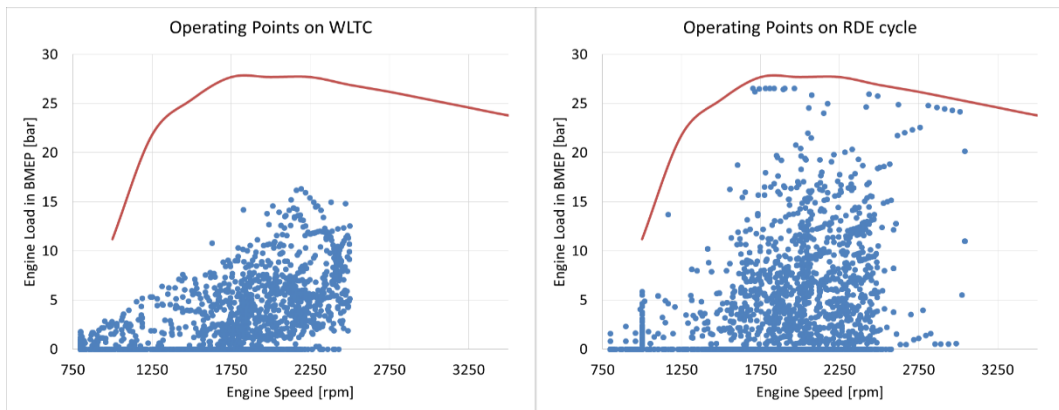


Figure 1-6 Engine operating points for a C segment car on the WLTC and a RDE cycle

Chapter 2

State of the Art Engine Calibration Methods

With such advancements in various components of diesel engine the number of control parameters have increased a lot. The increased number of control parameters while provide more flexibility and better control over the combustion process, make the task of engine calibration more difficult. In this chapter a brief introduction of engine calibration has been provided before explaining the problems associated with the traditional methods and motivations behind this research work.

2.1 What is Engine Calibration

For understanding the basics of engine calibration, it is essential first to explain the functioning of the engine control. When the accelerator pedal of the vehicle is pressed, the change in position of the pedal is translated by the Engine Control Unit (ECU) in terms of torque request at a given speed. Inside the ECU there are maps of different control parameters mentioned in the previous chapter. These maps are a function of speed and load. The ECU reads the maps for different control parameters for the given speed and load and controls the engine to provide the desired torque while minimizing the fuel consumption and engine emissions. This process is shown in Figure 2-1.

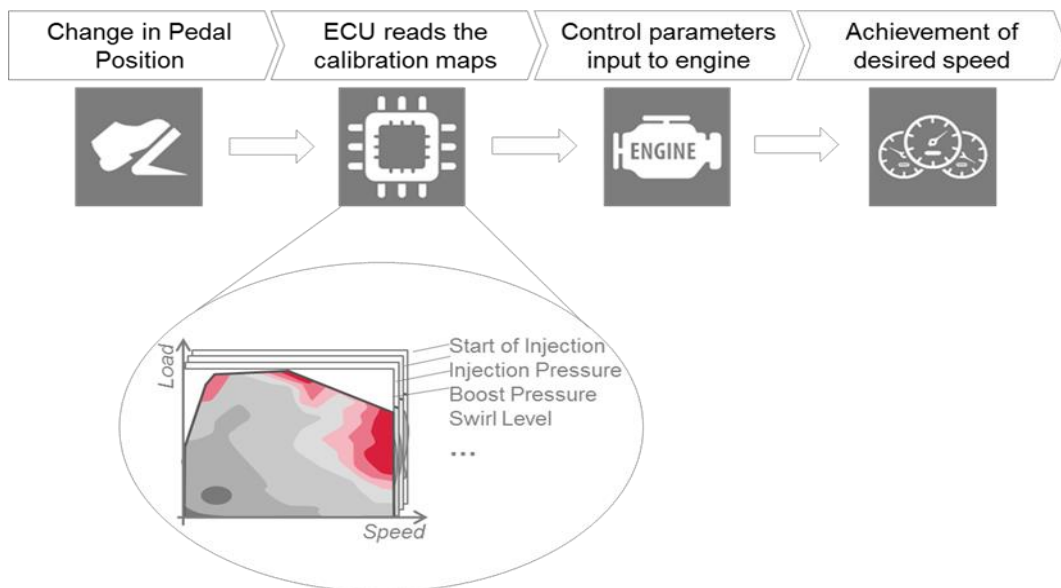


Figure 2-1 Engine control using the lookup tables stored in ECU

These maps for different control parameters stored in the ECU for optimum performance of the engine are known as the engine calibration maps. Besides the optimization of the engine performance, the engine calibration maps must fulfill additional constraints in terms of smooth drivability, low engine vibrations, and noise. These constraints depend on the mission profile of the vehicle. Furthermore, the engine calibration maps should be smooth enough. The smoothness of calibration maps essentially means the absence of any sudden variations in the values of the control parameters for the adjacent operating points. The smoothness of the calibration maps has to be ensured to avoid problems in drivability especially during transients. For certain control parameters, like EGR and boost pressure that have low dynamics this becomes even more important. Some time is required for the control parameters with low dynamics to achieve the requested target value [21,22]. For this reason, during the transient, when the requested target values change quickly, smooth maps are required to achieve the steady behavior as soon as possible.

Of course, the engine needs to be controlled in the complete operating range, and therefore, the engine calibration must be optimized for the complete operating range. However, the reference cycles mentioned in Chapter 1 are used as targets for the engine calibration task as they provide targets in terms of emissions and fuel consumption for homologation. Furthermore, with the introduction of RDE the optimization of engine calibration in the complete operating range has to be ensured.

This task of optimization of engine control parameters for the complete engine operating range and storing them in the form of maps in the ECU is known as the engine calibration task. This chapter will now go in deeper detail of how engine models are used to aid in engine calibration task. This will be followed by the different calibration methods that are commonly used for diesel engine calibration.

2.2 Model Based Calibration

Diesel engine combustion is a very complex phenomenon which is difficult to fathom and even more difficult to optimize. Furthermore, as mentioned earlier, with increasing the number of control parameters, it is possible to better manage the combustion process, but it also increases the complexity of the system. As for many other complex systems, modeling and simulation tools are employed to reduce the development time and cost of the diesel engines. In the context of engine calibration, these models are used to predict emissions and other engine quantities like temperature and pressure for any change in control parameters. Different kinds of models are available and can be used to simulate the combustion in diesel engines. These models can be broadly classified in physical and experimental models. Both of these model categories will now be described in detail along with their advantages and disadvantages.

2.2.1 Physical Models

A physical model uses physical and mathematical concepts and equations to describe a system. These equations can be solved to predict the outcome of any change in the input of the system. Depending on the type of phenomenon being described, these models can vary in complexity. Based on the discretization of the control volume, these models can be classified into Three Dimensional (3D), Two Dimensional (2D), and One Dimensional (1D) models. For simulating different processes in diesel engines, they are quite common. A brief description for each of these kinds of models is provided here.

3D Models

As combustion in diesel engines is a 3-dimensional phenomenon, 3D Computational Fluid Dynamics (CFD) models are quite good in terms of predictive capabilities. This is especially true for prediction of emissions like Soot and NO_x. However, these models have a massive drawback in terms of time. These models are not only computationally costly to solve but also requires an enormous effort for creating the models. Due to this shortcoming, use of these models is limited to concept validation and enhancing the knowledge of combustion inside the diesel engine [23,24]. As an example, if a new injector or a combustion chamber concept has to be tested, 3D CFD simulations would be the best choice to evaluate the design [25,26]. However, the use of these kinds of models for engine calibration is not possible because of too large computational time and cost.

2D Models

These models discretize the control volume in two directions. A very commonly used example of this type of model is Direct Injection Diesel Jet Model by Gamma Technologies that discretizes the jet of the injected fuel in radial and axial direction [27]. These kinds of models have lower computational time than 3D models, but still considerably high for calibration activity. Furthermore, this savings in computational time comes at the cost of accuracy in terms of predicting emissions. 2D models can predict the trend of emissions accurately for change in control parameters but are not very accurate in providing the exact values (especially soot).

1D Models

1D CFD models can be effectively used for simulating the phenomena or systems in which the flow is predominant in just one direction. A typical example of this would be simulating gas exchange in diesel engine. Even though these models are very fast to compute and solve, they cannot be used for prediction of emissions. For this reason, experimental models, described in detail in the next section, are preferred for carrying out the engine calibration task.

2.2.2 Experimental Models

These models or methods are based on experiments performed on the engine test bench. During the early development of diesel engines, when the number of control parameters were very limited, these parameters could be optimized experimentally at the test bench by changing one parameter at a time and evaluating the effect of this variation. This method is simple if there is no interaction between different parameters. However, in diesel engines the different control parameters interact with each other. For example, higher boost pressures allow higher EGR to be used for NO_x control. In order to exploit this relationship, it is important to vary both boost pressure and EGR simultaneously. This simultaneous variation of the control parameters is carried out using full factorial experiments. If we consider a full factorial experiment for two control parameters each having 10 different discrete levels or values of variation, then this would give 100 experiments to be carried out. This is shown in Figure 2-2.

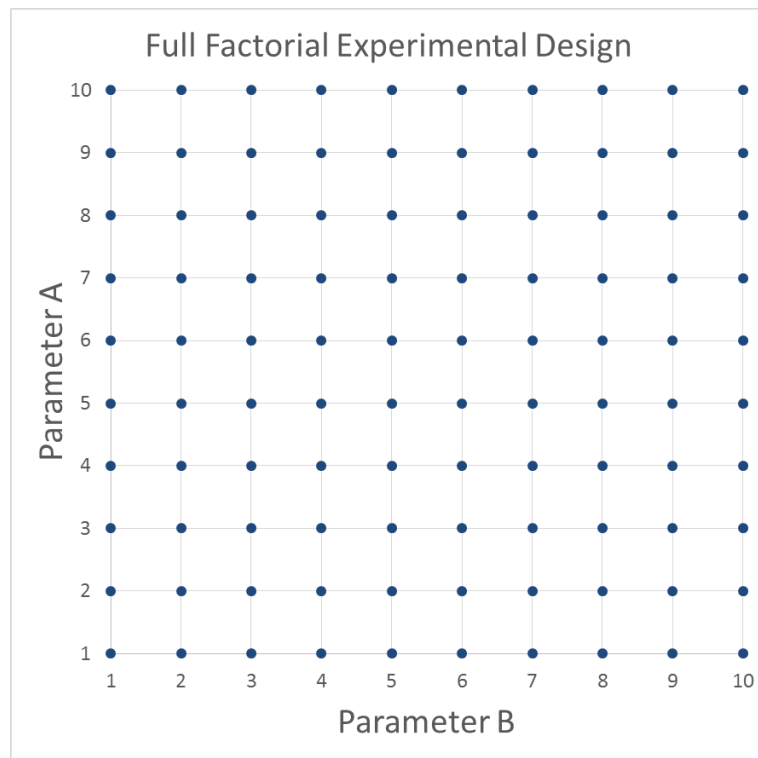


Figure 2-2 Full factorial experimental design for two parameters each having 10 levels

In fact, as the number of control parameters increase, the number of experiments increase exponentially with a relation mentioned in Equation (1).

$$\text{No. of experiments} = \text{No. of levels of each parameter}^{\text{No. of Parameters}} \quad (1)$$

Using this relation, Figure 2-3 shows that for a system with eight control parameters, each having three discrete levels, we will need almost 6500 experiments for a full factorial analysis. As mentioned before, a modern diesel engine can easily have up to 15 control parameters. It is therefore infeasible to perform a full factorial experimental analysis for such a complex system.

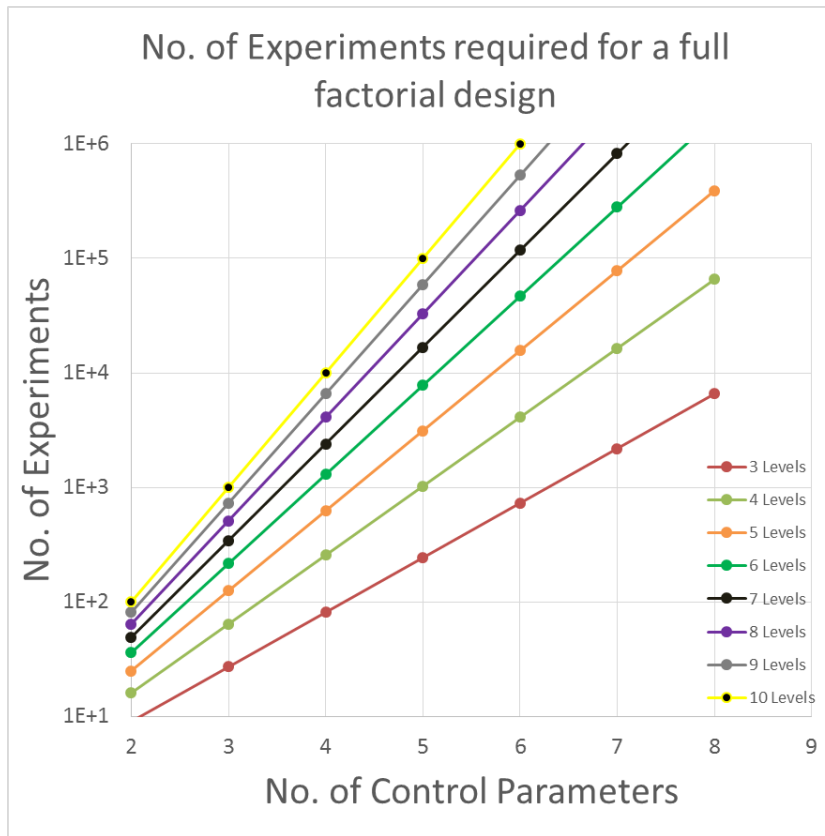


Figure 2-3 Number of experiments required for a full factorial design as a function of number of control parameters and levels of each control parameter

For this reason, Design of Experiment (DoE) techniques are used to reduce the number of experiments required [28]. Using DoE, a shorter experimental test campaign is generated that can be performed at the test bench in a shorter time than full factorial design. The size of the experimental campaign still depends a lot on the required model type and complexity. To reduce the experimentation time and cost even further, a lot of research have been performed in the area of experimental modelling of the diesel engines [28–30]. The commonly used experimental engine models can be broadly classified into two categories, Polynomial and black-box models, both of which will be now described in brief.

Polynomial Models

An experimental model defines the relationship between the inputs and the outputs. In polynomial models, this relationship is defined using polynomial equations. A typical example for a quadratic polynomial model with two inputs is shown in Equation (2). If the relationship between the two inputs is not linear, then this degree of polynomial has to be used to model the relationship.

$$\hat{y} = a_1 + a_2x_1 + a_3x_2 + a_4x_1^2 + a_5x_2^2 + a_6x_1x_2 \quad (2)$$

As it can be seen from the equation, at least 6 experiments are required as there are 6 unknown variables. The number of experiments increases as the degree of the polynomial increases. These higher degree polynomials are required to model

complex relationships like the ones between different control parameters of a diesel engine. However, even with the higher degree polynomial functions, the number of experiments required to be performed, in order to model the engine behavior correctly, is still much less than required in a full factorial experiment. Due to this benefit of reduced experiments, DoE along with polynomial models are quite often used for modeling and optimization of diesel engine performance [29–31]. Even if these models are quite popular because of their simplicity, they are not suitable to model higher dimensional space problems with a large number of inputs. Due to the increased number of control parameters in diesel engines, black box models are also gaining popularity for the engine optimization problem.

Black Box Models

These are a category of models in which the input is provided to the model, and the output is obtained without having any information or knowledge about the internal functioning of the model. In this way, the model itself behaves like a black box inside which the inputs are processed but cannot be observed. This is shown in Figure 2-4.

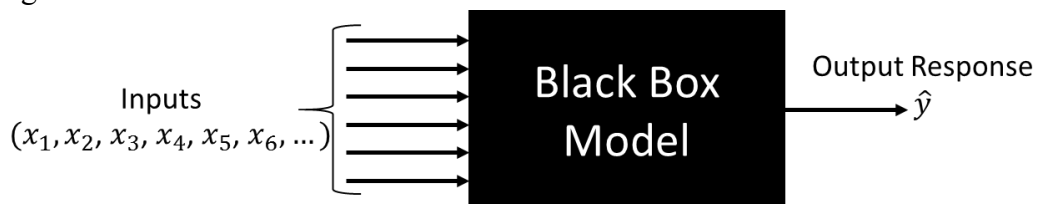


Figure 2-4 Output response estimation using a black box model

Typical examples of black box models include Neural Network (NN) models and Gaussian Process (GP) models. Even though Black Box models are difficult to comprehend and interpret, they are quite useful in modelling system with high dimensional space such as diesel engines. For this reason, such models are being increasingly used for modelling and optimization of diesel engines [22,32,33].

2.3 Different Approaches for Engine Calibration

Once the models have been created using the above-described methods, the next step is to use these models to optimize the engine in the complete operating range and creating the calibration maps. For carrying out this task, different approaches can be adopted. Some of the popular calibration approaches along with their pros and cons are discussed in brief in this section.

2.3.1 Local Approach for Calibration

Local approach for engine calibration is one of the most commonly used approaches. In the local approach, the operating points of the driving cycles are first grouped into a reduced number of points which are commonly referred to as Key Points (KPs). This definition of KPs is carried out using certain clustering

algorithms such as the nearest neighbor algorithm. This is shown in Figure 2-5, where the operating points on WLTC are associated to the nearest KPs. The operating points are shown on normalized axes so that load and engine speed have the same scale for the clustering algorithm to work. The engine load and speed have been normalized using the respective maximum and minimum values encountered on WLTC. In Figure 2-5 the operating points are shown by the same symbols (smaller) and the same color as of the KP they are associated with.

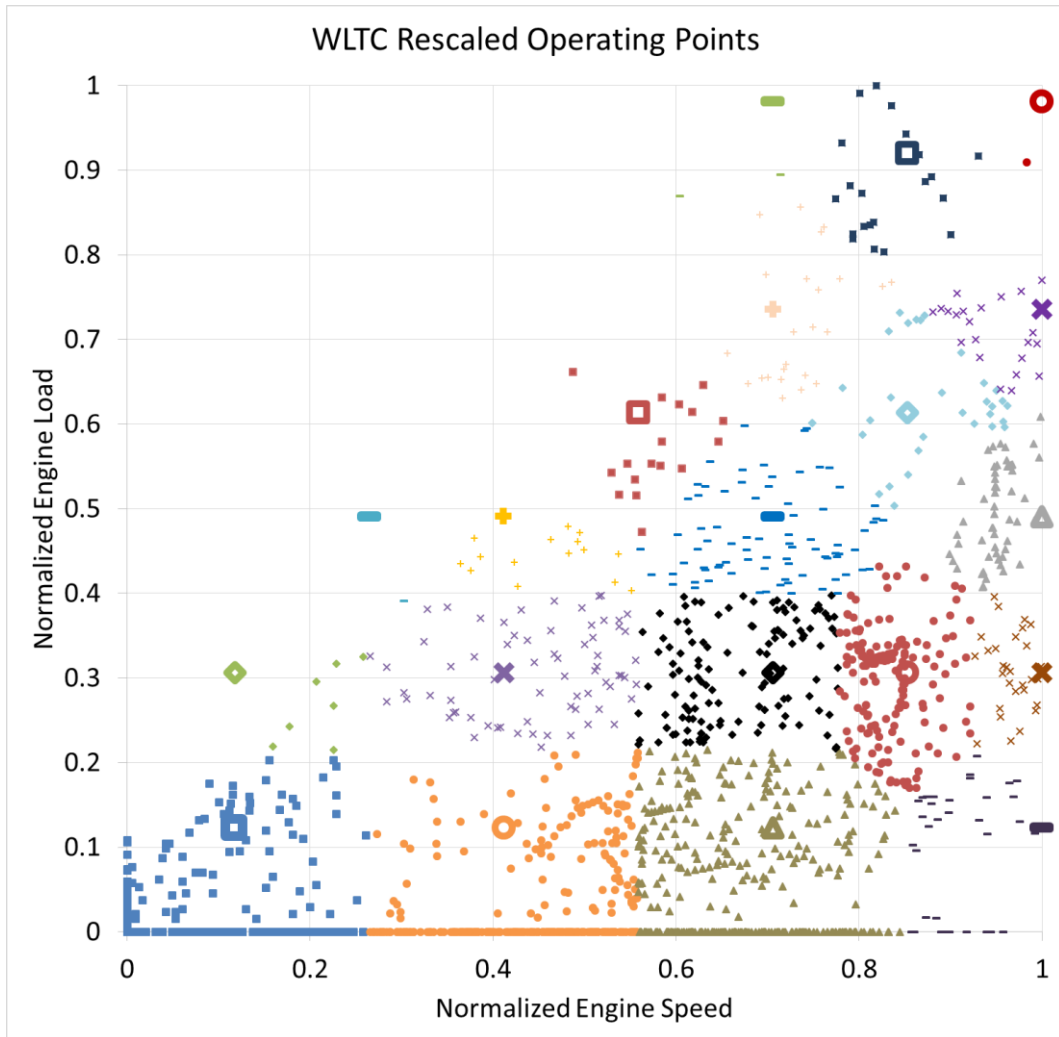


Figure 2-5 Key point definition for WLTC using a clustering algorithm

It can be seen in Figure 2-5 that about 80% of the operating points of WLTC could be represented by just 7 to 8 KPs. However, higher number of KPs are used as at different engine speed and load conditions different control parameters are active. For example, at low loads two pilot injections are used to control the engine combustion noise but at high loads the second pilot is not used as it is not very effective. Similarly, at low loads boost is not a controllable parameter, as the exhaust gases entering the turbine at low loads do not have enough enthalpy to produce sufficient power to drive the compressor. Therefore, the desired boost pressure cannot be achieved at low loads. In this way, each KP may have different number of active control parameters associated with them. Furthermore, to avoid

extrapolating the control parameters or engine calibration maps, a higher number of KPs are selected. For a driving cycle as the WLTC, to adequately model the engine behavior the number of KPs can be anywhere between 18 and 25. For RDE, the number of KPs are typically between 25 and 30.

Once the KPs are defined, they can be considered as the statistical representation of the engine operation over the given driving cycle. The experimental models are therefore created for only these points. These experimental models are called local models. Using the local models, each KP is optimized for some objective subjected to some constraints. It should be mentioned here that each KP is modelled and optimized independently of the other KPs. This means that value of the control parameter or emission at different KPs do not influence each other in any way. Thus, both the modelling and optimization is carried out locally for each KP. This is the reason that the approach is known as local approach for calibration.

Once the optimum value of the control parameters for all the KPs are found, the calibration maps are generated using interpolation and extrapolation. The calibration map generation from the optimal values at different KPs for one such parameter, SOI is shown in Figure 2-6

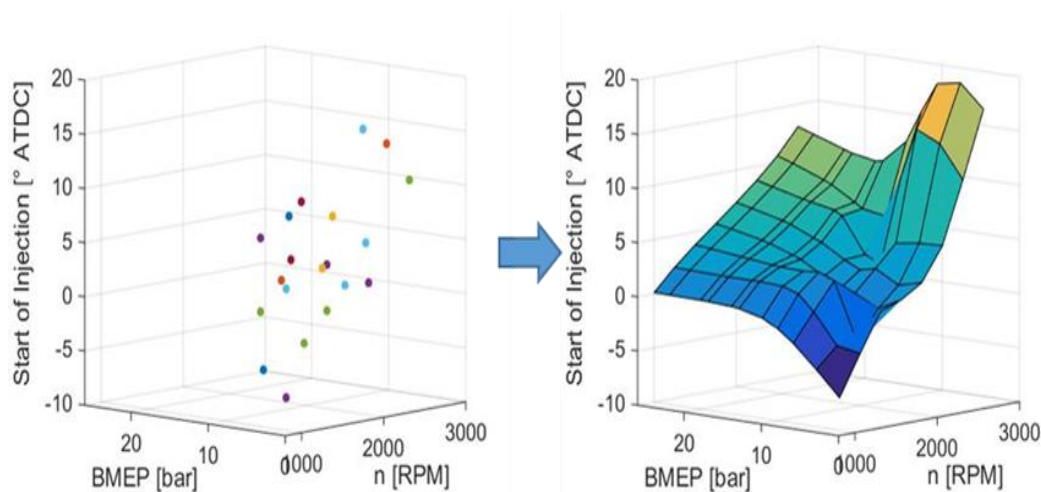


Figure 2-6 Start of Injection map creation from the optimum values at different Key Points

Since all the KPs are optimized locally, the value of the control parameters for the neighboring KPs can be very different. This can result in rough calibration maps, for example Figure 2-6, which is not acceptable due to the violation of the smoothness requirement. Therefore, the final step is to smoothen the calibration map manually. As a consequence, the values of the control parameters can be moved away from their optimal value to smoothen the map as shown in Figure 2-7.

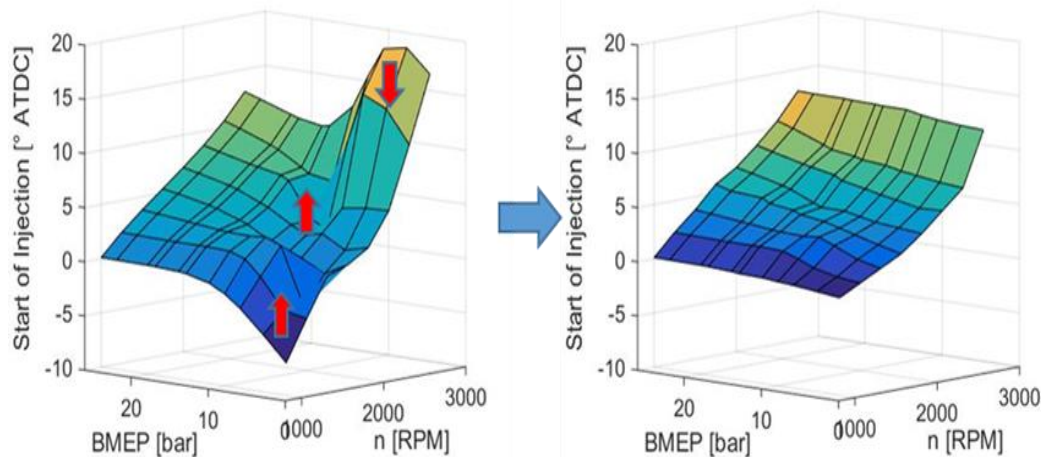


Figure 2-7 Manual smoothing of Start of Injection map

At each KP, the local models are highly accurate in predicting emissions for changes in control parameters. However, due to their local nature, there is no information available between different KPs. Furthermore, one of the major drawbacks of the local models is the loss of optimality due to manual smoothing procedure. However, local approach is still widely used in the industry for calibration due to the accuracy of the local models. Moreover, the local approach is much simpler than its counterparts, which are described next.

2.3.2 Global Approach for Calibration

In the global approach, the engine models are constructed for an operating region instead of a point. Therefore, the engine speed and load are also inputs to the global models. This means that the global models can predict the result of variation in engine speed and engine load in addition to the variation in control parameters. Typically, more than one DoE is defined to cover the entire operating range of the engine. The reason is same as mentioned before; a different number of control parameters are active in different areas of engine operation. The areas of engine operation having similar control parameters are combined together, thus resulting in 3 or 4 global DoEs. This is shown in Figure 2-8.

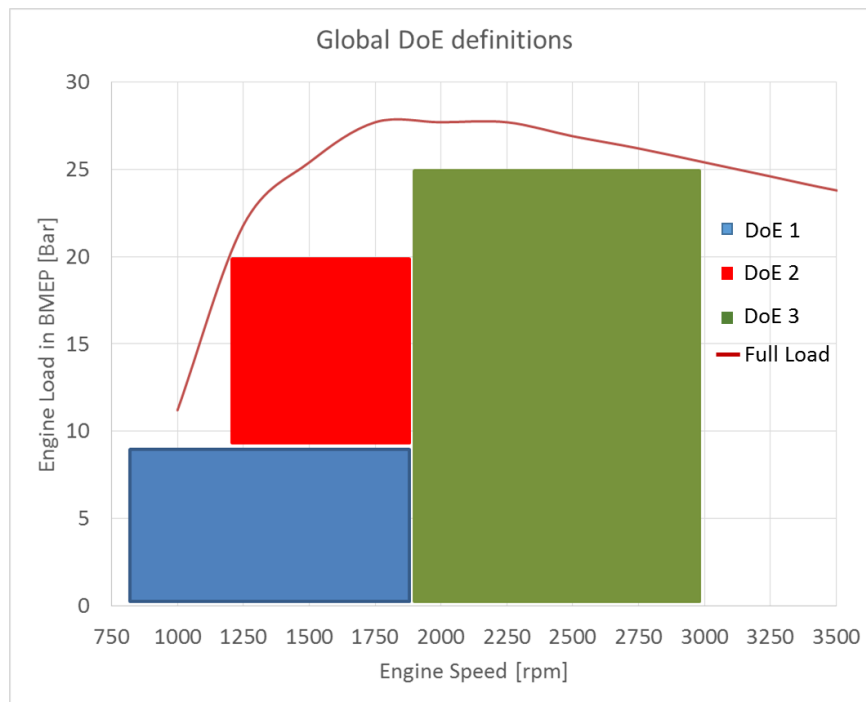


Figure 2-8 Modelling of the complete engine operating range using global Design of Experiment

Once the global models are constructed for each region, these models are then used to optimize the engine calibration. The difference with respect to the local method is that there instead of local optimization of KPs, here the complete set of engine calibration maps are optimized globally. This essentially means that using different techniques like Local Linear Model Tree (LoLiMoT), polynomial models, splines etc., the calibration maps can be built by optimization of global models while imposing smoothening constraints directly on the maps. In this way, in global approach, both modelling and optimization processes are global.

Global approach eliminates the manual smoothening procedure that is present in the local approach. Due to the removal of the manual smoothening procedure, this approach has become quite popular for engine calibration [34,35]. In addition, due to the use of global models, information is available in the complete engine operating range and not just at some KPs as in the case of local approach. However, global models are not as accurate as the local models. Furthermore, in order to build global models, very large DoE campaigns are required (typically 6-8 times larger than local ones). These large campaigns require a long testing time and therefore are prone to instrument drift during the testing [36]. This drift can further reduce the accuracy of the models. Due to these shortcomings, local models are still preferred over global models.

2.3.3 Mixed Approach for Calibration

As the name suggests, mixed approach is intermediate between local and global. Mixed approach uses local models to maintain the accuracy and global optimization to avoid loss of optima due to smoothening of the maps. In this way, mixed approach combines some of the advantages of the two approaches. However,

as local models are used in mixed approach also, the information between different KPs is still missing. Furthermore, the mixed approach involves a lot of step and is more complex than both local and global approach [37]. That is why this approach is sometimes used in the industry, but it is not very popular [38].

2.4 Motivations for Improving Calibration Methodology

The above-mentioned approaches are state of the art for diesel engine calibration. However, they are slow, time consuming and most importantly, dependent on the skill of the calibrators. In all the three approaches, the calibrators give the constraints required for optimization. These constraints may not always result in the optimum solution of the problem and can further slowdown the calibration process.

With the aim of reducing the effort for diesel engine calibration, a faster and automated calibration methodology for last generation of automotive diesel engines has been developed in this work. Furthermore, it cannot be argued that when using models to carry out the calibration task, accuracy of the models is most important parameter to be considered. Local models are certainly at an advantage in terms of accuracy. If the loss of optima associated with the local approach can be tackled, then this can bring the local approach at par with the other methods of calibration, if not make it better. For this reason, local models have been selected to carry out the work further. In order to remove the loss of optima occurring in local models, smoothness and optimization steps have been integrated in this methodology. Moreover, a Multi Objective Optimization (MOO) method based on Genetic Algorithm (GA) have been developed in this work to find the optimum values for the control parameters for different KPs.

In Chapter 3, a description of the local models used for carrying out the calibration task is provided. This is followed by the description of optimization methodology in Chapter 4. The results from the optimization are used in Chapter 5 to describe the smooth calibration map generation methodology. In Chapter 6, the results for the calibration map generation methodology have been shown and discussed. This is followed by concluding remarks in Chapter 7.

Chapter 3

Engine Emission Models

Some parts of this chapter have already been published in the following journal article:

- Millo F, Arya P, Mallamo F. Optimization of automotive diesel engine calibration using genetic algorithm techniques. *Energy* 2018. doi:10.1016/j.energy.2018.06.044.

The experimental models used in the research activity were provided by FEV Italy. The engine used in the experimental activity is equipping a C segment vehicle in European market, and it features a two-stage turbocharger and a short route EGR, without any VVA system. For calibrating the engine for the European market, 25 KPs were selected. However, 5 of these KPs were at high loads and high speed that are not encountered during WLTC and therefore have not been considered in this study. However, this does not mean that the methodology has been defined only for WLTC. It can be extended to any type of driving cycle and to any number of KPs.

In the first section of the chapter, the main engine control parameters have been highlighted along with the modelling domain. Following this short introduction, the modelling process has been described. In the last section of the chapter, the quality of the models used has been assessed and reported.

3.1 Model Domain and Process

The following parameters were used as inputs for the empirical models.

1. Start of Injection (SOI)
2. Air Quantity
3. Rail Pressure or Injection Pressure
4. Swirl level
5. 1st Pilot Quantity
6. 1st Pilot Dwell Time (DT)
7. Boost Requested
8. 2nd Pilot Quantity
9. 2nd Pilot DT

The number of inputs for all the KPs were not that same as some of the control parameters (last three) mentioned above were only partially active. Boost requested was not an active control parameter at lower loads because the exhaust gases arriving at the turbine cannot generate enough power to drive the compressor.

Furthermore, 2nd pilot injection, which is quite effective in reducing the CN at low loads, was not used at high loads as this can affect the combustion stability.

As mentioned earlier, DoE was used to create empirical models, which were then used to reduce the calibration effort. For creation of local models for each KP, the experiment was carried out in such a way that all the control parameters were varied in some range. This range is typically known as the model domain. While using the models for predictions, the quality or the predictability of the models is valid only in the model domain. Of course, the exact value of model domain for each control parameter changes according to the KP, but the range of variation in the value is usually constant. As, it is not possible to show the model domain for each KP, therefore the range of variation is shown in Table 3-1. This range of variation, as mentioned earlier, is typically constant, but might be subjected to small changes depending on the feasibility of the values that the control parameters take.

Table 3-1 Range of variation of each control parameter for the experiments to generate empirical models [39]

Parameter Number	Input Quantity	Unit	Range of Variation for Domain
1	SOI	°bTDC	±4
2	Air Quantity	mm ³ /stroke	±40
3	Rail Pressure	MPa	±30
4	Swirl level	%	±30
5	1 st Pilot Quantity	mm ³ /stroke	±0.8
6	1 st Pilot DT	μs	±500
7	Boost Pressure	kPa	±25
8	2 nd Pilot Quantity	mm ³ /stroke	±0.8
9	2 nd Pilot DT	μs	±500

Once the experiments were carried out for each KP, the results from the experiments were used to construct the empirical models using a Gaussian Process (GP) regression. GP regression uses the concept of maximum likelihood to train the models. As it is a vast topic and has been extensively covered in literature, it has not been explained here [40–42]. The experiments were designed in such a way that for each KP, there were 140 design points, 16 repetition points and 20 validation points. Design points were used for generating the empirical models, whereas repetition points were used to correct any drift in the instruments used for testing. Instrument drift is typically common while performing long test campaigns at the engine test bench. However, most importantly, the validation points were used to validate the models and check the predictive capability of each model. As these points are not used for training of the model, they can provide useful information about the models overfitting the training data. To add another check for the quality of the models, Leave One Out (LOO), a cross validation technique, was also used

[43]. With LOO technique, the model is trained on all the design points but one and the model prediction is then carried out for this particular point. This process is repeated until all the design points have been left out once. Together, these three parameters, R^2 , R_{Val}^2 and R_{LOO}^2 were used to assess the quality of the models generated. If the value of any of these correlation coefficients was less than 0.95, the models were rejected and the experimental activity was performed again for that KP. The next section shows the quality of the models generated for one of the KPs.

3.2 Model Quality

The following engine outputs were modelled as a function of the control parameters:

- Brake Specific Fuel Consumption (BSFC)
- Brake specific emissions (NO_x, Soot, HC, CO)
- Combustion Noise (CN)
- Exhaust Temperature

In this way, 7 models were created for each KP. As an example, the model quality using the correlation coefficients for one of the KPs (2000 rpm x 5 bar) has been reported in Table 3-2. Following this, the model response plots for each of the empirical model for the same KP are shown from Figure 3-1 to Figure 3-7.

Table 3-2 Different correlation coefficients used for evaluating the model quality [39]

Model	R^2	R_{Val}^2	R_{LOO}^2
BSFC	0.966	0.956	0.953
NO _x	0.996	0.990	0.988
Soot	0.996	0.960	0.972
CO	0.993	0.976	0.971
HC	0.956	0.954	0.950
CN	0.987	0.967	0.967
Exhaust Temperature	0.988	0.969	0.973

As it can be seen from the Figures and the table, all the models showed very high predictive capabilities. These models are used to optimize the engine calibration in a computer environment, thus reducing the cost and development time. However, as mentioned earlier, traditional optimization techniques are not well suited for such a complicated task. Therefore, in the next chapter, a novel optimization methodology using these empirical models have been described.

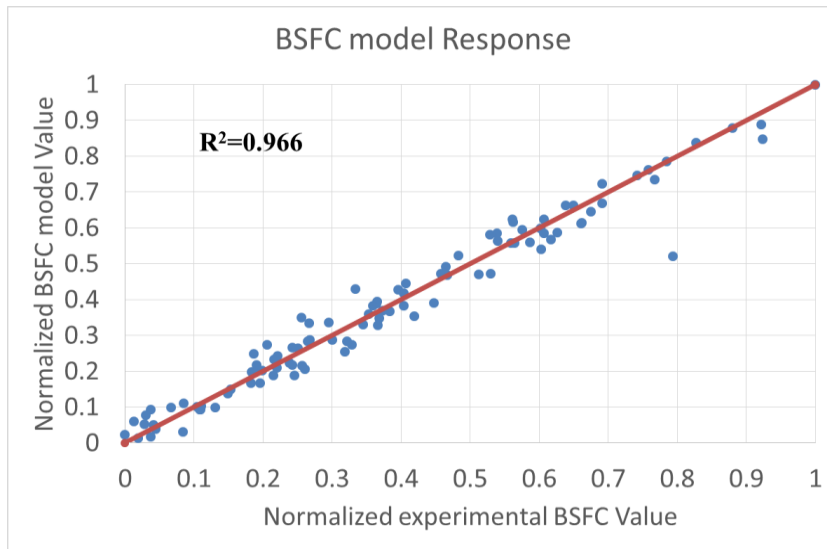


Figure 3-1 BSFC model response [39]

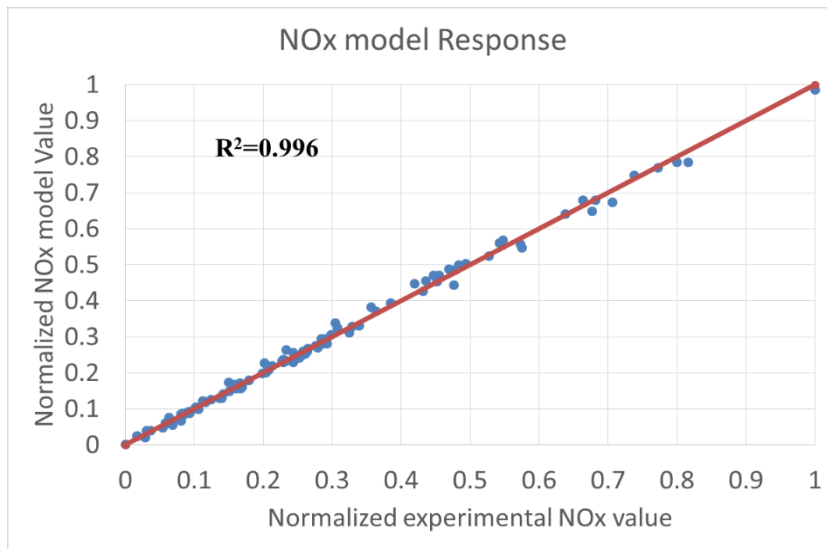


Figure 3-2 NOx model response [39]

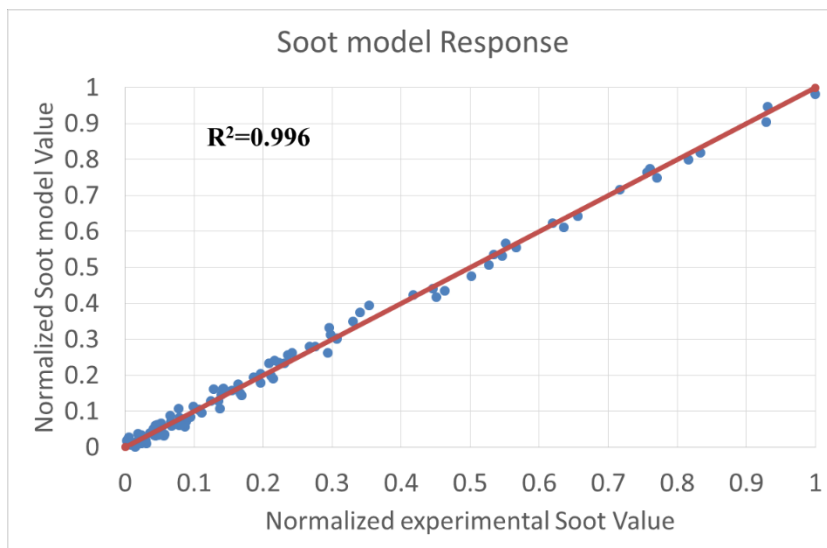


Figure 3-3 Soot model response [39]

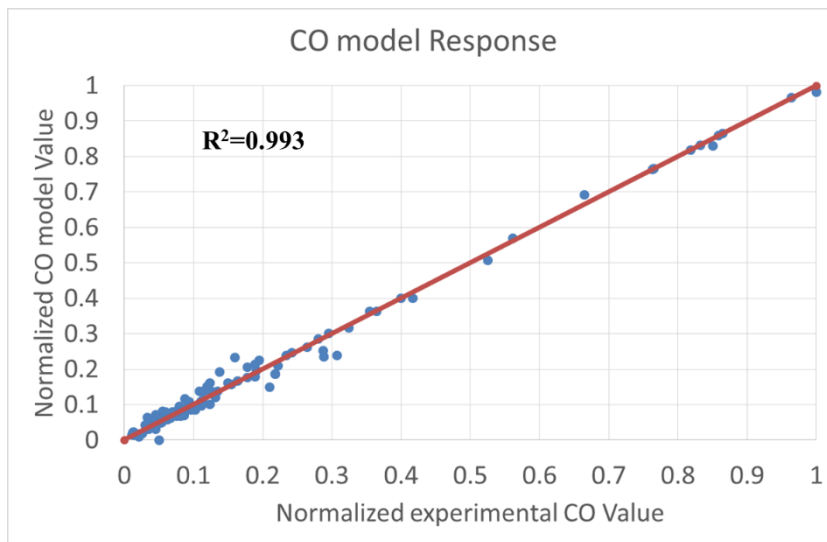


Figure 3-4 CO model response

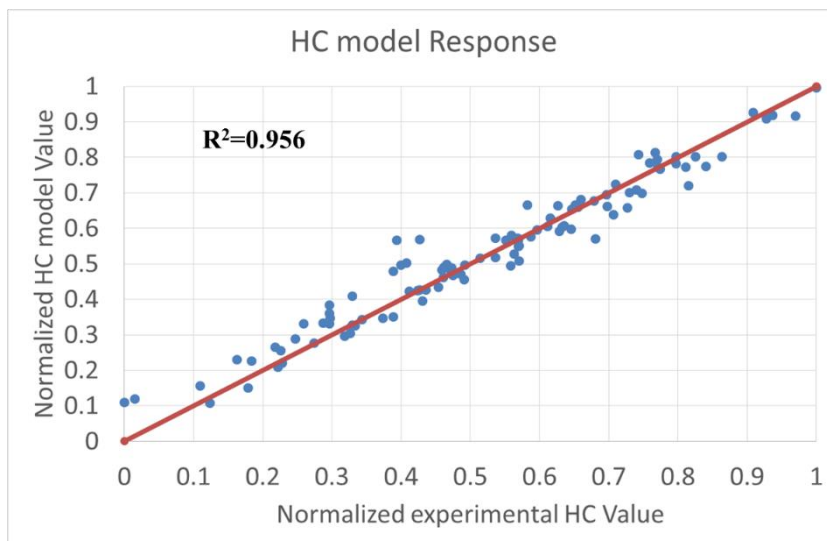


Figure 3-5 HC model response

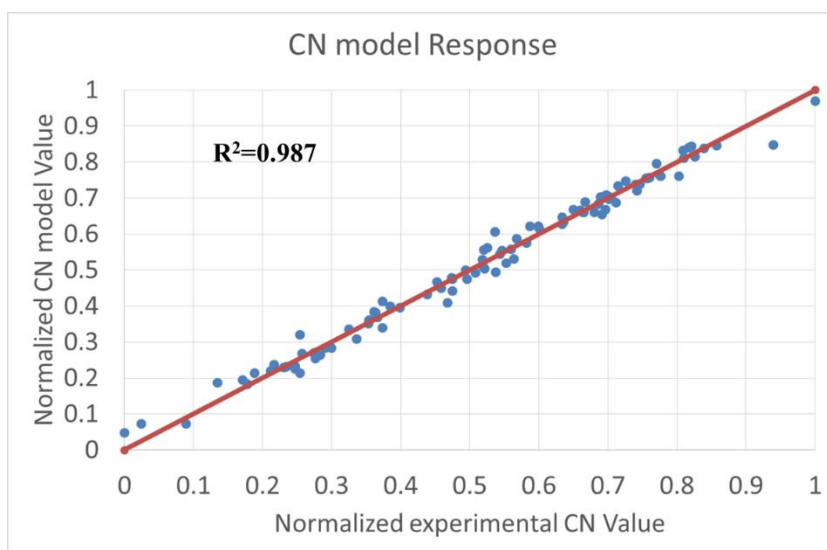


Figure 3-6 CN model response [39]

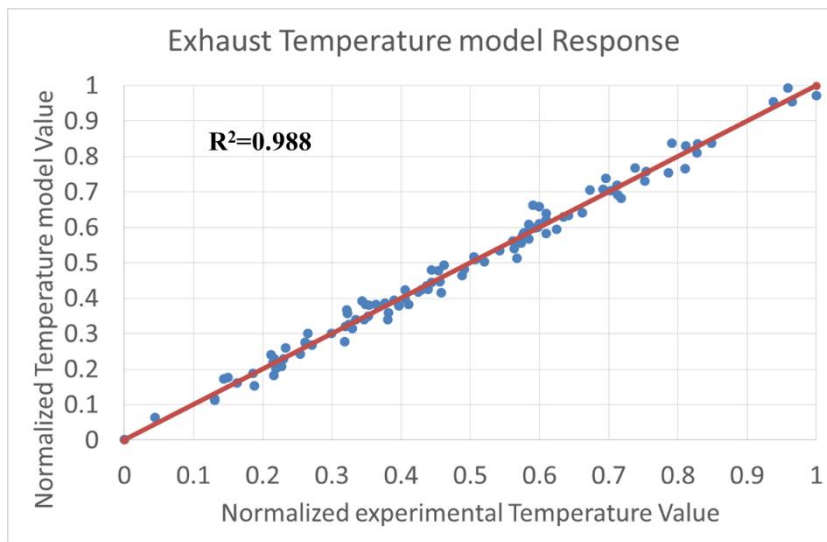


Figure 3-7 Exhaust temperature model response

Chapter 4

Optimization

Some parts of this chapter have already been published in the following journal article:

- Millo F, Arya P, Mallamo F. Optimization of automotive diesel engine calibration using genetic algorithm techniques. Energy 2018. doi:10.1016/j.energy.2018.06.044.

Optimization of a diesel engine is a multi-objective optimization (MOO) problem since many objectives like fuel consumption; emissions, combustion noise etc. have to be optimized. Moreover, because of the trade-off relationship between the different objectives like Soot and NOX this optimization task is further complicated. Traditionally, the solution to a MOO problem is found by breaking down the problem into multiple Single Objective Optimization (SOO) problems. Out of these multiple problems, the optimization problem with the most significant objective is then considered and solved. The choice of the most significant objective is dependent on the calibration target. In these single objective problems, the optimization is carried out for one objective while the rest of the objectives act as constraints. This is also known as bounded objective function method [44]. Furthermore, the solution to the optimization problem is typically found using classical optimization techniques such as steepest descent or simple gradient method. Mathematically, this type of optimization can be described by the Equation (3) to Equation (7):

$$Target = \min(FC) \quad (3)$$

$$NO_x \leq a \quad (4)$$

$$PM \leq b \quad (5)$$

$$CN \leq c \quad (6)$$

$$Exh Temp. \geq d... \quad (7)$$

Although, the calibration activity can be carried out using the conventional methods, there are some significant drawbacks associated with these methods. Firstly, the traditional optimization methods are not suitable for such a kind of optimization. Traditional optimization methods like gradient descent are not very useful for solving the higher dimensional optimization problems such as diesel engines, which can easily have up to 15 control parameters. These methods worked

well with convex functions and trivial non-convex functions [45]. Moreover, the application of such optimization methods is confined to continuous differentiable functions. Furthermore, the solutions from these methods depend on the initialization as these methods suffer from a possibility of being trapped in local minima.

A single objective optimization is not the ideal scenario, especially for local models, since this limits the possibility of selecting a solution that can give better result in tradeoff between emissions and fuel consumption. For example, with a MOO solution that generates a Pareto front between different objectives, it might be possible to select a solution that gives much lower NO_x for a very small penalty in fuel consumption. Pareto front with multiple optimized calibrations also provides more flexibility in selecting the calibration that can provide smoother calibration maps.

Furthermore, the constraint definition coupled with traditional optimization methods pose even a bigger problem. Typically, these constraints come from the experience of the calibration team. This is not always the best choice for defining the constraints as it is dependent on human judgement and might be prone to errors. In addition, in some particular cases, such as a newly designed engine, it is impossible to determine the adequate value of these constraints. Moreover, since the aim of this work is to develop a methodology that is automatic, definition of constraints coming as human input proves to be a roadblock towards achieving the aim.

In the direction of improving the calibration methodology for diesel engines, an optimization methodology has been described in this chapter, the code for which was developed in house using MATLAB v2016b. In the described optimization method, a similar bounded optimization has been followed. However, the constraints have been defined dynamically and systematically in such a way that a Pareto front is obtained. Furthermore, the optimization is carried out using Genetic Algorithm (GA) that have become quite popular due to their stochastic nature and capability to avoid local minima.

In the first part of the chapter, a MOO methodology has been described. For illustration purpose, the methodology has been described using one KP (2000 rpm and 5 bar BMEP). The starting point of this methodology are the local empirical models described in the previous chapter. Following the description of the methodology, some results achieved have been shown. In the second part of the chapter, a specific case of the optimization problem has been considered. This is a case when a calibration is already present for the engine, but a reduction is required for one of the emissions, while preserving the smoothness of the calibration maps.

4.1 Multi Objective Optimization

As mentioned earlier, traditionally the MOO problem is broken down into multiple SOO problems and then solved for the most significant objective. However, in the described methodology, instead of solving for just one objective,

the multiple SOO problems have been solved in a systematic way to obtain a Pareto front.

Before going on with the description of how the Pareto front is obtained, it is necessary to first introduce the optimization method used to solve a one SOO problem, which has been described using a flow chart shown in Figure 4-1.

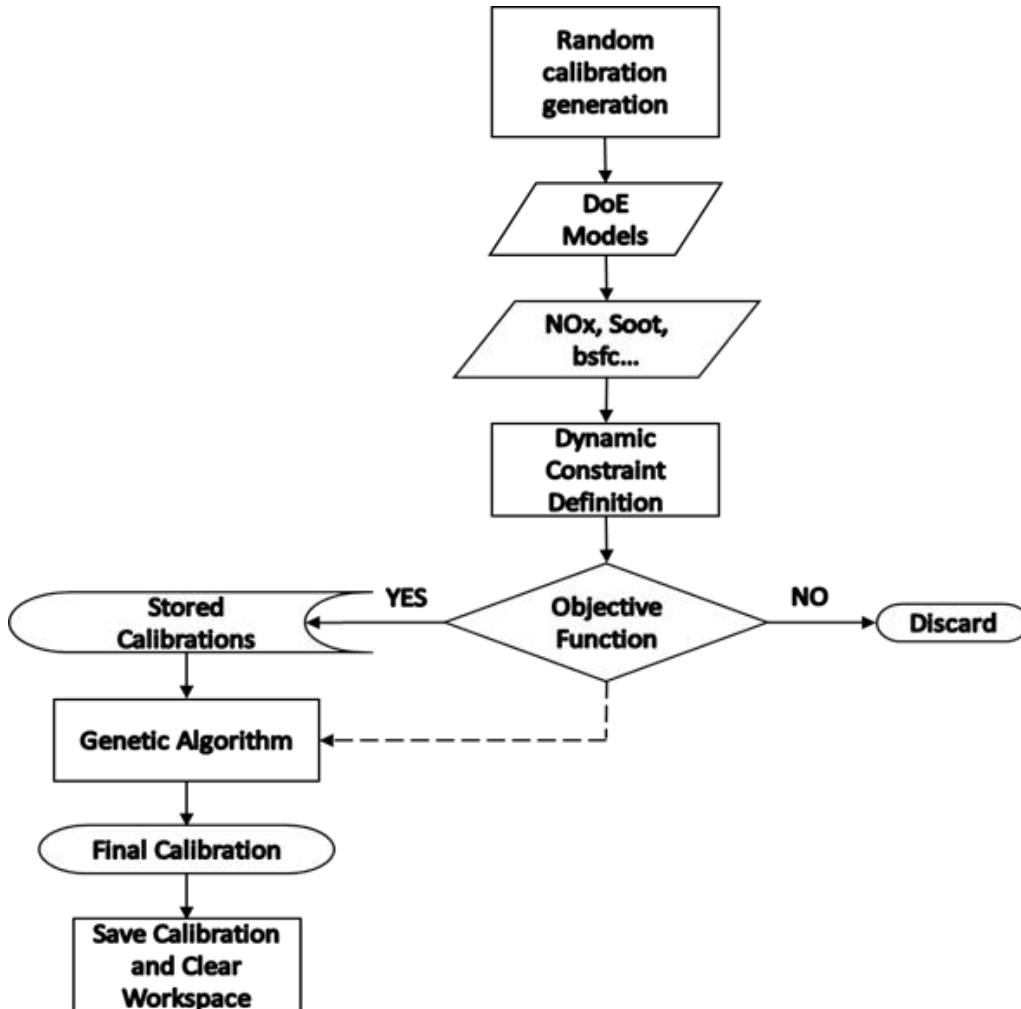


Figure 4-1 Flow chart describing the methodology to solve one optimization problem [39]

As a first step of the optimization, a large number of random calibrations (100,000) are generated using the random number generator of the MATLAB. This large number of calibrations are created by varying the value of each control parameter randomly within the model domain. The various emissions, FC, exhaust temperature and CN are then calculated using the empirical models/DoE models. Once the values of the different model outputs have been calculated, dynamic constraints are used to reduce the size of the population. This is done using an objective function check. In this component, all the calibrations that result in the model outputs lower than the constraints (and higher in case of exhaust temperature, since minimum value of exhaust temperature is required) are stored and are passed on to the GA optimizer as an initial population. In addition, the information regarding the objective to be optimized is also passed on to the GA optimizer. The

GA optimizer uses this initial population and the objective information to converge to one optimum calibration for a given set of dynamic constraint. This optimum calibration and set of constraint are saved in the hard disk and the workspace of MATLAB is cleared to be initialized for another optimization with different constraints and different optimization objective.

The process shown in Figure 4-1 is carried out multiple times with different set of dynamic constraints and different set of optimization objectives to achieve the final Pareto front solution. However, the two most important components of the methodology for solving a SOO problem are dynamic constraint definition and GA. Therefore, before moving on to the Pareto front generation, these two modules have been described in detail.

4.1.1 Dynamic Constraint Definition

The final solution obtained for a SOO optimization is predominantly dependent on the constraints provided as an input. Therefore, the dependency on human input for the constraints can sometimes result in not so optimum solution. Furthermore, for the sake of keeping the methodology of calibration automated, these constraint values cannot be provided as an input and therefore needs to be defined in a self-executing way. In this section, the logical approach to define these constraints in an automatic manner has been described.

Firstly, it is important to differentiate between the two types of constraints used in this approach. As mentioned earlier, for each iteration, the optimization objectives and constraints are varied systematically. However, not all the constraints need to be varied for each iteration and depending on this variation, two types of constraints identified are:

- **Static/Fixed:** These constraints are fixed for all the iterations of the optimization process for one particular KP. The value for these types of constraints is typically coming from hardware limits, early heating of EATS, targeted comfort level and so on. The value of fixed constraints is typically known or set for each KP before the starting of the calibration activity. Exhaust temperature, CN, HC and CO¹ are considered as fixed constraints parameters in this activity.
- **Dynamic:** These constraints need to have different value for each iteration. Therefore, they are defined dynamically before each GA optimization. NO_x, Soot and BSFC are chosen as dynamic constraints parameters.

Once the constraints that are to be varied dynamically are selected, the following steps are used to define their value:

¹ The emission models used for the activity are for warmed up EATS condition. In this condition, the efficiency of DOC is high and almost constant. However, CO and HC can be used as dynamic constraints with an additional computational cost.

STEP 1 Generation of Scatter Plots: The 100,000 random calibrations, which are generated as a first step of optimization iteration, are evaluated using empirical models. Once the value of different emissions has been obtained, the normalized² scatter plots for soot-BSFC and NO_x – BSFC are created. It should be added here that every point in these scatter plots represents emission values coming from a distinct calibration. These normalized scatter plots are shown in Figure 4-2 and Figure 4-3.

STEP 2 Gridding of Scatter Plots: The normalized scatter plots are then divided into 400 small squares by using a grid (20x20). The number of points included in each square are counted.

STEP 3 Grouping: The small squares are clustered in a manner that they form a rectangular shape. Furthermore, it is ensured that a minimum number of points (5000 in this work) are enclosed in this rectangle. One of the vertices of this rectangle is always at the origin point. The idea behind this choice is to capture the lower left corner of the plot where the values of both the emissions would be low and a sufficiently large number of points (i.e. possible calibrations) are enclosed in the constraint boundaries. This is shown by the red rectangle in the Figure 4-2.

STEP 4 Value Definition of Constraints: The borders of the selected rectangle are used as the constraints. As an example, again using Figure 4-2, the value of the soot cannot be higher than 35% of the maximum value of soot achieved during the random calibration generation. Similarly, the value of BSFC cannot be higher than 25% of the maximum BSFC. However, as two sets of constraints (Soot-BSFC and NO_x-BSFC) are obtained, two different values for BSFC constraint is available. Therefore, out of these two sets, the higher value of BSFC is adopted as the final constraint for BSFC. This is because the two sets are evaluated independently, if the lower value is selected, then for one of the sets inclusion of minimum number of points might not be ensured. It should be added here that if HC and CO are also considered as dynamic constraint parameters, then 10 such sets of constraints would be obtained (C_2^5), out of which the higher value for each parameter can be adopted as the final constraint value.

² The BSFC, Soot and NO_x are normalized in a range of 0 to 1 by using the maximum and minimum values obtained by evaluation of the random calibrations.

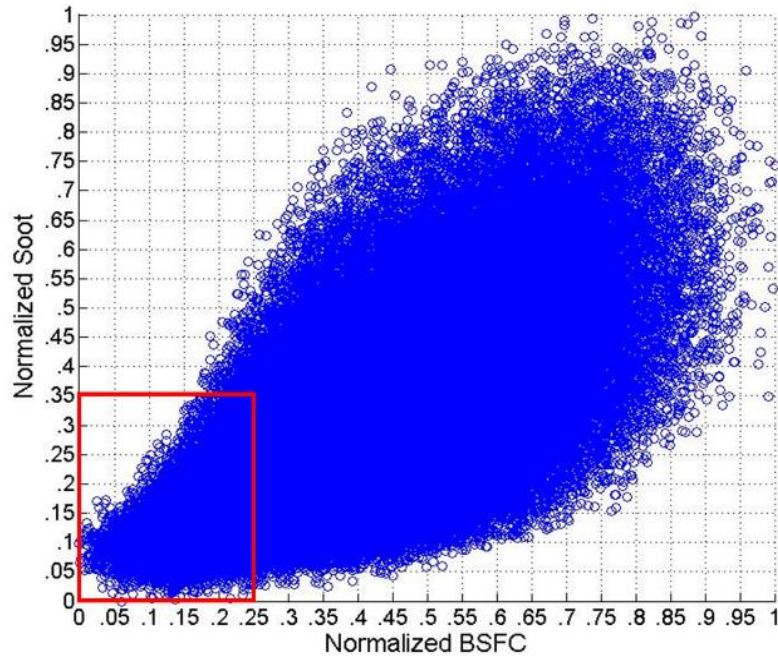


Figure 4-2 BSFC-Soot normalized scatter plot calculated from randomly generated calibrations [39]

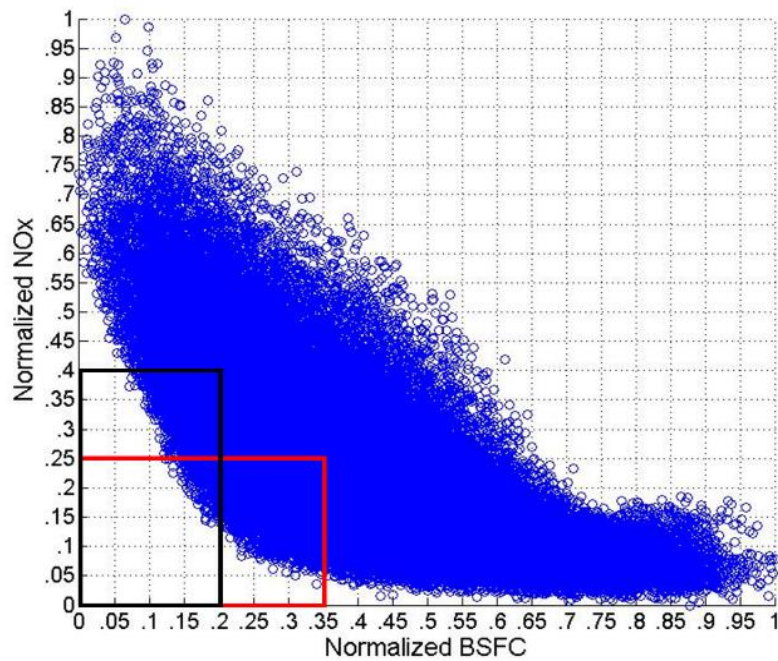


Figure 4-3 BSFC-NO_x normalized scatter plot calculated from randomly generated calibrations [39]

In Figure 4-3 two constraint rectangles (black and red) are presented as an example. As it might be expected, a huge number of such rectangles and thereby value of constraints can be obtained by using combinations of different width and height. The rationale of the approach is to use these different combinations and change the value of constraints in a systematic way to obtain a Pareto front.

However, before the complete optimization process can be described, following key terms need to be defined:

- **Constraint Biasing:** Constraint biasing is described as the bias a rectangle has, due to its inherent shape, towards a constraint parameter. The red rectangle in Figure 4-3 for example is biased towards NO_x thus giving a lower value of NO_x constraint and a higher value of BSFC constraint. The bias is decided by the orientation of the rectangle. There are only two possible orientations for each set of constraint, horizontal or vertical. Moreover, as the two sets are evaluated independently, four possible combinations of orientations from the two sets of constraints (Soot-BSFC and NO_x-BSFC) can be obtained. These possible combinations along with some explanation are highlighted in Table 4-1.
- **Bias Quantification:** This term is introduced to quantify the bias that exist towards a constraint parameter. This can be considered as the absolute difference between the height and width of the rectangle mentioned above. For a normalized constraint value, this can be written mathematically as:

$$Bias = |1^{st} Constraint Value - 2^{nd} Constraint Value| \quad (8)$$

Three distinct possibilities are considered:

- **Mild Bias:** For mild bias, the absolute difference between width and height of the rectangle is equivalent to two squares ($Bias = 0.10$). Going back to Figure 4-3, red rectangle is shown as an example of mild biasing.
- **Soft Bias:** If the absolute difference between height and width is increased to three squares, then this is considered as soft bias ($Bias = 0.15$).
- **Hard:** For hard bias, the absolute difference is further enlarged to four squares ($Bias = 0.20$). Black rectangle in Figure 4-3 is an example of Hard Bias.

Table 4-1 Different combinations for biasing of constraints [39]

CASE (<i>jk</i>)	BIAS (1 st Set)	BIAS (2 nd Set)	Comments
11	BSFC	BSFC	Limits the value of BSFC constraint.
12	BSFC	Soot	Limits the value of Soot constraint but not of the BSFC constraint
21	NO _x	BSFC	Limits the value of NO _x constraint but not of the BSFC constraint
22	NO _x	Soot	Limits the value of both Soot and NO _x constraints

As mentioned earlier, value of the BSFC constraint is evaluated for both the sets of constraints, the higher of which is finally adopted as the final value for the BSFC constraint in order to ensure that a minimum number of points are included in the constraint boundaries. It is because of this that cases 12 and 21 do not limit

the value of the BSFC constraint, even if one of the set in both the cases is biased towards BSFC.

Figure 4-4 and Figure 4-5 show the zoomed in version of the Figure 4-2 and Figure 4-3 with the focus on the points inside the constraint boundaries (Red rectangle in both Figure 4-2 and Figure 4-3). This is an example of case 21 (Table 4-1), as the 1st set of constraint is biased towards NO_x and the 2nd set is biased towards BSFC. It can be noticed from Figure 4-4 and Figure 4-5 that the value of the BSFC constraint is set to 35% of the maximum value obtained using random calibrations. This is because the higher value of the BSFC constraint is coming from the 1st set. Furthermore, it should be pointed out here that the algorithm only ensures minimum number of points enclosed in the constraint boundaries and the actual number of points can be above this threshold.

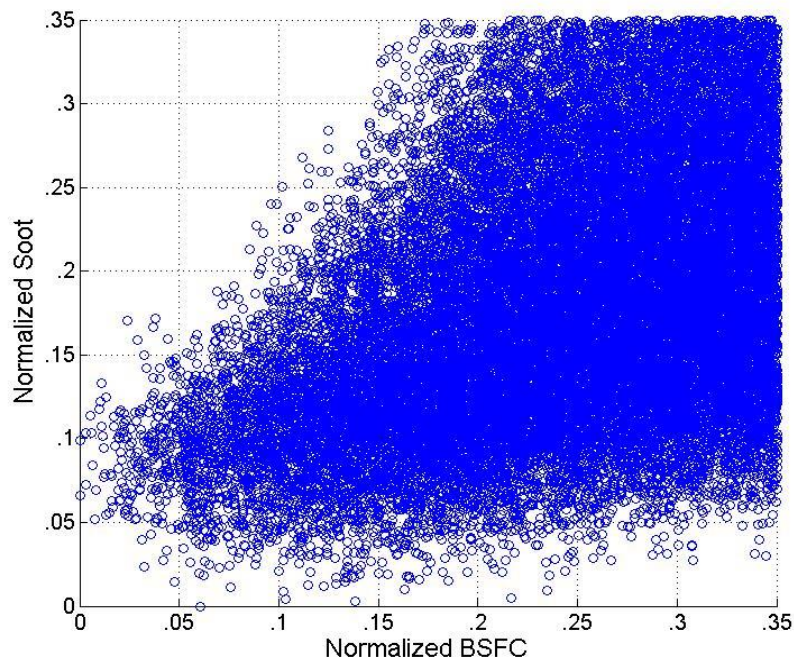


Figure 4-4 BSFC-Soot scatter points included inside the constraint boundary [39]

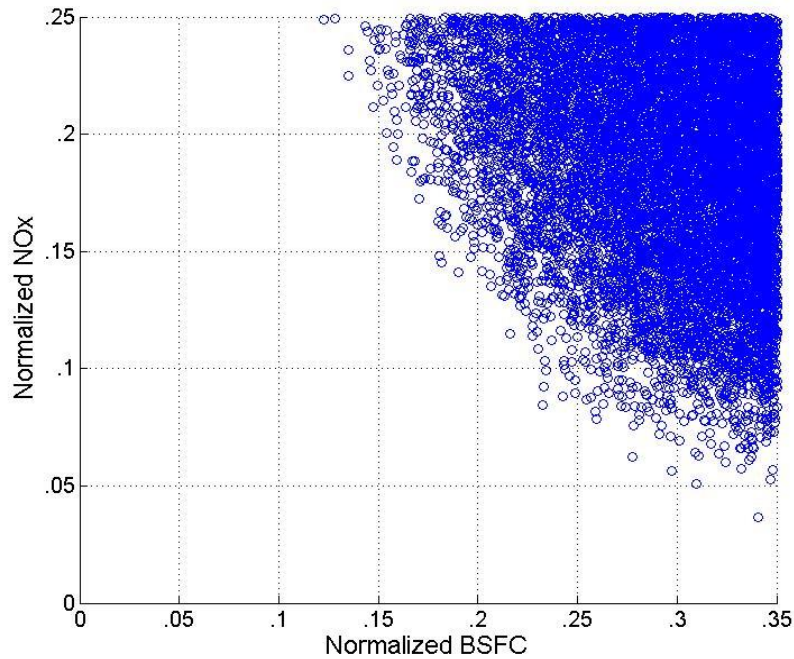


Figure 4-5 BSFC-NO_x scatter points included inside the constraint boundary [39]

Once the value of dynamic and static constraints is decided, these values are passed on to the objective function check (Figure 4-1). The calibrations that result in the emission values below these constraints are stored and passed on to the GA optimizer that is described in the next section. To highlight the effect of this objective function check, the Soot-BSFC and NO_x-BSFC scatter of the stored calibrations is shown in Figure 4-6 and Figure 4-7. On comparison of Figure 4-4 Figure 4-6, it can be seen that more than 5000 calibrations have been reduced to a much smaller numbers because of application of other constraints (static and NO_x). A similar comparison can be carried out for Figure 4-5 and Figure 4-7.

Furthermore, it is ensured that the number of calibrations provided as an input to the GA optimizer is not too high, as this will slow down the convergence and performance of the optimizer. Therefore, the maximum number of stored calibrations is limited to 500. If the number of calibrations passing the constraint check is higher than this number, then 500 calibrations are selected out of this larger group. This selection is carried out in a way to ensure that the calibrations are well distributed throughout the input model domain. This means that if two calibrations, that are close to each other in the model input domain (similarity in values of SOI, Air....), pass the constraint check then the one resulting in lower emissions will be selected and the other one will be discarded.

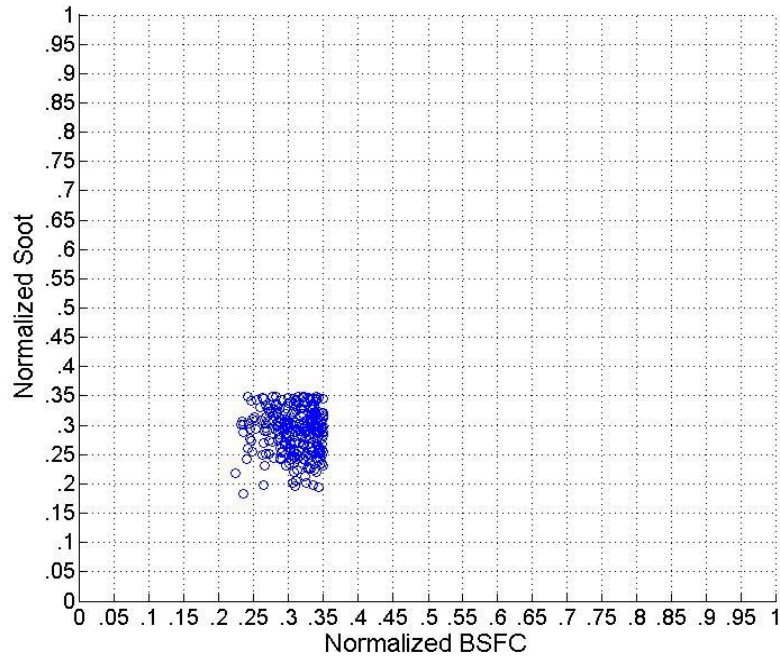


Figure 4-6 BSFC-Soot scatter for stored calibrations, i.e. calibration passing the objective function test [39]

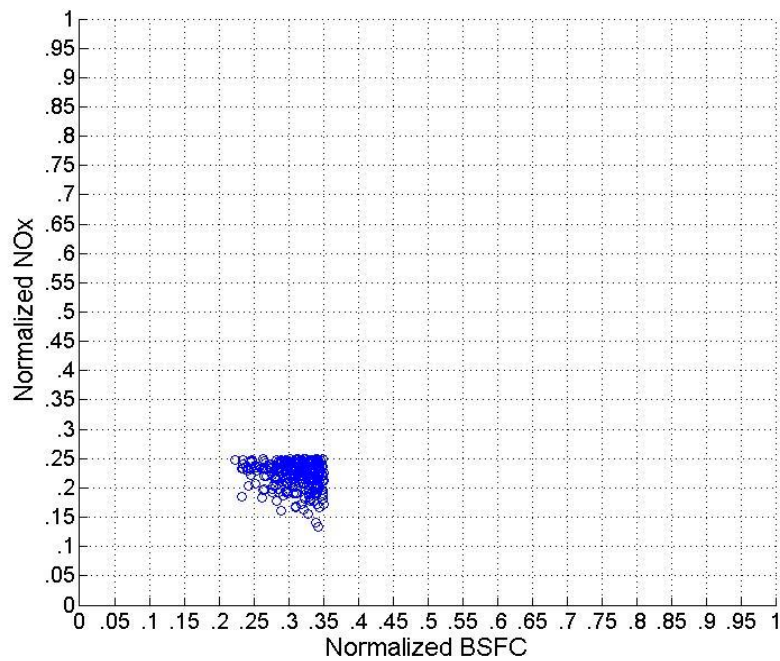


Figure 4-7 BSFC-NO_x scatter for stored calibrations, i.e. calibration passing the objective function test [39]

These stored calibrations shown in Figs. are provided as an input to the GA optimizer, along with the dynamic constraints and the objective function information, which then converges to a final solution for each SOO problem. This convergence process is described in the next section.

4.1.2 Genetic Algorithm Optimizer

GA works on the theory of natural selection to achieve the optimal solution over a large number of generations. However, this large number of generations differs from problem to problem. GA is a well-known optimization technique and well defined in the literature [46]. However, since the optimization code was developed in house, it has been described here in detail. Moreover, it is important to describe the exact procedure used to convert the control parameters of each calibration into a suitable data input for the GA.

Each calibration that passed the objective function check is converted to a form of a string or a row vector. To define the terminology of GA more clearly, this row vector is known as a chromosome. Each element of this chromosome or row vector is called a gene and the value that is stored in a gene is known as allele. It should be pointed out here that the location of each gene is fixed in the chromosome and cannot be exchanged with position of another gene. Thus, in reference to the specific case under discussion, each calibration is considered as a chromosome. The set of control parameters is considered as a gene and the value that control parameters take is known as allele. This representation of engine calibration as a chromosome is shown in Figure 4-8. In Figure 4-8 depending on the number of control parameters active for the KP in discussion only 9 genes have been shown, but the methodology can be easily extended to a larger number of control parameters.

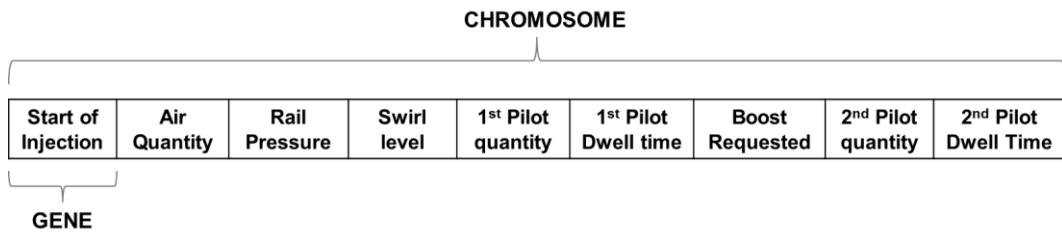


Figure 4-8 Engine control parameters represented in a form of chromosome [39]

Once the calibrations are converted into chromosomes, a fitness value is assigned to each chromosome using Equation (9):

$$Fitness = (Obj_{x,Base} - Obj_{x,i}) / Obj_{x,Base} \quad (9)$$

where, $Obj_{x,Base}$ is the quantity obtained for the optimization objective from Dynamic constraints and $Obj_{x,i}$ is the value of the optimization objective in the i^{th} generation of the optimization.

The GA optimization tries to achieve the highest fitness values. Therefore, this equation is only valid for the objectives where reduction is desirable such as FC and emissions. In case of exhaust temperature that needs to be increased as much as possible, $1 - Fitness$ values can be used.

Figure 4-9 shows the different steps of GA optimization that will be described in further detail now.

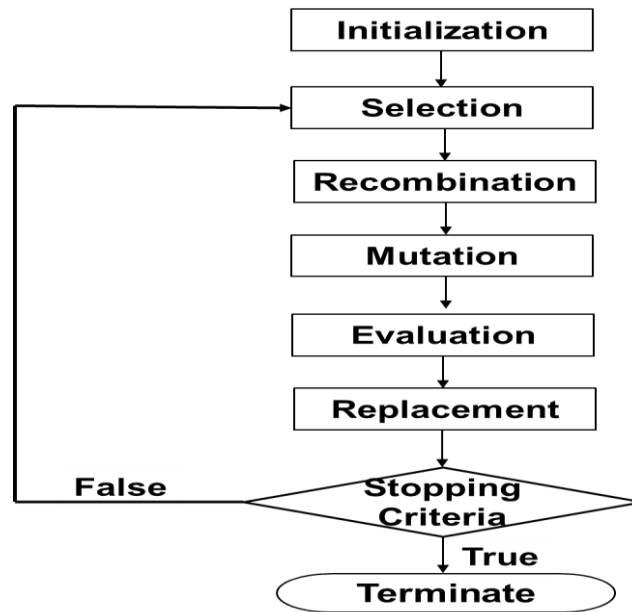


Figure 4-9 Sequence of steps for optimization using genetic algorithm [39]

Initialization

Commonly GA is initialized using a population generated randomly over the complete search domain. However, if the search domain is big, then GA can take long time to converge. In such cases, some intuitive measures, such as the described method of using dynamic constraints, are required to reduce the computational effort and time.

Selection

50 calibrations are selected as parents out of the stored calibrations using a roulette wheel selection method. Roulette wheel method is a standard method for selection and there for it has not been explained here [47].

Recombination

During the recombination stage, some random genes of the parent chromosomes are exchanged, and children chromosomes are generated that usually have a higher fitness value than the parent chromosomes. Various techniques are available for carrying out the recombination operation. In the described optimizer, a uniform crossover technique has been used. In uniform crossover, the swapping probability of each gene is considered separately and is equal to 0.5. Thus, each gene has a 50% chance of being swapped irrespective of what happens to the other genes. In order to carry out recombination operation in a fast manner, a row of random bits is generated that has the same length as that of the chromosome. The

genes are swapped between parents P1 and P2, if the bit corresponds to 0. Otherwise if the bit is 1 the genes are copied as it is to the children chromosomes C1 and C2. An example of recombination using uniform crossover is shown in Figure 4-10.

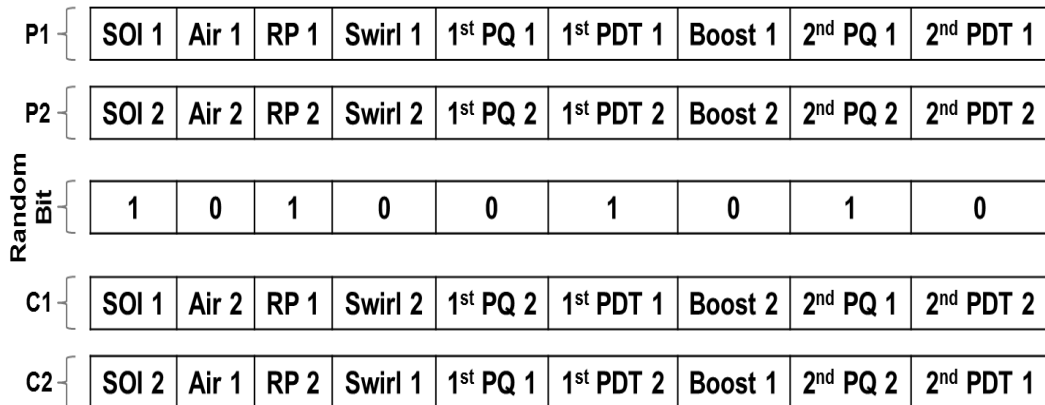


Figure 4-10 Uniform crossover-based recombination technique [39]

Mutation

In order to introduce further randomization in the GA optimization, after every certain number of generations, 10 for the specific case, one of the genes is selected at random and the allele of this gene is replaced with a random value generated across the valid domain.

Evaluation and Replacement

Each chromosome of the new population created using mutation and recombination functions is evaluated for fitness. If there is an increase in fitness without violation of the constraints coming from dynamic constraints definition, the child chromosome is passed on to the next generation. If any of the constraint is violated or if there is no increase in fitness, parent chromosome is copied as it is to the next generation. In this way, an increase of fitness, over a sufficiently large number of generations is ensured, while adhering to the constraints.

As an example, assuming NO_x is the target objective and the rest of the emissions are constraints. If there is a reduction in NO_x without any decrease in exhaust temperature and without any increase in emissions and FC, only then the child chromosome, or calibration, is passed on to the next generation. In this way, NO_x value is lowered after some generations, while the value of other emissions remains the same.

Stopping Criteria

Stopping criteria can be based on a number of generations or convergence to a final solution. For the purpose of this work, in order to achieve a good trade-off between computational time and performance, the GA optimization is run for 200 generations, thus adopting a fixed number of generation criterion. For the

application in discussion, typically GA optimization converges to a single solution within 200 generations. If this does not happen, then the chromosome with the highest fitness is considered as the final solution. In this way, one KP is optimized for a given target objective and constraints. In the next section, the systematic variation of the objectives and constraints in order to obtain the Pareto front is described.

4.1.3 Pareto Front Generation

By systematically varying the dynamic constraints and the optimization objectives during multiple iterations of the SOO optimization, multiple optimized calibrations can be obtained. These multiple optimum calibrations together form a Pareto front. Figure 4-11 shows the flow chart (nested loop structure) for the methodology for carrying out these multiple iterations.

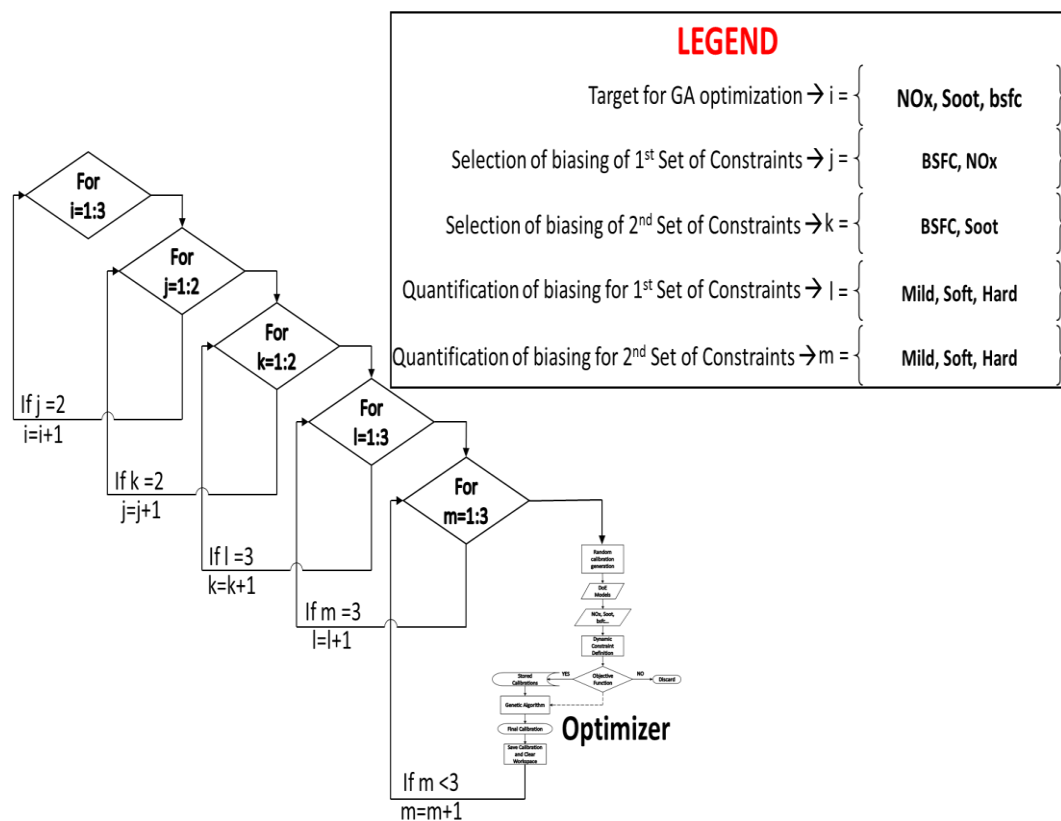


Figure 4-11 Generation of Pareto front using systematic variation of dynamic constraints and optimization objective [39]

In Figure 4-11, i is the variable that determines the optimization objective. As in the work described three optimization objectives are considered, NO_x, Soot and BSFC, i can take values from 1 to 3 representing these objectives respectively. Similarly, variables j and k are responsible for selecting the constraint biasing for BSFC-NO_x (1st set of constraint) and BSFC-soot (2nd set of constraint) respectively. Thus, both j and k can take value of either 1 or 2. For example, if j is equal to 1, then the 1st set of constraint is biased towards BSFC. Variables j and k along with the two sets of constraints have also been described before in Table 4-1. At the same

time, the two variables l and m are used to quantify the bias (Mild, Soft, and Hard) present in the two constraints sets. Thus both l and m can take 3 values. In this way, optimizing all the SOO problems obtained by varying the optimization objectives and constraints according to this nested loop structure, a Pareto front can be obtained.

It should be mentioned here that with the levels of variations in each of the 5 variables, it is possible to obtain 108 different SOO problems ($3 \times 2 \times 2 \times 3 \times 3$). However, it is possible that not all of these optimization problems will result into a solution. In some of the cases, it is possible that the dynamic constraints are too tight and therefore the number of stored calibrations passed on as input to the GA are really less (less than 10). In these cases, the GA optimization is likely to fail. In this work, this problem was repeatedly observed for the case 22. In this case, as both the NO_x and Soot constraints were limited, it was difficult to achieve a sufficiently large initial population. This happened as it is very unlikely to obtain simultaneously low Soot and low NO_x even with a high BSFC. Of course, it was possible to relax the BSFC constraint even further to obtain a higher number of stored calibrations, but it was not considered as practical to increase the constraint more than 50% of the normalized constraint. Considering the feasibility of the constraints, the non-converged SOO problems were ignored. As a result, the number of multiple optimized calibrations obtained for each KP varied in the range of 75 to 100. There is a large variation because the constraints and the possibility to achieve simultaneously low Soot and low NO_x is very much dependent on the operating conditions.

It should also be mentioned here that a single optimization iteration took less than a minute to converge and all the iterations for one KP were finished in about one hour on a machine with 8 GB RAM and Intel i5 2.3 GHz processor.

4.1.4 Results

For the KP (2000 rpm and 5 bar BMEP) in discussion, 75 different calibrations obtained using the iterative procedure described are shown in the form of scatter plots for BSFC-soot and BSFC- NO_x in Figure 4-12 and Figure 4-13 respectively. The calibrations with BSFC as the optimization target are shown in black. The ones optimized for NO_x and soot are shown in blue and pink respectively.

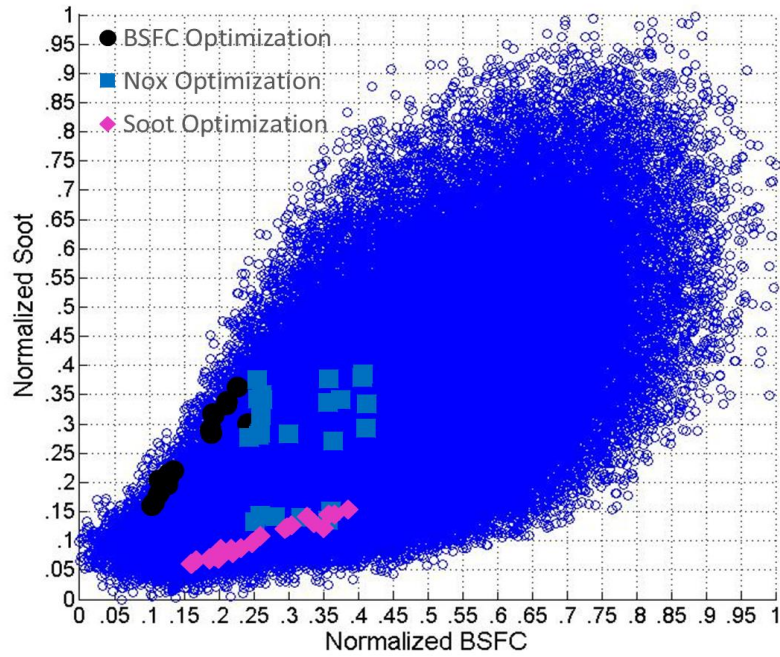


Figure 4-12 BSFC-Soot scatter for optimized calibrations [39]

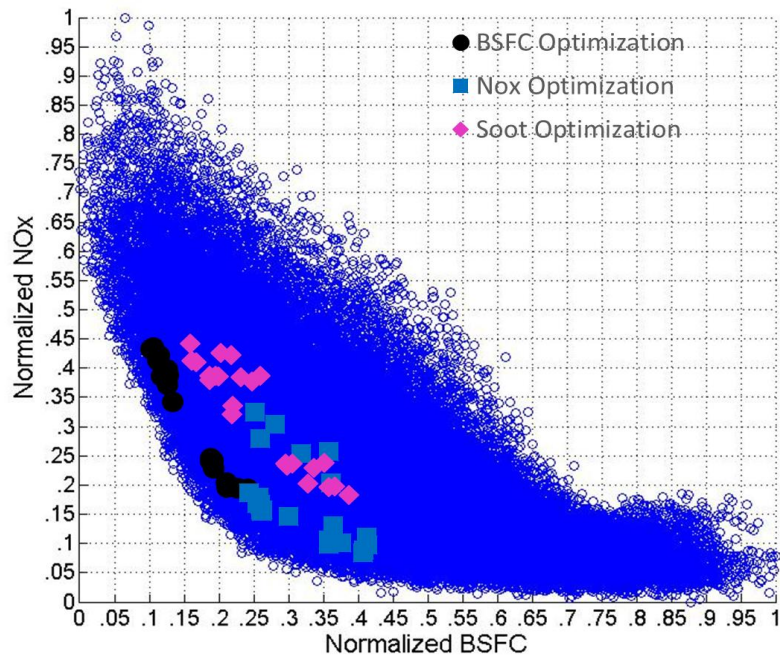


Figure 4-13 BSFC-NO_x scatter for optimized calibrations [39]

In the two figures, the emissions from the optimized calibrations are plotted along with the scatter of the emissions obtained from the random calibrations. This has been done to display the distance between the border of the scatter plots and the optimized calibrations. The border of the scatter plot indicates the most superior Pareto front that can be obtained if the optimization is carried out in absence of any constraints. However, due to application of the constraints, both dynamic and fixed,

a small gap appears between the border and the optimized calibrations, but due to the efficiency of the GA optimization, this gap is minimized. In fact, to show the efficiency of the optimization method, the results achieved have been compared with a calibration carried out using traditional optimization techniques. This optimization is referred as BaseCal in this work.

Before carrying out the comparison, a short description of the method used to generate these calibration maps has been provided here. The empirical models mentioned in the previous chapter were used to optimize the different KPs of BaseCal using a gradient descent method. After the optimization, the calibration maps were generated using interpolation and extrapolation. For the map generation from the KPs, CAGE a quite popular tool (part of Model Based Calibration Toolbox) in MATLAB was used. Following the map generation, manual smoothening procedure was carried out to achieve the desired smoothness level. It should be mentioned here that these calibration maps generated using the traditional methods were already satisfying Euro 6d emissions standards for a C segment car with an approximate curb mass of 1650 kg.

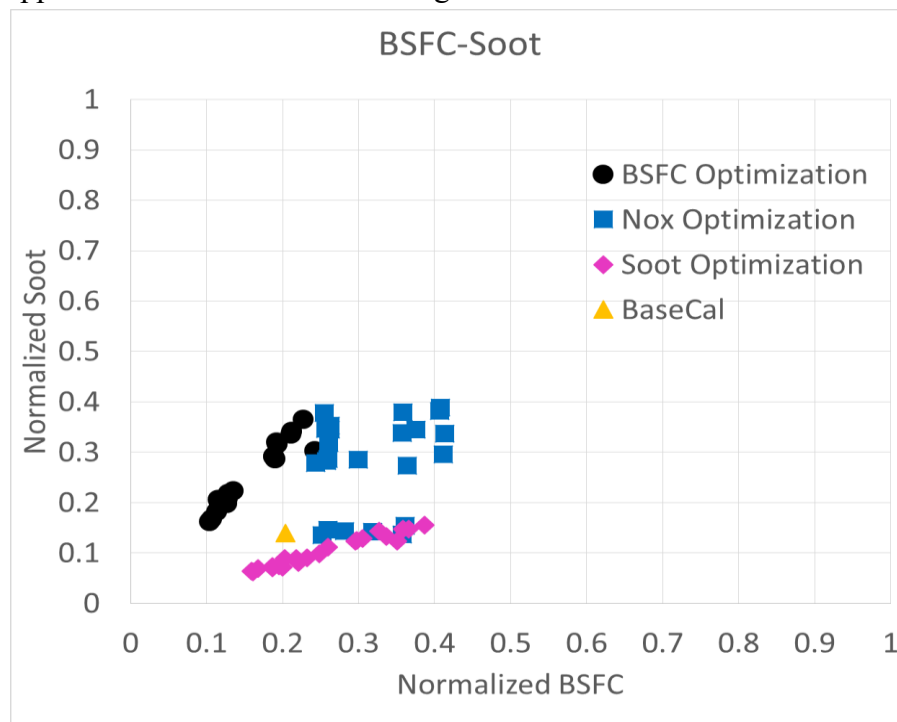


Figure 4-14 BSFC-Soot scatter for optimized calibrations in comparison with a base calibration [39]

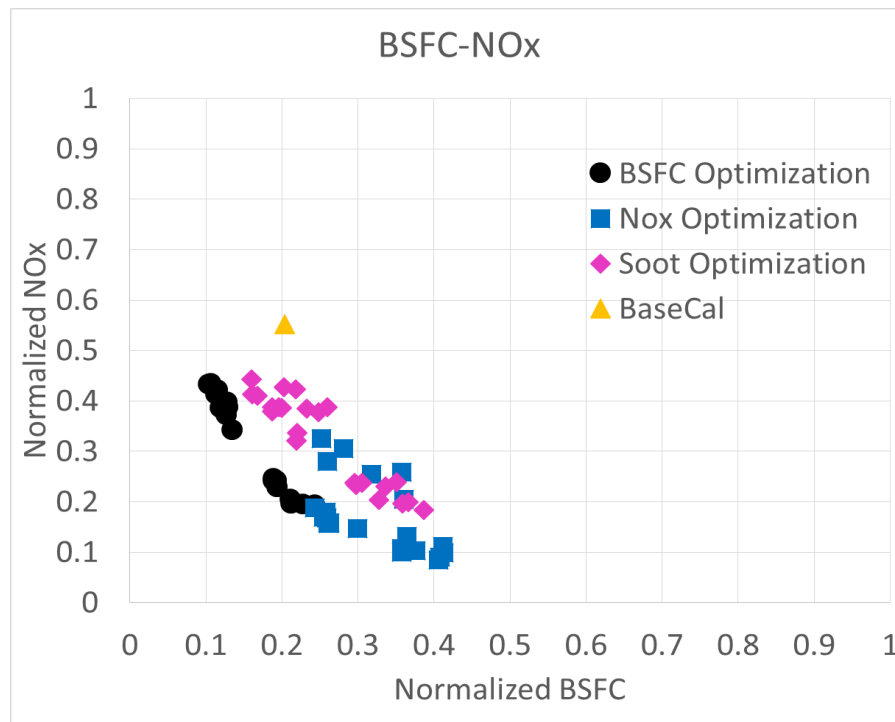


Figure 4-15 BSFC-NO_x scatter for optimized calibrations in comparison with a base calibration [39]

Figure 4-14 and Figure 4-15 shows the comparison between the emissions from the optimized calibrations and the BaseCal. Looking at Figure 4-14, it can be observed that the BaseCal has been optimized for low Soot. It can also be clearly seen from Figure 4-15 that a low NO_x is achieved for all the optimized calibrations even for the cases where the NO_x optimization is not the objective. Furthermore, it can also be clearly noticed that there are multiple calibrations with lower Soot, lower NO_x and lower BSFC than the BaseCal. Moreover, to have a fair comparison, the fixed constraints for the MOO are the taken from the BaseCal. This means that all the calibrations shown in the two figures also have lower CO, HC, CN and higher exhaust temperature than the BaseCal.

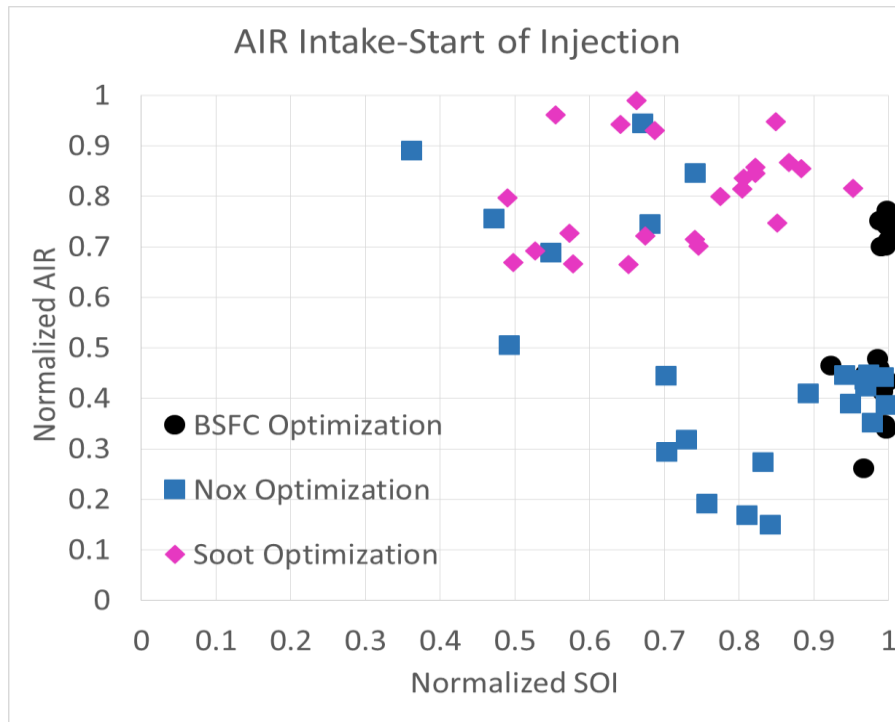


Figure 4-16 SOI-Air scatter of the optimized calibrations [39]

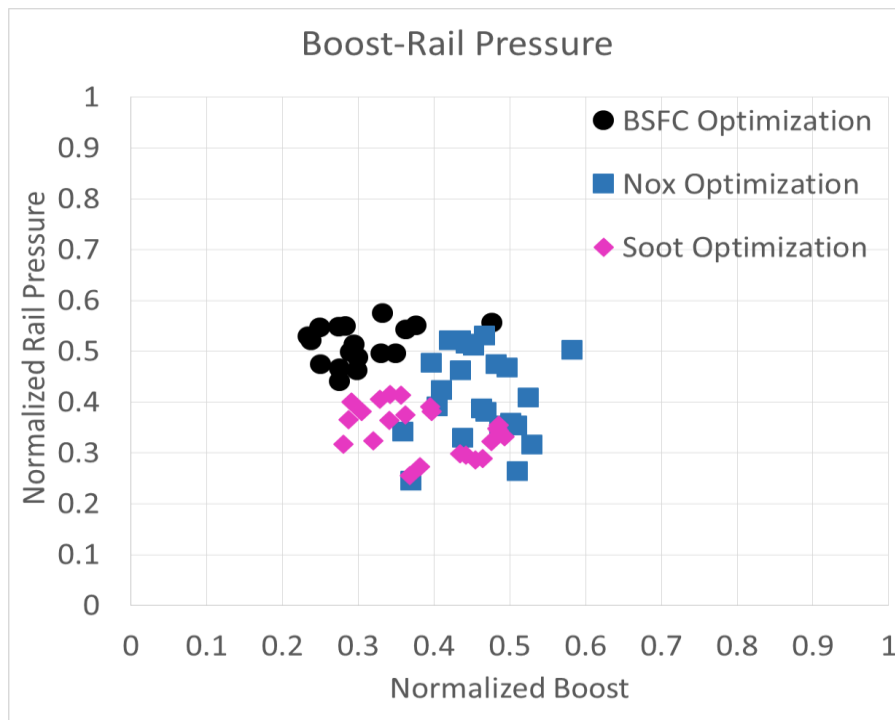


Figure 4-17 Rail pressure-Boost pressure scatter of the optimized calibrations [39]

Figure 4-16 and Figure 4-17 show the distribution of 4 of the 9 control parameters in the model domain. This distribution is shown on normalized scatter plots with 0 referring to the minimum permitted value for the control parameter and 1 referring to the maximum. From these two figures it can be seen that the control parameters are somewhat well distributed in the model domain. Due to this distribution, it is possible to select a calibration with a same or different

optimization target with significantly different input parameters. Therefore, if by selecting one of the optimized calibrations, the resulting calibration maps are not smooth enough, then it is always possible to select another good calibration that can provide better results in terms of smoothness.

The main aim of this work is to develop a one-click methodology that is capable of carrying out an automatic diesel engine calibration optimization while generating sufficiently smooth calibration maps. The first step towards this aim is to have multiple optimum calibrations that are distributed throughout the model domain. Using these multiple optimum calibrations for each KP, an algorithm has been defined that is capable of automatically generating smooth calibration maps using the trade-off between smoothness and performance of the maps. This methodology is defined in chapter 5. However, before going into the details of map generation, a special case of optimization has been considered and explained in the next section.

4.2 Single Objective Optimization with Existing Calibration

It is a quite common scenario in the industry that an existing engine calibration has to be modified slightly to suit a different purpose. This calibration change can be due to the use of same engine with a different EATS architecture or due to the change in homologation cycle or legislation limits (introduction of the same engine in different market). For such cases, it would be a waste of time and money to recalibrate the engine from scratch.

With such scenarios in mind, a small modification of above-mentioned methodology has been proposed in this section to quickly able to generate the new calibration maps capable of achieving the desired target. In the next subsection, the changes with respect to the previously defined method will be highlighted. This will be followed by the results achieved for a typically scenario of reducing NO_x.

4.2.1 Methodology

It should be mentioned here that the existing calibration used for this study is the same as mentioned earlier. Again, calling the existing calibration as BaseCal, the two main premise for developing this method are:

- The BaseCal maps are sufficiently smooth and this smoothness should be preserved at all costs.
- The BaseCal is already optimized. Therefore, the achievement of the desired objective should happen without any deterioration in any emissions, CN and exhaust temperature.

Starting with these two points, a similar method that make use of random calibration generation and GA optimization is described here. The flow chart for the methodology is shown in Figure 4-18. On a closer look, Figure 4-18 looks a reduced form of the workflow given in Figure 4-1. The main difference is, the

dynamic constraint definition module is no longer required as the values of constraints are coming from the BaseCal. Furthermore, there is no module for saving and clearing the workspace, as the case in discussion does not require multiple optimum calibration. Therefore, the iterative approach described in section 4.1.3 is not used here. The remaining methodology is same.

To quickly go through it again, random calibrations are generated in a given domain. These calibrations are then evaluated using the DoE models to give the value of emissions (also CN and exhaust temperature) for each of these generated calibrations. The objective function check stores the calibrations that result in lower target quantity without violating any constraint. These stored calibration serves as an initial population to GA based optimizer that works exactly in the same way as described in section 4.1.2.

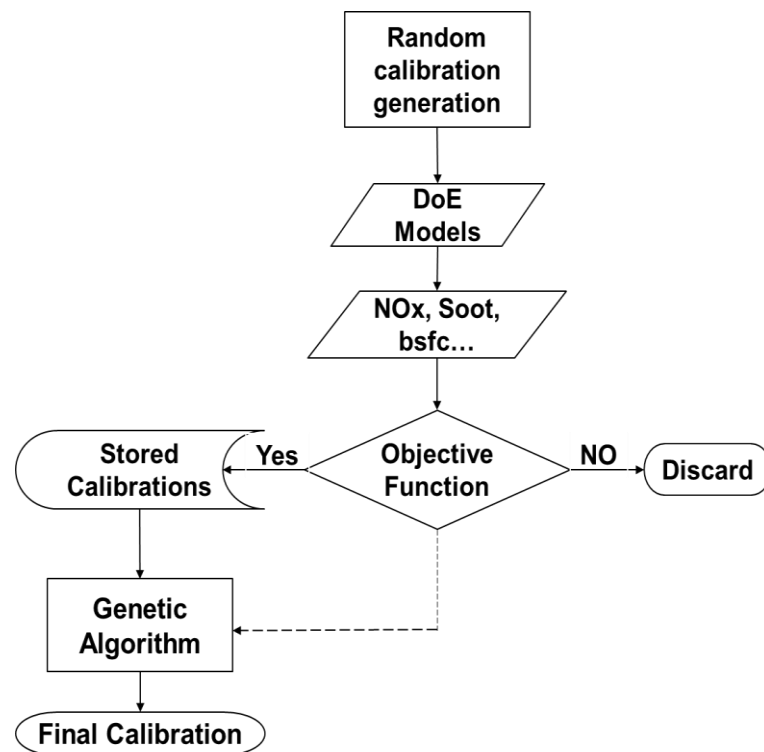


Figure 4-18 Reduced work flow for the single objective optimization methodology with an existing calibration present [39]

However, for preserving the smoothness of the calibration maps, a method needs to be defined. For this purpose, a simple yet novel method is adopted. Since the calibration maps are already smooth, the variation allowed in the control parameter for the purpose of optimization is restricted to a very small value. The range of variation to generate random calibrations from empirical models is reduced to about 10-20% of the original domain. In this way, the empirical models are used to explore only a narrow domain centered around the BaseCal. This reduced domain is shown in the last column of Table 4-2.

Table 4-2 Reduced range of variation for generation of random calibrations in order to preserve the smoothness of the existing calibrations [39]

Parameter Number	Input Quantity	Unit	Range of Variation for Domain	Reduced range of variation
1	SOI	°bTDC	±4	±0.4
2	Air Quantity	mm ³ /stroke	±40	±10
3	Rail Pressure	MPa	±30	±5
4	Swirl level	%	±30	±5
5	1 st Pilot Quantity	mm ³ /stroke	±0.8	±0.2
6	1 st Pilot DT	μs	±500	±100
7	Boost Pressure	kPa	±25	±5
8	2 nd Pilot Quantity	mm ³ /stroke	±0.8	±0.2
9	2 nd Pilot DT	μs	±500	±100

To explain this reduced range of variation more clearly with an example, a SOI map from the BaseCal is shown in Figure 4-19.

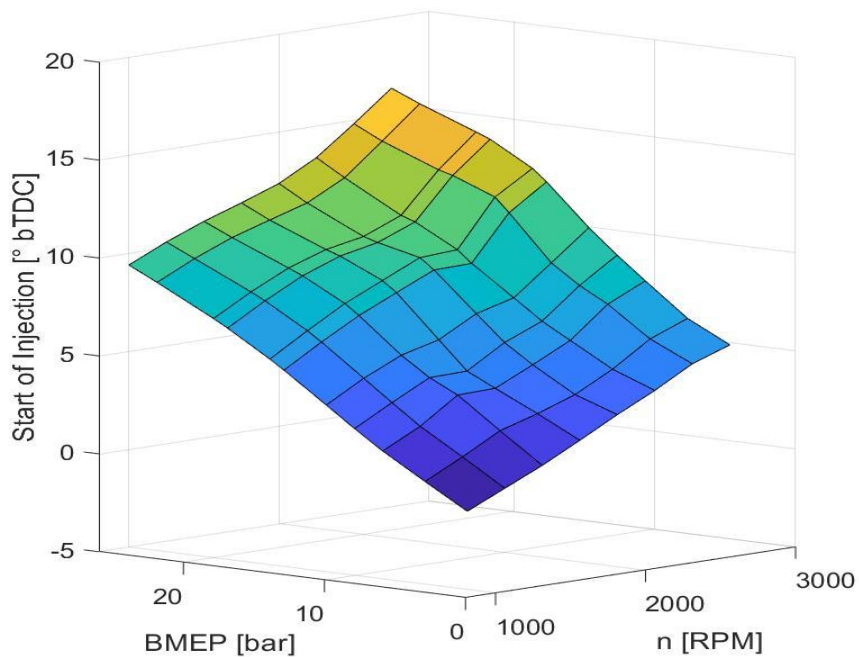


Figure 4-19 SOI map from the base calibration [39]

The reduced range of variation essentially means that there are two surfaces parallel to this SOI map and the value of SOI for the purpose of generation of random calibration and optimization can only exist between these two surfaces. These two surfaces are shown in Figure 4-20. As it can be observed from the Figure 4-20, the two surfaces are quite close to the actual SOI map. Therefore, no matter

how much the SOI values changes during the optimization, the final map generated after the optimization would always retain the smoothness.

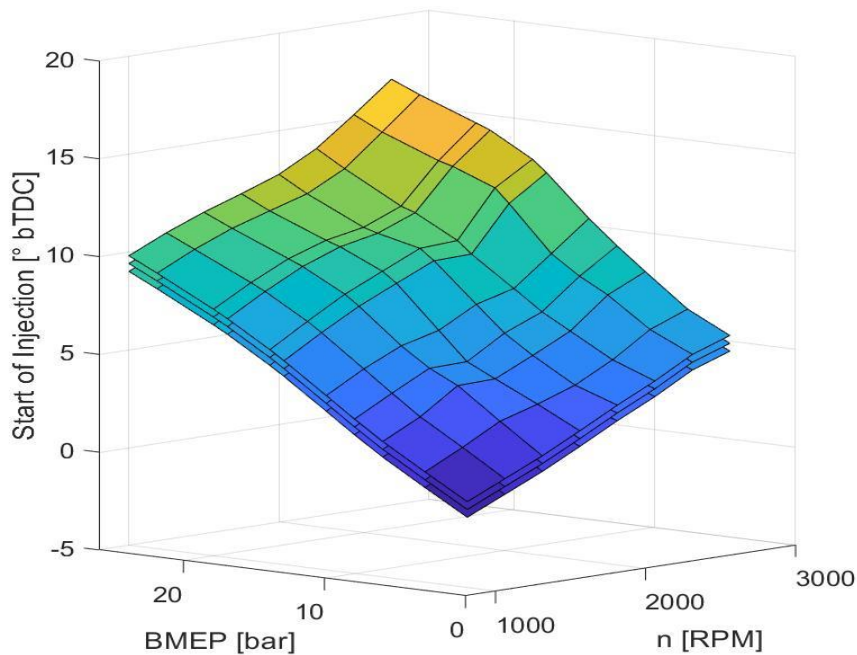


Figure 4-20 Parallel surfaces around the SOI map to preserve the smoothness [39]

It should also be added here that since a much narrow domain is being used in comparison to MOO, the number of random calibrations generated are reduced to 10,000 from 100,000 to increase the speed of optimization.

The advantage of using this methodology is that is very efficient and fast. For one KP, the optimization takes less than a minute using a machine with 8 GB RAM and Intel i5 2.3 GHz processor. Thus, a significant reduction can be achieved in any target quantity for any driving cycle in less than a quarter of an hour. The results from one such optimization to reduce the NO_x from the same engine mentioned earlier have been shown in the next subsection.

4.2.2 Results

In this section, the normalized results achieved for the NO_x reduction for one KP (2000 rpm x 5 bar), when using BaseCal as an existing calibration, have been shown. Figure 4-21 shows the reduction in NO_x over the complete optimization process i.e. 200 generations. It can be clear observed from Figure 4-21 that the optimizer is able to converge to a single optimum solution within the stopping criterion. Also, it can be observed that the GA optimizer NO_x plot is starting from 88% of the calibrated NO_x value. This is because a significant 12% reduction is coming from the initial population generated using random number method as the first step of optimization. The further 7% reduction is achieved due to GA optimizer.

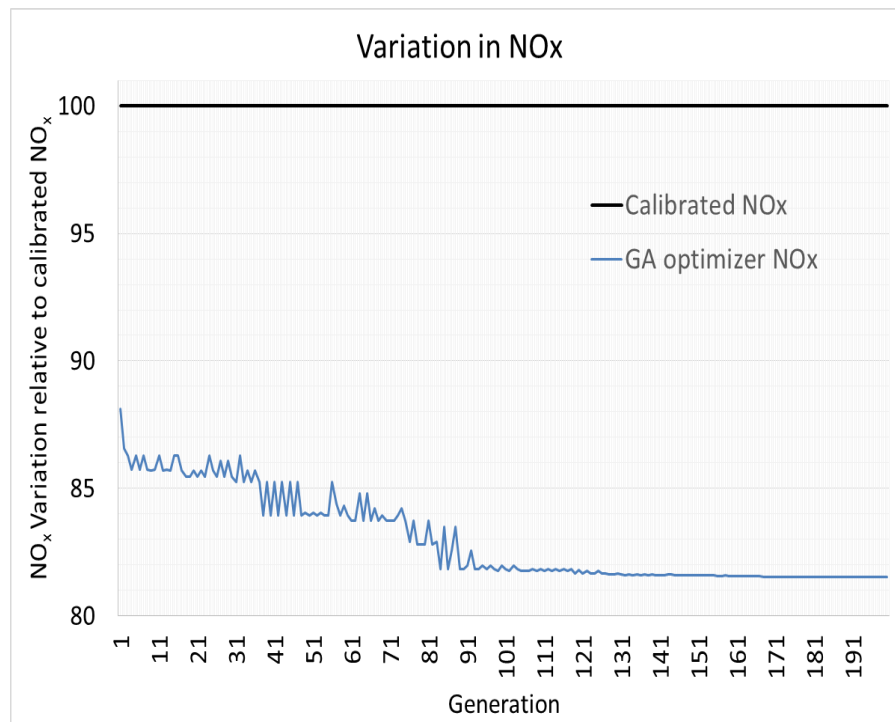


Figure 4-21 NO_x variation in comparison to the base calibration during the complete optimization process [39]

A similar plot highlighting the fitness over the number of generations can be seen in Figure 4-22. It should be pointed out that the Figure 4-21 and Figure 4-22 give the same information but in a different manner. The fitness function is defined in the same manner as mentioned in Equation (9). Therefore, fitness is a direct measure of reduction in NO_x value but presented as a fraction and not as a percentage. Following this, in Figure 4-23 and Figure 4-24, CO and HC variation during the optimization are highlighted. It can be seen from these figures that the constraints are not violated at any point during the optimization. Furthermore, even though CO and HC are not the optimization target, yet an approximate 5% reduction is achieved for these two quantities also. Similarly, in Figure 4-25, Figure 4-26 and Figure 4-27, CN, Soot and BSFC variations have been shown and as expected the values of these quantities are always lower than the constraints.

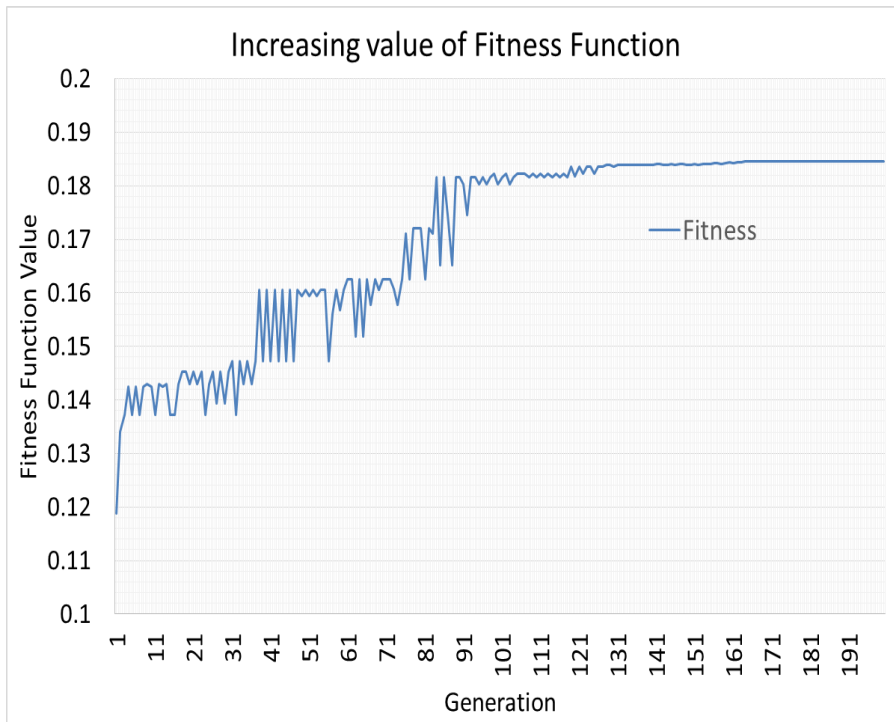


Figure 4-22 Increase of fitness over the complete optimization process [39]

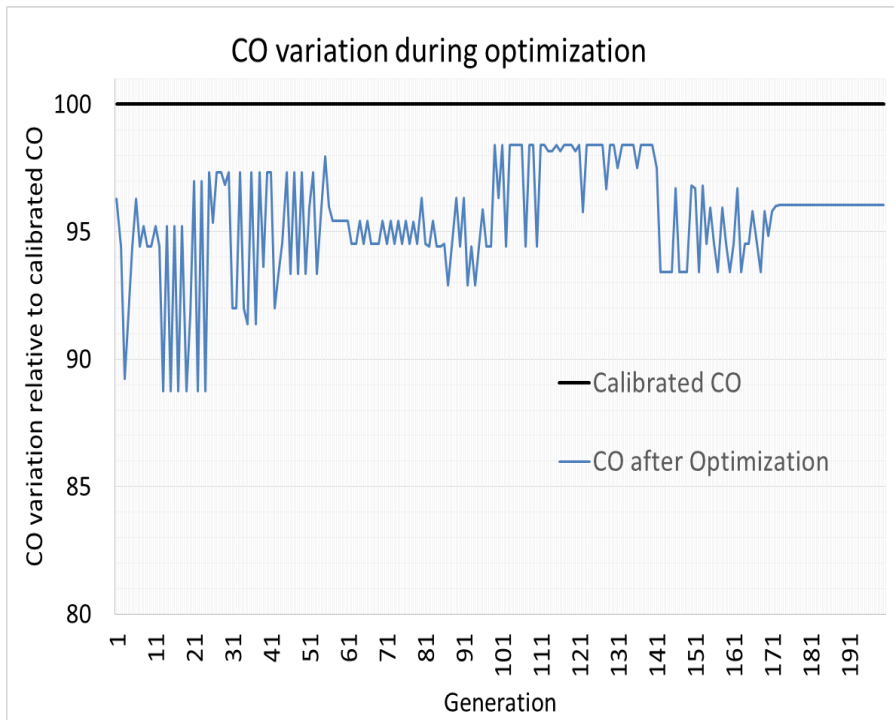


Figure 4-23 CO variation in comparison to the base calibration during the complete optimization process [39]

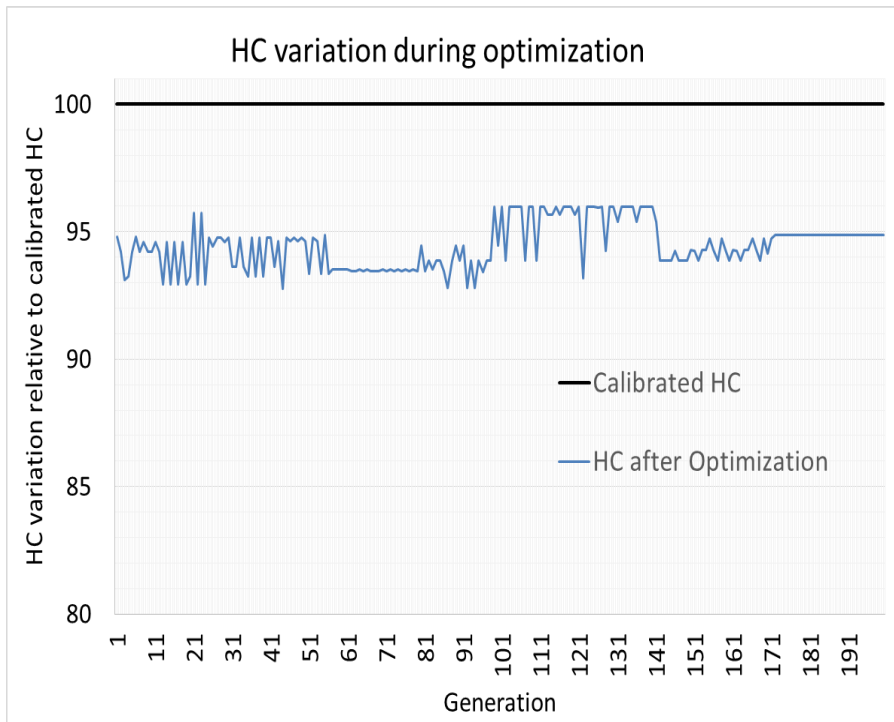


Figure 4-24 HC variation in comparison to the base calibration during the complete optimization process [39]

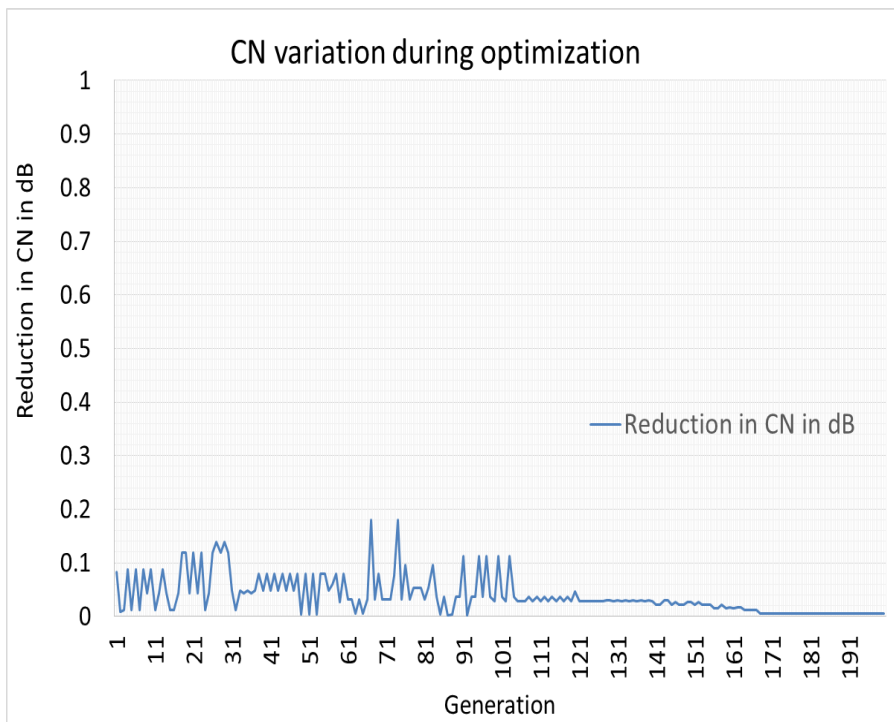


Figure 4-25 CN variation in comparison to the base calibration during the complete optimization process [39]

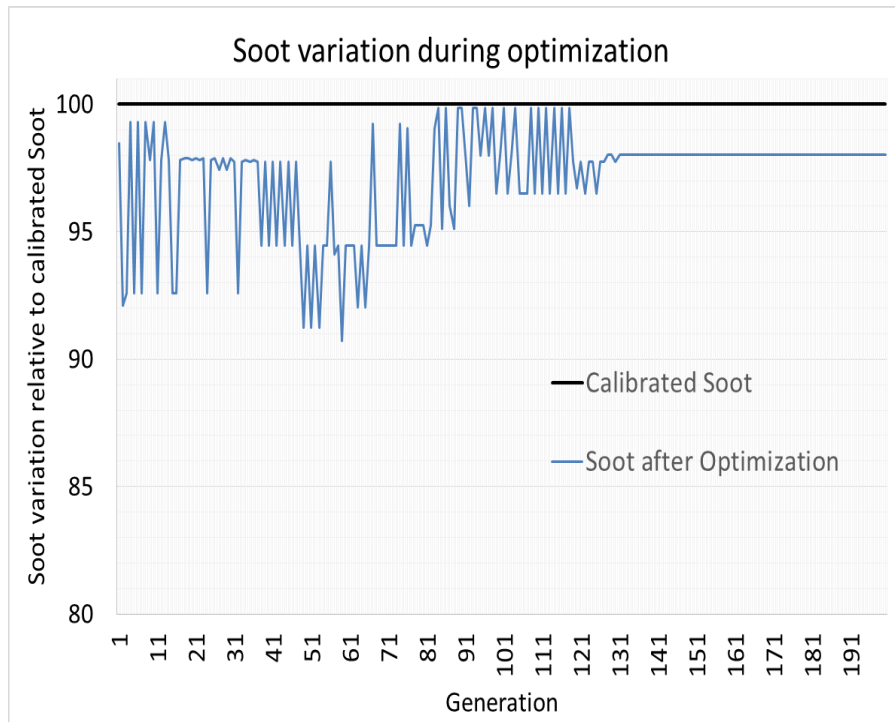


Figure 4-26 Soot variation in comparison to the base calibration during the complete optimization process [39]

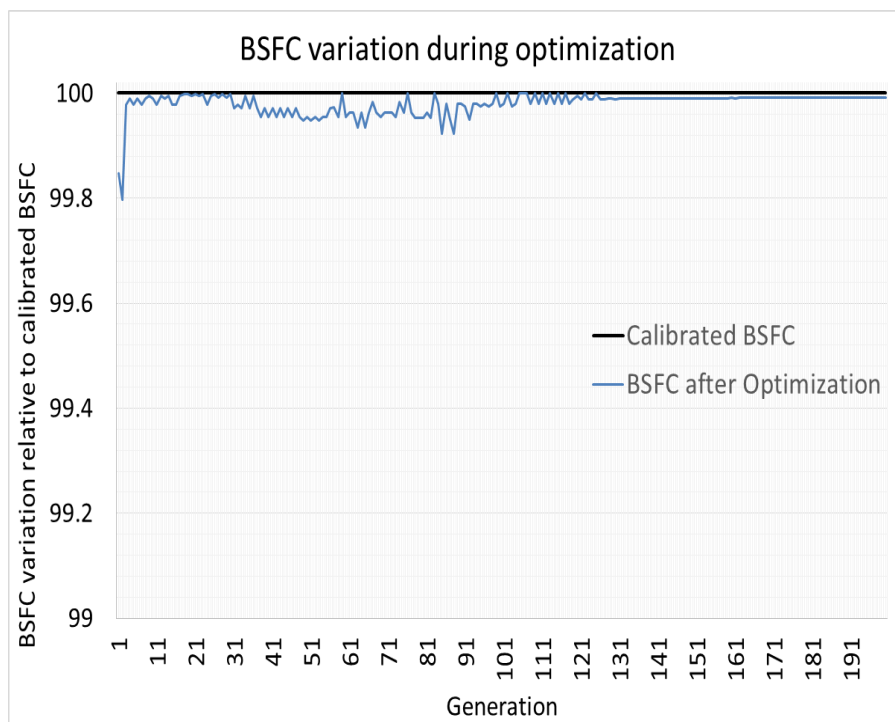


Figure 4-27 BSFC variation in comparison to the base calibration during the complete optimization process [39]

As mentioned earlier, the results shown here are just for one KP. However, to give an idea of the true potential of this methodology, the NO_x reduction achieved for all the KPs is shown in Figure 4-28. It can be clearly observed that over all the KPs an average of roughly 17% reduction is obtained. This reduction is obtained without deteriorating any other emissions and without any loss of smoothness of

existing calibration maps. It should also be added here that a similar reduction can be achieved in other emissions by simply changing the target.

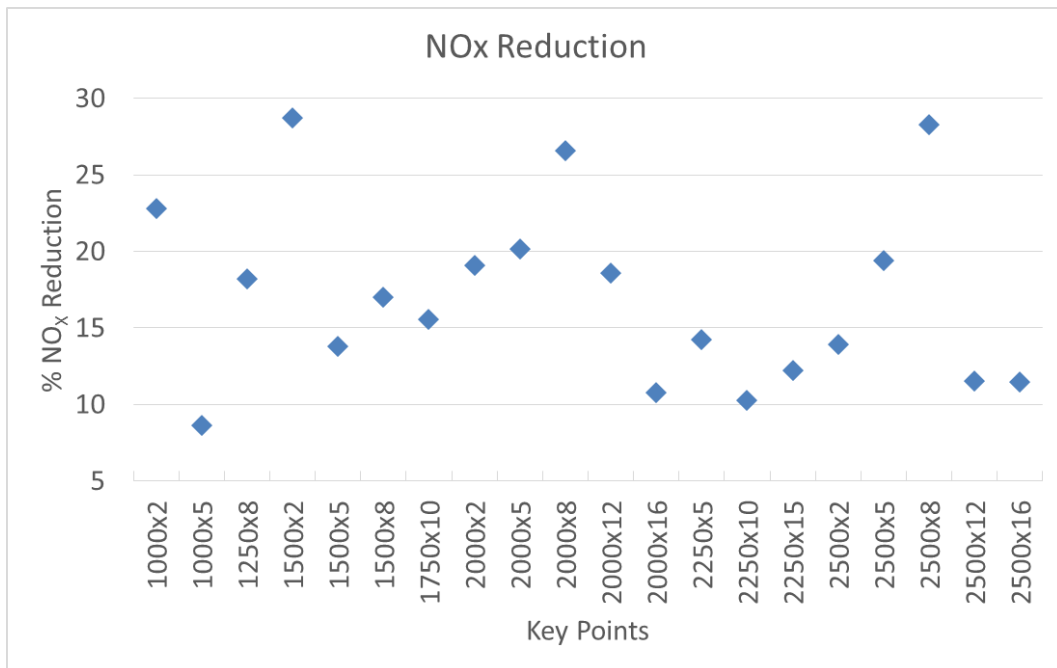


Figure 4-28 Percentage NO_x reduction possible for all the selected key points using the described optimization methodology

For single objective optimization case, it is easy to maintain the smoothness of the existing calibration maps while achieving significant reductions in the target. However since for MOO, the calibration maps are being generated from scratch a dedicated methodology needed to be defined, which has been described in the next chapter.

Chapter 5

Smooth Map Generation

Some parts of this chapter have already been published in the following journal article:

- Arya P, Millo F, Mallamo F. A fully automated smooth calibration generation methodology for optimization of latest generation of automotive diesel engines. *Energy* 2019. doi:10.1016/j.energy.2019.04.122.

As mentioned in the previous chapters, beside the achievement of emission and fuel consumption targets, the smoothness of the calibration maps generated is also very important. The smoothness of the calibration maps affects not only drivability and engine operation, but it also influences the experimental costs and time required for calibration, especially when using local models. Not only manual smoothing can result in loss of optima, but each iteration of manual smoothing may require testing the newly generated maps to check compliance with emissions, thus increasing the experimental time and cost.

Thus, with the aim of reducing the loss of optima associated with the local method and making the calibration procedure automatic and more robust, a methodology to generate smooth calibration maps have been defined in this chapter. This methodology uses the multiple optimum calibrations for each KP, generated as illustrated in the previous chapter, to produce a large number of calibration maps out of which the maps resulting in the desired smoothness and low emissions can be selected.

In the first part of the chapter, a quick introduction of time-based weight calculation has been provided. This time based weighting factor is used to select the three most prominent KPs, using which firstly a single calibration map generation has been described in section 5.2. These large number of calibration maps are generated for different cases according to the smoothness requirement of each control parameter map. These different cases are mentioned in section 5.3, following which an iterative method to generate a large number of calibration maps is described in section 5.4. In the end, a method to evaluate the smoothness and performance of each calibration map is described in section 5.5.

5.1 Time-Based Weight Calculation

Time based weight for each KP is calculated using the exact same approach described in Chapter 2. Clustering algorithms like nearest neighbor algorithm is

used to associate each operating point to the nearest KP. This is shown again in Figure 5-1 which is the same figure as shown in Chapter 2. The ratio of number of associated operating points with each KP to the total number of operating points (1800 for WTLC) gives the weight of each KP. The weights of 20 different KPs in decreasing order are given in Table 5-1.

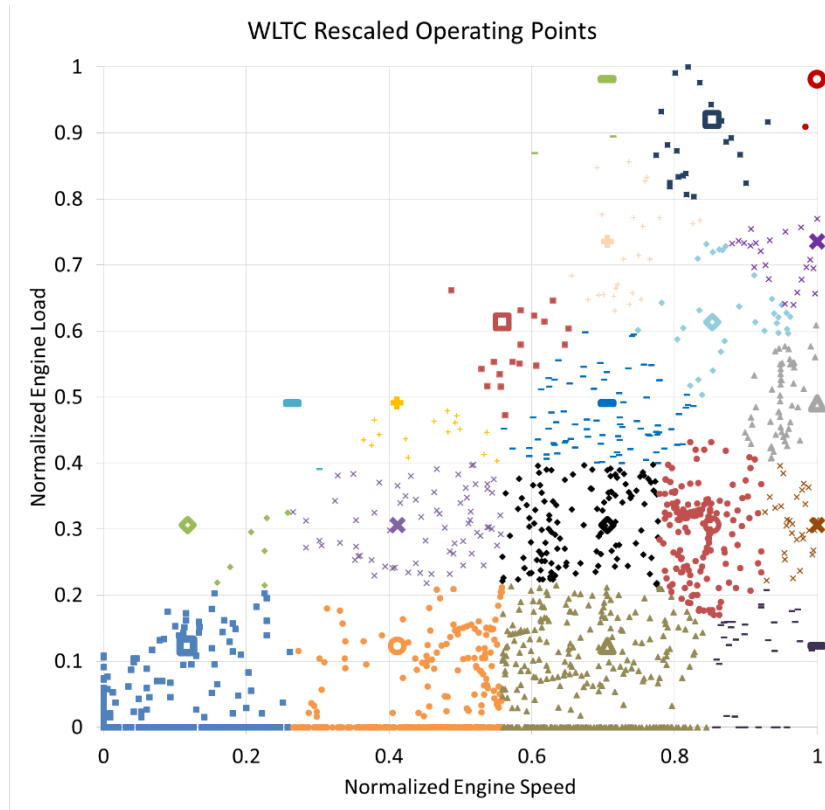


Figure 5-1 Time based weight evaluation of each point using a clustering algorithm [48]

Table 5-1 Time based weight of each key point in a decreasing order

KP #	RPM	BMEP	Weight	Normalized Engine Speed	Normalized Load
4	1000	2	22.90	0.12	0.12
1	2000	2	19.22	0.71	0.12
2	1500	2	15.95	0.41	0.12
3	2250	5	12.10	0.85	0.31
5	2000	5	6.89	0.71	0.31
6	2000	8	4.61	0.71	0.49
7	1500	5	3.83	0.41	0.31
8	2500	8	3.11	1.00	0.49
9	2500	2	1.89	1.00	0.12
10	2250	10	1.76	0.85	0.61
11	2500	5	1.61	1.00	0.31
12	2000	12	1.32	0.71	0.71
13	2500	12	1.21	1.00	0.71
14	2250	15	1.15	0.85	0.92
15	1750	10	0.93	0.56	0.61

16	1500	8	0.92	0.41	0.49
17	1000	5	0.38	0.12	0.31
18	2000	16	0.11	0.71	0.98
19	1250	8	0.06	0.26	0.49
20	2500	16	0.05	1.00	0.98

Out of these multiple KPs, three most weighted KPs are selected and a plane is generated for each control parameter. Using these planes, the maps for each control parameter are then further calculated. This plane generation and map creation is described in the next section 5.2.

It should be pointed out here that the three selected KPs are 2000 rpm x 2 bar (KP1), 1500 rpm x 2bar (KP2), and 2250 rpm x 5 bar (KP3). The first KP in the table, 1000 rpm x 2 bar, is not selected because of two reasons. Firstly, as the idea is to generate a plane, a minimum of three non-collinear points are required for this. If the first three KPs are selected, then there is no variation in the engine load and all the three KPs lie in a straight line. Thus, a plane cannot be generated using the first three KPs. Secondly and more importantly, 13% of the weightage of 1000 rpm x 2 bar KP is due to the stop phase of the vehicle, which for the simplification of the KP weighting strategy have been considered as 800 rpm and 0 bar load (idle condition). So there are over 230 points overlapping at (0,0) position in the Figure. This reduces the effective weight of this KP to less than 10% and therefore less than all the three selected KPs. It is for this reason also that the 1000 rpm x 2 bar KP is labelled as #4 in Table 5-1.

In addition, other strategies like start and stop and fuel cut off have not been considered while calculating the effective weight of the KPs, but it can be taken into account. In that case, the weights of KPs will change and some other KPs than the chosen 3 will be selected.

5.2 Calibration Map Generation

The three most weighted KPs are selected as a minimum of three non-collinear points are required to generate a plane and a plane is the smoothest calibration map that can be obtained. Thus, for a moment, if we forget about the rest of the 20 KPs and use these planes for different control parameters as the calibrations maps, then the loss of optima is already minimized to some extent. As the planes are generated using the optimum calibrations for the three most weighted KPs, together which have a combined weight of roughly 50%, these planes can provide quite good results. Of course, this is a very rough estimation and may not be entirely correct, but the main takeaway is that these planes are already a good starting point to generate the calibration maps. Furthermore, this level of smoothness of maps is not required and therefore is useless. Therefore, now considering the remaining 17 KPs, an intuitive and simple methodology will be defined to create a calibration map from these planes.

Considering that out of the large number of multiple optimum calibrations for each KP, the first one is selected for the three most prominent KP and a plane is

generated for each control parameter. These generated planes are a function of engine load (*BMEP*) and engine speed (*n*). Mathematically these can be described as:

$$z_i = a * n + b * BMEP + c ; i = 1:m \quad (10)$$

Where z_i represents the value for i^{th} control parameter (in the same order as mentioned in chapter 3 and chapter 4), a, b, c are constants and m represents the number of control parameters (9 in this case).

One such plane for SOI (z_1) is displayed as an example in Figure 5-2.

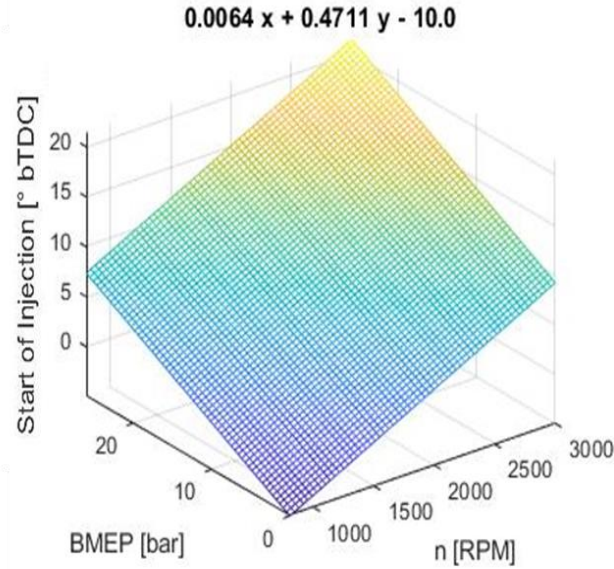


Figure 5-2 SOI plane shown as an example of the map generation method [48]

It should be reminded here that for each of the KPs, there are large number of optimum calibrations present generated using the methodology defined in the previous chapter. Out of these large number of calibrations, it is possible to choose any value for SOI for the remaining KPs. However, in order to minimize the distortion of the above shown surface, the value of SOI closest to the plane is selected for the remaining 17 KPs. Mathematically, for i^{th} control parameter, the distance of each of the optimum value from the generated plane can be calculated using Equation (11):

$$\delta z_i^{KP} = |z_{i,eq}^{KP} - z_{i,opt cal}^{KP}| ; z_{i,opt cal}^{KP} \in Opt cal^{KP} ; KP = 1:20 \quad (11)$$

Where δz_i^{KP} is a distance vector for i^{th} control parameter one particular KP.

Thus δz_1^4 is a vector contains the distance of each of the SOI value (from multiple optimum calibrations) from z_1 plane for the KP 1000 rpm x 2 bar. Therefore, for each KP, the minimum value from the vector δz_1^{KP} can be selected to generate a really smooth map. The closest value selected to the SOI plane for the remaining 17 KPs is shown in Figure 5-3 and the consequent map generated using these values is shown in Figure 5-4.

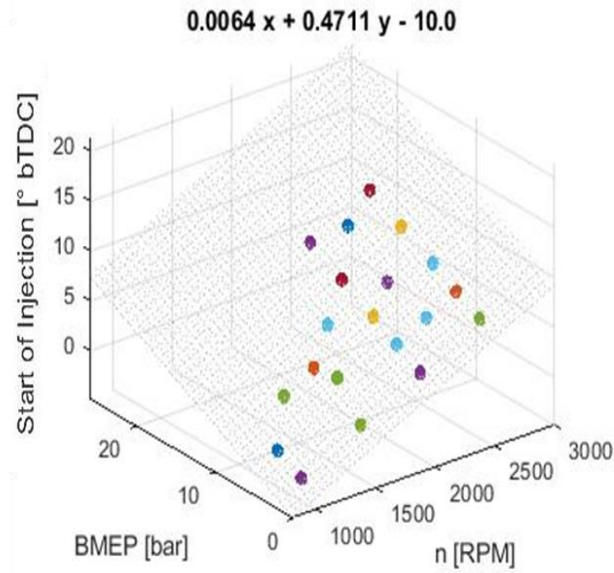


Figure 5-3 SOI value closest to the generated plane for the remaining 17 key points [48]

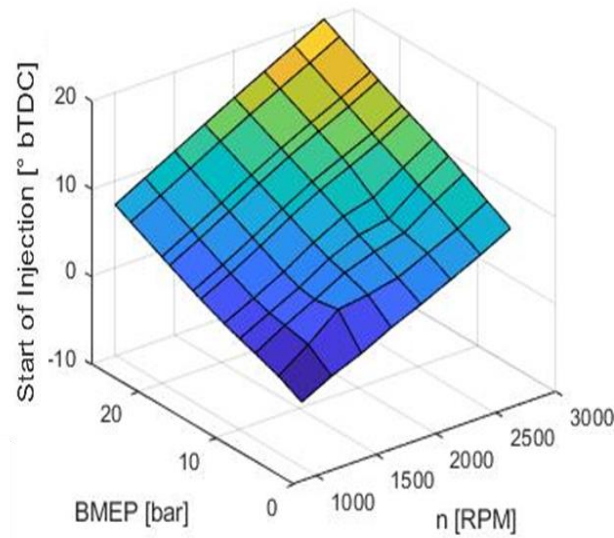


Figure 5-4 SOI map generated using multiple optimum calibrations and SOI plane [48]

However, a calibration is a set of values for different control parameters and these values are only valid when used together as a set. Therefore, if a calibration is selected in such a way that it gives smooth SOI maps, then it is a possibility that for rest of the control parameters the maps may not be smooth. In order to avoid this, the smoothness of different control parameters is considered simultaneously using Equation (12):

$$Target = \min(\sum_{i=1}^m w_i \times norm(\delta z_i^{KP})) \quad (12)$$

where w_i represents the smoothness weight of the i^{th} control parameter.

Equation (12) means that the weighted sum of the deformations for the different control parameter surfaces is to be minimized. Parameter weights have been introduced here as some control parameter maps need to be smoother than others.

As it can be understood from Equation (12), a higher control parameter weight will result in a smoother map. Moreover, it can also be seen in equation that the normalized values have been used for the distance vectors. This is because the range of values that each control parameter takes is quite different. For example, recalling from the Chapter 3, the variation in SOI for each KP is $\pm 4^\circ$, whereas for Airflow this variation is of the order ± 40 mm³/stroke. This means that the distance vector for SOI (δz_1^{KP}) would be quite lower in magnitude in comparison to distance vector of Airflow (δz_2^{KP}). To avoid this, the distance vectors are normalized in the range of 0-1.

Equation (12) should result in sufficiently smooth maps for all the control parameters. However, it requires the information regarding the smoothness weight for each control parameter (w_i), the selection for which is defined in the next section.

5.3 Smoothness Weight Settings

As mentioned before, not all the control parameters map require the same level of smoothness, and therefore, these weights should be selected carefully. Moreover, not every control parameter is active in the complete engine operating range. Out of the 9 control parameters mentioned previously, only 6 are active for the complete engine operating range. The three partially active control parameters are Boost Pressure, 2nd Pilot Quantity and Dwell Time. Due to this partially active behavior of these control parameters, a different smoothness requirement is imposed on these parameters. In fact, the maps generated for these control parameters are required to be smooth in only a limited area of engine operation.

Furthermore, it is quite common in the automotive industry to utilize the same engine in a variety of vehicles to cut down on the development cost and time of the new vehicles. To put it simply, one engine can be readily equipped, with some minor changes, in a family car, in a sporty vehicle or in a pick van. It is quite often that the minor changes that permits such a diversified usage of the same engine are related to the modification of the engine calibration. Depending on the calibration, an engine with a same displacement is able to provide different peak torque and peak power. These calibration changes are necessary because of different mission profiles for different vehicles. As an example, in a sports vehicle there is an immediate response to a very small change in accelerator pedal position, on the other hand for a family car, the response is milder. Moreover, the calibration changes because of different mission profiles means different calibration maps need to fulfill different smoothness requirements. In addition, this difference in calibration can also result in tightening of the desired smoothness for a particular control parameter and slackening for another one. Therefore, the smoothness weight for each control parameter (w_i), can change a lot depending on the mission profile and application of the engine.

However, the more difficult part is to anticipate the smoothness weights for different control parameters. Depending on the variation of control parameters throughout the engine map, some control parameter maps might be inherently

smooth. Due to this difficulty in anticipating the smoothness weight setting for the control parameters, a small number of different weight settings are evaluated. Table 5-2 shows the five different weights settings (or referred to as cases from now on) used for the 6 different control parameters. As it is clear from Table 5-2, only the 6 parameters that are active for the complete engine operation are considered. Moreover, the weights for three parameters, swirl, 1st pilot quantity and 1st pilot DT, are kept low in all the 5 different cases. This is because for the application in consideration in this study, these maps of these parameters are not very critical from the smoothness point of view.

Table 5-2 Different cases for smoothness weight settings of different control parameters [48]

Weight Setting	Parameter	SOI Weight	Injection Pressure Weight	Air Flow Weight	1 st Pilot Quantity Weight	1 st Pilot Dwell Time Weight	Swirl Weight	$\sum_{i=1}^m w_i$
Case 1		0.5	0.2	0.1	0.067	0.067	0.067	1
Case 2		0.3	0.2	0.2	0.1	0.1	0.1	1
Case 3		0.2	0.2	0.3	0.1	0.1	0.1	1
Case 4		0.077	0.154	0.538	0.077	0.077	0.077	1
Case 5		0.167	0.167	0.167	0.167	0.167	0.167	1

Up to this point, the method for generating calibration maps using the calibration from three most prominent KPs and parameter smoothness weight have been defined. However, as it has been mentioned earlier, there are large number of optimum calibrations for each KP. For each of the three selected KPs (referred to as KP1, KP2 and KP3), there are more than 80 optimum calibrations. In the section 5.2, the calibration map generation was illustrated using the first calibration of each of these three KPs. However, if a different calibration for any of these KPs is selected then the shape of the maps, the smoothness, the emissions, everything will change. Using this idea, an iterative approach for generation of large number of calibration maps is defined in the next section.

5.4 Multiple Calibration Maps Generation

The advantage of generating a calibration map by selecting the nearest optimum calibration from the plane for each KP is that the smoothness and performance are already ensured to some extent. However, this approach along is not sufficient to achieve the required targets for performance and smoothness. Therefore, the before mentioned approach is combined with an iterative method to optimize the performance while maintaining the smoothness. Each combination of the optimum calibration from three most weighted KP gives a different set of calibration maps, as it results in a different set of planes for each control parameter. If there are more than 80 optimum calibrations for each of the three KPs, that gives more than half a

million combination ($80 * 80 * 80$). Furthermore, there are 5 cases of smoothness weight settings that can increase the number of combinations to over 2.5 million. Now the intention is to generate more than 2.5 million sets of calibration maps (each set has 6 control parameter maps mentioned in Table 5-2) using the systematic variation of the selected calibration for the three KPs and the smoothness weight settings. Out of these large number of calibration maps, the ones optimizing the performance and providing a sufficient level of smoothness can be selected. This is more clearly explained with the help of a flow chart (nested loop structure) shown in Figure 5-5.

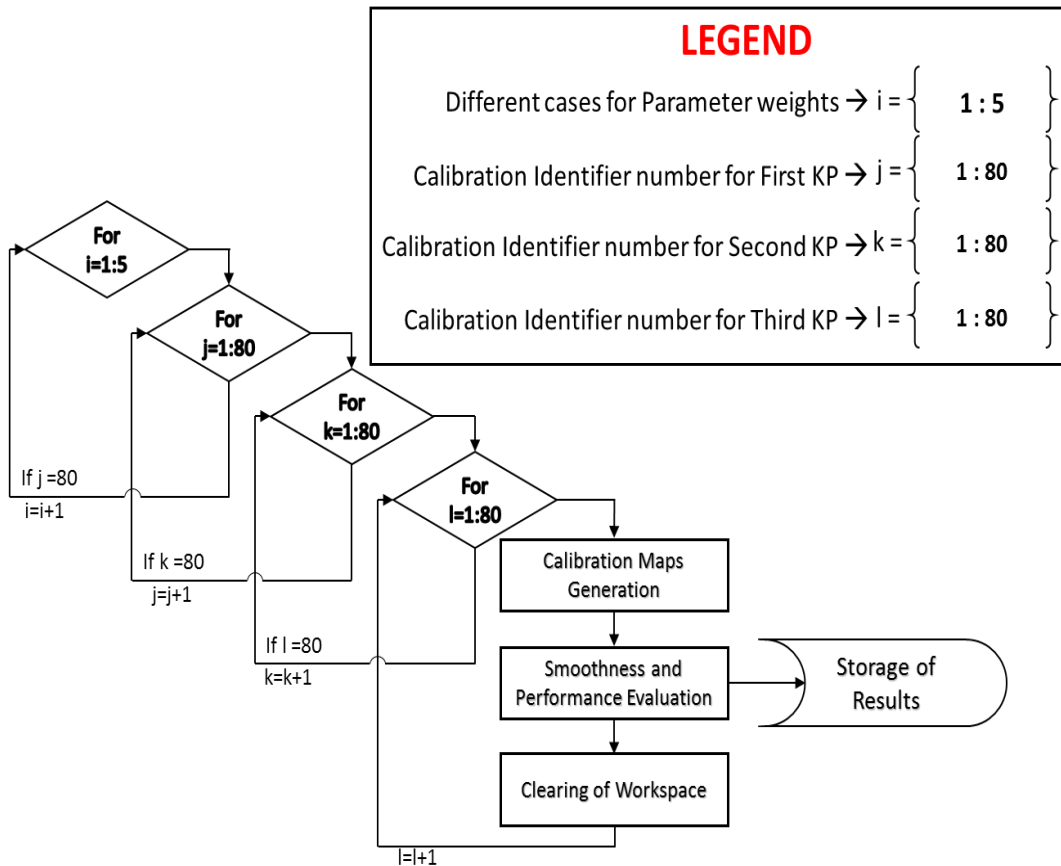


Figure 5-5 Iterative methodology using nested loop structure to generate a large number of calibration maps [48]

In Figure 5-5, i represents the different cases of smoothness weight settings and therefore can take the value from 1 to 5, representing the 1st to 5th case shown in Table 5-2 respectively. The selected optimum calibration for KP1 is represented by j . In a similar manner, k and l represents the selected optimum calibration for KP2 and KP3 respectively. In this way, more than 2.5 million sets of calibrations maps are generated and stored in the memory. These maps are evaluated using suitable and fast criteria for smoothness and performance that is defined in the next section 5.5. The benefit of having such a large number of calibration maps is that a trade-off can be obtained between smoothness and performance. In this way, for every desired level of smoothness, the calibration map resulting in minimum emissions can be selected.

5.5 Calibration Evaluation

In order to select the best calibration maps out of these large number of maps, it is necessary to evaluate the smoothness and performance of each map. Therefore, some criteria need to be defined according to which these generated maps can be assessed. In addition, since the number of maps generated is quite large, the evaluation criteria has to be fast to evaluate. In this section, a smoothness evaluation criterion has been described that is followed by a description of performance evaluation criterion.

5.5.1 Smoothness Evaluation

The idea of surface smoothness is quite commonly used in Computer Aided Design (CAD). In the literature many methods can be found for evaluating the smoothness of any given surface. If the calibration maps can be considered as regular surfaces, then their smoothness can be calculated in a similar way. Building on this idea, in this work one such method that utilizes Gaussian curvature to quantify the smoothness of any given surface has been used [49].

The value of Gaussian curvature K for a point (a, b) on any given surface is calculated as:

$$K = \frac{f_{xx}(a, b) \times f_{yy}(a, b) - f_{xy}(a, b)^2}{(f_x(a, b)^2 + f_y(a, b)^2 + 1)^2} \quad (13)$$

It is understandable from the Equation (13) that Gaussian curvature method utilizes the first order and second order differential to calculate the smoothness at any given point. An overall measure of the smoothness for a complete map can be calculated by summing up the square of Gaussian curvature obtained at each point of the map. This is shown in Equation (14):

$$E_K = \sum_{x=1}^X \sum_{y=1}^Y K_{x,y}^2 ; \quad XY = \text{grid of Map}(n, BMEP) \quad (14)$$

In the literature E_K is defined as the normalized curvature energy [50]. The normalized curvature energy gets smaller and smaller as the map becomes smoother. In fact, for a plane, the value of Gaussian curvature is zero at all the points (second order differentials at all the points are zero). Therefore, as mentioned earlier and now proved mathematically, a plane is the smoothest map that can be obtained with a normalized curvature energy corresponding to zero. It should be added here that as the different control parameters are varied in different range of values, it is better to perform the energy calculation for normalized maps (0-1). This normalization of maps makes it possible to have a comparison of smoothness between the different control parameters maps.

5.5.2 Performance Evaluation

The performance evaluation of the set of calibration maps is carried out using the cumulative NO_x and soot emissions and fuel consumption over the driving cycle. Since performance of many calibration maps need to be evaluated, a fast method is required. Therefore, the engine out NO_x and Soot emissions are used for comparison and in this way EATS simulation is avoided.

Chapter 6

Results and discussion

Some parts of this chapter have already been published in the following journal article:

- Arya P, Millo F, Mallamo F. A fully automated smooth calibration generation methodology for optimization of latest generation of automotive diesel engines. Energy 2019. doi:10.1016/j.energy.2019.04.122.

In this chapter, the results of the smoothness and performance evaluation for the generated calibration map sets are shown and discussed. Of course, it is not possible to show the 2.5 million sets. Therefore, in the first section of the chapter, the smoothness and performance for each case of smoothness weight setting, averaged over half a million calibration sets included in each case, have been shown. Furthermore, due to the large number of calibration maps in each case, there is a high variance in results. This high variance signifies that some calibration maps lead to really low emissions but can be really bad from the perspective of smoothness and vice versa. Due to this high variance, it is better to highlight the averaged results. However, it is also important to present and compare some of the individual sets of calibration maps to provide a better overview of the achieved results. Therefore, in section 6.2, performance and smoothness of some shortlisted calibrations have been shown and compared with the existing calibration, referred to as BaseCal in the earlier chapters. It should be mentioned here again that even though the BaseCal have been optimized using traditional methods, it is capable of meeting Euro 6d emission target and therefore serves as a fair point of comparison.

6.1 Case Wise Comparison of Average Smoothness and Performance

As the smoothness, calculated using normalized curvature energy E_K , have been averaged over half a million calibration sets present in each case, each of the 6 control parameter mentioned in Table has one averaged value for E_K for each case. This averaged E_K value for two of the control parameters, SOI and air flow, along with the smoothness weight value of each case for these parameters are shown in Figure 6-1 and Figure 6-2. Also, as a point for comparison, the E_K value for the BaseCal SOI and air flow map have been shown in these figures. Only 2 of the 6

parameters are shown here as these two are the most crucial from the smoothness point of view for the case in discussion.

As it is expected and can be observed from Figure 6-1 and Figure 6-2, the average values for E_K increases as the values of the weight decreases. Again, the lower the E_K , smoother are the maps. Also, in all the results shown in this chapter, $\log_{10}(E_K)$ has been used as the y-axis. This means, the bigger is the bar in a plot, lower is the E_K and therefore smoother is the map.

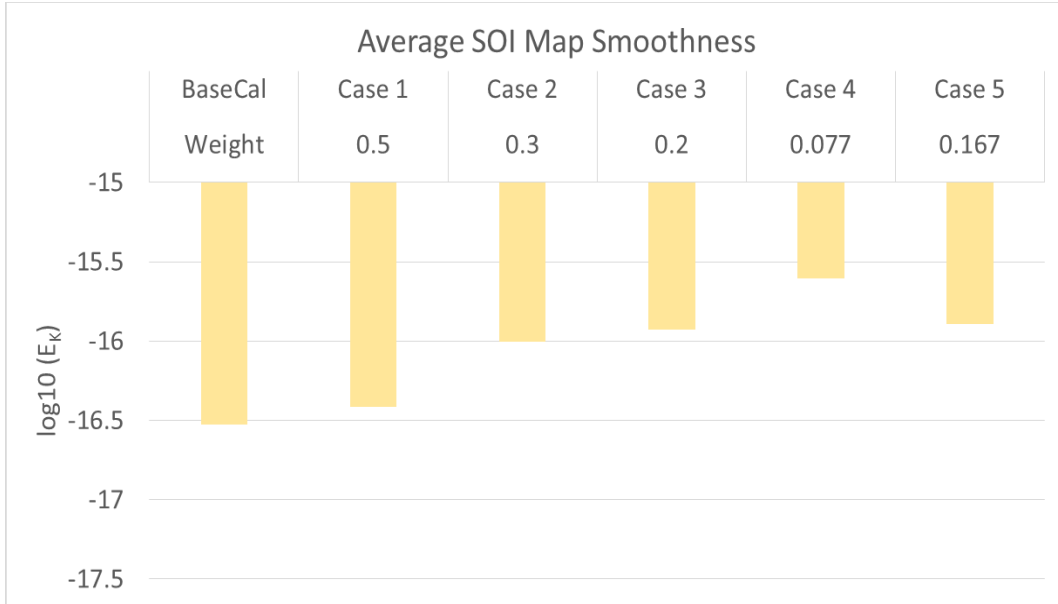


Figure 6-1 Average SOI map smoothness for the five different parameter weight settings [48]

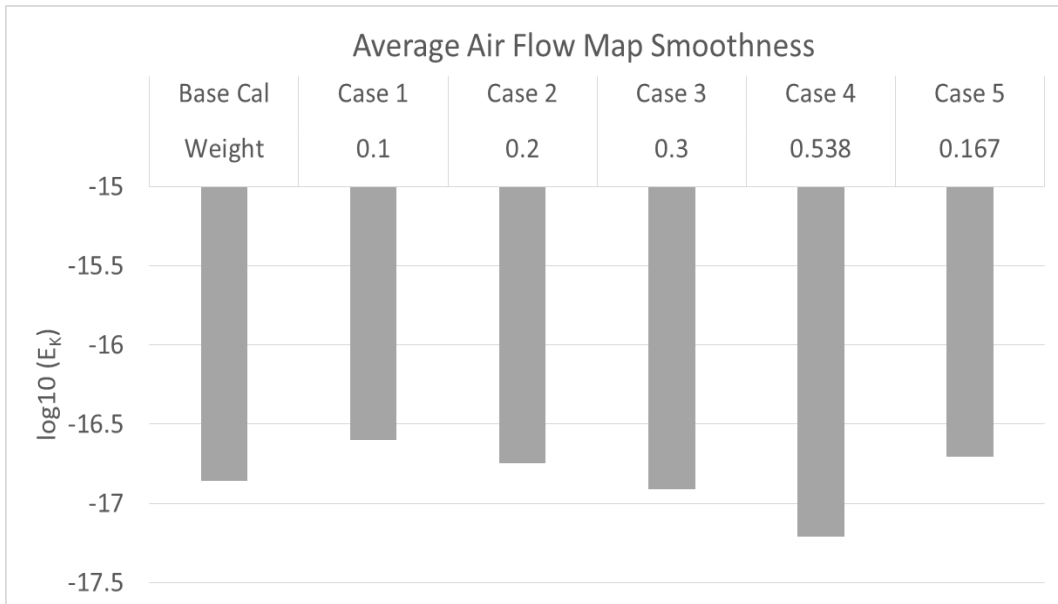


Figure 6-2 Average air flow map smoothness for the five different parameter weight settings [48]

Interestingly, on comparing the 1st Case in Figure 6-1 and Figure 6-2, even though the SOI weight of 0.5 is much higher than air flow weight of 0.1, the average smoothness of the air flow map is still higher. This behavior is consistent with the statement mentioned earlier that the smoothness of the different calibration

parameter maps depends a lot on how the parameters are varied during the engine operation. Due to this, some calibration parameter maps may be inherently smoother and therefore will not require a high smoothness weight, as is the case for air flow. However, this is very difficult to judge in advance. In fact, using BaseCal as an example, the air flow map is smoother than the SOI map and if a similar behavior is required by the new calibration maps then that would typically mean assigning higher smoothness weight to air flow map. However as explained earlier using results in Figure 6-1 and Figure 6-2, this high smoothness weight for air is definitely not required. Therefore, it is difficult to decide the smoothness weights of the different calibration parameters in advance and it justifies the rationale of adopting different cases of smoothness weight settings.

More interestingly in Figure 6-3 the average reduction in NO_x, soot and BSFC in comparison with BaseCal over WLTC are shown for each case. As it can be quite clearly seen from Figure 6-3, for all the cases there is roughly a 0.5% reduction in BSFC and a 10% reduction in NO_x. Also for soot there is a significant reduction in the first two cases, and a marginal penalty in the last two cases.

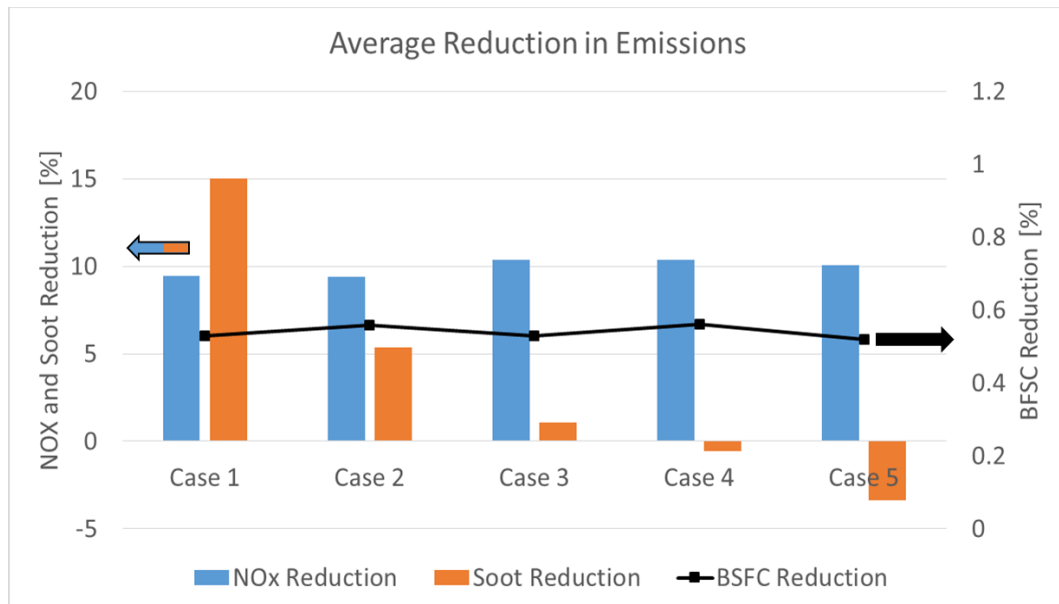


Figure 6-3 Average reduction in emissions over WLTC for the five different parameter weight settings [48]

Looking at Figure 6-1, Figure 6-2, and Figure 6-3, it is quite evident that the 1st case provides a considerably lower emissions along with satisfactory smoothness level. Nonetheless, it should be reminded here that the values shown in these figures are the average values over half a million sets of calibration maps which are just highlighting the trend. Therefore, out of these half a million calibrations for the 1st case it is necessary to select some calibrations based on satisfaction of thresholds on performance and smoothness. Moreover, these sets of maps also have to satisfy the upper and lower bounds for each control parameter. Many of the calibration maps are therefore rejected as they do not satisfy the performance requirement or the smoothness requirement or a portion of a map lies outside the acceptable range.

Only the calibration maps that satisfy the thresholds are finally selected and stored to be reviewed by the calibration team. These performance and smoothness of these shortlisted calibration maps is shown in the next section.

6.2 Smoothness and Performance of Shortlisted Calibrations

It is necessary to be recalled here that the performance and smoothness are in a trade-off relationship. The described approach makes it very easy utilize this trade-off relationship as it enables to select the calibrations (from the large number of stored calibrations) that result in much lower emissions at the expense of smoothness and vice a versa. In order to show the potential of the developed methodology and to make the comparison easy, the threshold for the smoothness criteria was kept close to the value of smoothness of BaseCal that was achieved by manual smoothing. In this manner while keeping one component of the tradeoff same, the possible reduction in the other one was highlighted.

Having mentioned the comparison method, 6 sets of the calibration maps from the 1st Case satisfied the decided criteria for smoothness and performance. The log of normalized curvature energy for three of the control parameters (injection pressure, SOI and air flow) of these 6 sets of maps are shown in Figure 6-4. On the extreme left in the Figure 6-4, the smoothness for the same three control parameters from BaseCal have also been shown as a reference for comparison. It can be clearly seen in the Figure 6-4 that the smoothness level of the selected calibrations is quite close to the one of the BaseCal. It should also be added here that even if the smoothness of the other three control parameters (1st Pilot Quantity, 1st Pilot DT and Swirl) are not shown in Figure 6-4, the calibration sets were selected only if the smoothness of all the 6 maps were above threshold.

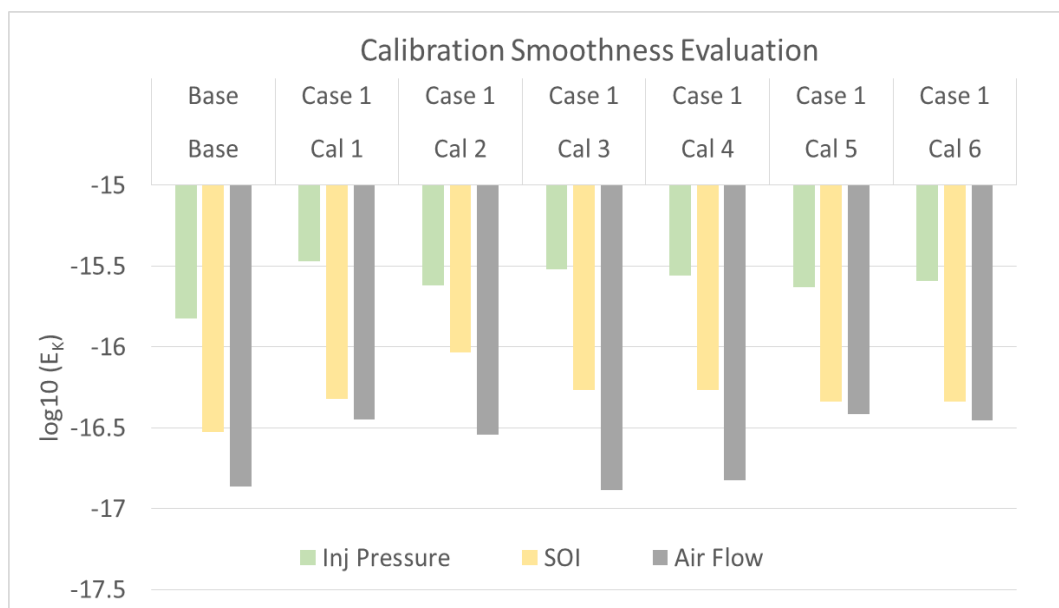


Figure 6-4 Smoothness of injection pressure, SOI and air flow maps for shortlisted calibration sets in comparison with BaseCal [48]

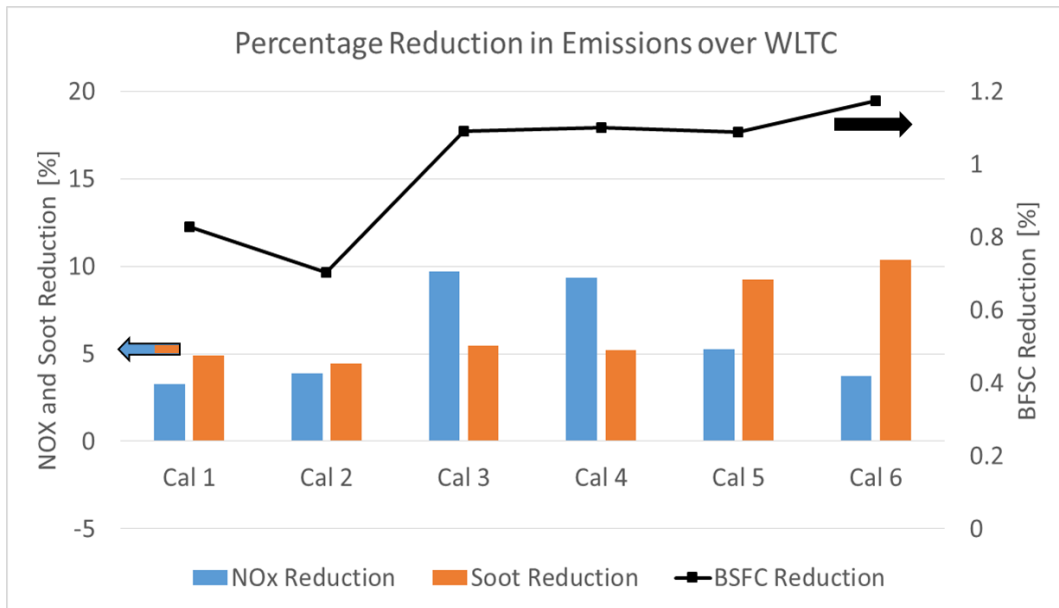


Figure 6-5 Simultaneous reductions in NO_x, Soot and BSFC for the shortlisted calibration in comparison to BaseCal over WLTC [48]

In Figure 6-5 the reductions in NO_x, Soot and BSFC in comparison to BaseCal over WLTC have been shown. The significant reduction in emissions in Figure 6-5 clearly highlights the loss of optima occurring in BaseCal due to the manual smoothening procedure. Furthermore, looking at both Figure 6-4 and Figure 6-5 it is quite evident that calibration set no.3 provides the maximum reduction in emissions while achieving the closest smoothness for all the control parameters maps. To show the achieved level of smoothness, the maps for injection pressure, SOI and air flow from calibration set no.3 have been shown in Figure 6-6, Figure 6-7 and Figure 6-8 respectively.

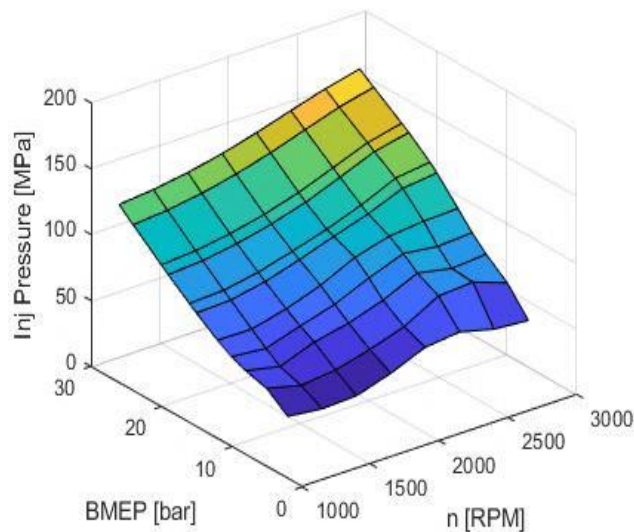


Figure 6-6 Injection pressure map from 3rd shortlisted calibration set [48]

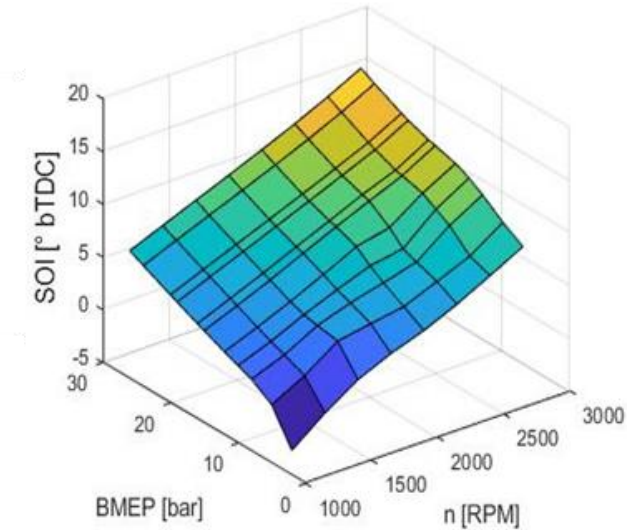


Figure 6-7 SOI map from 3rd shortlisted calibration set [48]

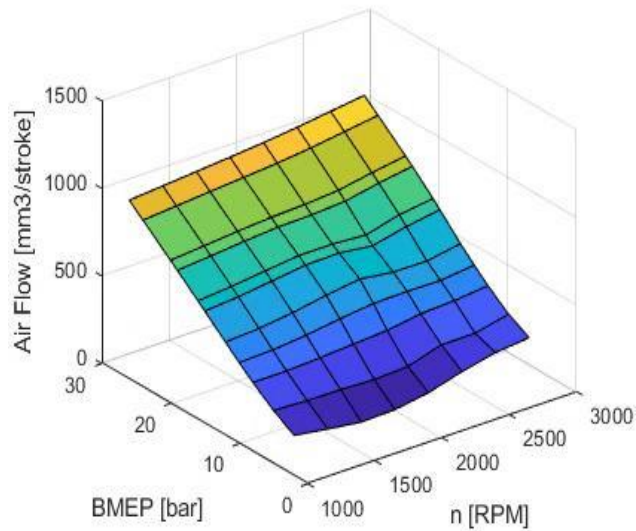


Figure 6-8 Air flow map from 3rd shortlisted calibration set [48]

Figure 6-6, Figure 6-7 and Figure 6-8 corroborates the data shown in Figure 6-4. Injection pressure map has the highest curvature, followed by SOI map and air flow map is the smoothest.

Finally, it should be mentioned here that this research work exploited the computational ability of the modern-day computers to rapidly compute and evaluate a huge number of calibrations generated using different combinations of the three most weighted KPs. The evaluation in terms of smoothness and performance for one such case (half a million calibrations) requires about 8 CPU hours on a machine with 8GB ram and an Intel i5 2.3 GHz processor. Moreover, with the GA optimization taking less than an hour for each KP, smooth calibration generation can be carried out in couple of days if the DoE or empirical models are available.

6.3 Discussion

The approach described in this work generates a large number of calibration maps using multiple optimum calibrations available for all the KPs. The approach is able to achieve significant results because of availability of multiple optimum calibrations that are scattered throughout the model domain. Table 6-1 shows 3 such optimized calibrations for KP1. It can be seen clearly that all the 3 calibrations are very different from each other in terms of the value of control parameters. Each of these calibrations have been picked from a group with different optimization objective. In fact, this is also clearly shown in Table 6-1 using the first two columns. At the same time Table 6-2 shows the emissions obtained from these three optimum calibrations relative to the BaseCal. It can be seen from the Table 6-2 that, irrespective of the optimization objective, low emissions have been achieved for all the three calibrations.

Table 6-1 Values of different control parameters for three diverse calibrations each optimized with a different objective [48]

Cal. Identifier	Optim. Obj.	SOI	Air Flow	1 st Pil. Quant.	Swirl	1 st Pil. DT	2 nd Pil. Quant.	2 nd Pil. DT	Inj. Pres.
		°bTDC	mm ³ /str	mm ³ /str	%	µs	mm ³ /str	µs	MPa
#22	NOx	-1.0	200	1.3	37.0	1490	2.0	1500	77
#30	Soot	3.6	221	1.8	61.6	1500	1.3	1500	65
#55	BSFC	4.9	213	2.0	31.1	660	1.4	1340	63

Table 6-2 Value of different emissions relative to BaseCal for three diverse calibrations each optimized with a different objective [48]

Calibration Identifier	Optimization Objective	NO _x relative to BaseCal	Soot relative to BaseCal	BSFC relative to BaseCal
		%	%	%
#22	NOx	33.8	97.4	99.9
#30	Soot	72.3	19.7	98.3
#55	BSFC	69.0	111.1	96.1

This availability of having low emissions for multiple calibrations gives the flexibility of selecting a calibration that can provide the required smoothness for the calibration maps and still managing to meet the emission targets. Furthermore, this methodology utilizes the idea that if, to obtain smooth calibration maps, a price in terms of one of the emissions must be given at a certain operating point, then that price can be recuperated at another operating point. For example, for smooth map generation if calibration #55 is selected from the Table 6-2 that result in a small penalty in terms of soot, then at another KP a calibration minimizing soot can be selected to compensate for this penalty. With the described methodology, all such possible mathematical combinations are explored, and the best ones are selected to

be finally reviewed by the calibration team. Moreover, the modules and the codes for the methods have been set up in a way that the optimization does not require a need to be monitored and can be evaluated directly the complete process is finished. In this way, the described approach is truly a one-click methodology.

When compared to other popular approaches of calibration such as global and local methods, one of the advantages of the defined methodology is that no information, such as value of constraints, is required a priori to the optimization. The local approach requires constraints for optimization for each KP and the global approach (also mixed local approach) requires constraints in terms of emissions and smoothness over the cycle. These values of constraint are largely dependent on the experience of the calibration team and might now always lead to the best results. Furthermore, many times the emission and the smoothness constraints change depending on the mission profile. As mentioned earlier, depending on what the engine is meant for, some control parameters may need smooth maps while some may not. Moreover, change in EATS calibration or addition or replacement of an EATS component will result in different emission constraints at the engine out level. These changes in constraints will lead to a completely new optimization process in the conventional approaches for calibration. However, with the defined approach, as all the possible combinations of different calibration maps with varying smoothness settings have already been evaluated and stored, no new optimization process is required. Any changes in the emission or smoothness constraint will just move the selection to another point in the established trade-off.

Although, in comparison with the global approach for calibration, the defined methodology being dependent on the local KP models, lacks the information about the emission and combustion processes between different KPs. However, as described earlier, the global models are not accurate enough yet, and that is why local models still remain the preferred choice for the calibration in the industry. Furthermore, the defined approach tackles the biggest problem associated with the local approach i.e. loss of optima which is clearly highlighted by the results shown.

Chapter 7

Conclusions

In this research work, keeping in mind the increased number of modern diesel engine control parameters and their impact on the calibration effort, an automated methodology for the optimization of last generation of automotive diesel engines have been described.

The review of the different state of the art engine calibration methodologies clearly highlights the need for a better optimization approach. The traditional methods for optimization are no longer sufficient to carry out a high dimensional optimization task such as a modern-day automotive diesel engine. The review also highlights the issues associated with the different calibration approaches. The local approach while is the most accurate from the modelling point of view, suffers from a loss of optima due to the smoothness requirement of the calibration maps. At the same time, global approach lacks in the accuracy of the model. Mixed approach, which uses local models, but global optimization, involves numerous steps and is slow. Moreover, all of these calibration methods require constraints, global or local, for carrying out the optimization task. These constraints are coming from the experience of the calibration team and sometimes are difficult to be defined for a newly designed engine.

With the aim of reducing the above-mentioned research gaps, starting from a local approach for calibration, firstly a Genetic Algorithm (GA)-based optimizer has been developed in house using MATLAB v2016b. The GA being a stochastic optimization method tackles the problem of entrapment in local minima that is associated with the traditional optimization methods. Moreover, the described optimization methodology generates multiple optimum calibration for several Key Points (KPs). All of these multiple optimum calibrations have shown to be significantly better than the optimization achieved using the traditional methods. For some KPs, a simultaneous reduction in 20% NO_x and 1% BSFC is achieved without deteriorating any other emissions, Combustion Noise (CN) or exhaust temperature. Furthermore, these multiple optimum calibrations form a Pareto front from which the calibrations providing the best tradeoffs in terms of different emissions can be easily picked.

Using this Pareto front, in the later part of this work, an approach has been defined to generate smooth calibration maps. Using the defined approach, a large number of calibration maps are generated and evaluated for performance and smoothness. These evaluations are stored in the memory and some calibrations can be quickly shortlisted based on a threshold criterion for smoothness and performance. The calibrations generated using the described methodology, when

compared with an existing calibration optimized for Euro 6d purposes using traditional methods, clearly show a remarkable reduction in all the emissions over WLTC. In fact, the selected calibration that has been highlighted finally in this work, shows a simultaneous reduction in NO_x (10%), Soot (5%) and BSFC (1.1%).

The most promising advantage of these stored evaluations is that since smoothness and performance of the calibrations are in a trade-off relationship, at any point it is possible to revert back to these evaluations and quickly choose a different point in this trade-off. In this way, if the application of engine is changed to suit a different mission profile, or if the calibration of EATS is changed or in any other combination of such scenarios, a calibration with the desired level of smoothness providing minimum emissions can always be easily selected without having to go through the calibration generation phase again. Therefore, this methodology has a potential to drastically reduce the development time and cost of modern day diesel engines. In fact, if the calibration generation is being done the first time, the task that would typically require couple of weeks can be carried out in couple of days only. Moreover, once generated and having stored the different calibration evaluations, it a matter of seconds to move to a different point in the trade-off between smoothness and performance.

References

- [1] Knecht W. Diesel engine development in view of reduced emission standards. *Energy* 2008;33:264–71. doi:10.1016/j.energy.2007.10.003.
- [2] Millo F, Mallamo F, Mego GG. The potential of dual stage turbocharging and miller cycle for hd diesel engines. SAE Tech. Pap., SAE International; 2010. doi:10.4271/2005-01-0221.
- [3] Zhang Q, Pennycott A, Brace CJ. A review of parallel and series turbocharging for the diesel engine. *Proc Inst Mech Eng Part D J Automob Eng* 2013. doi:10.1177/0954407013492108.
- [4] Ladommatos N, Abdelhalim SM, Zhao H, Hu Z. The dilution, chemical, and thermal effects of exhaust gas recirculation on disesel engine emissions - Part 4: Effects of carbon dioxide and water vapour. SAE Tech. Pap., SAE International; 1997. doi:10.4271/971660.
- [5] Kohketsu S, Mori K, Sakai K, Hakozaiki T. EGR technologies for a turbocharged and intercooled heavy-duty diesel engine. *Int. Congr. Expo., SAE International*; 1997. doi:https://doi.org/10.4271/970340.
- [6] Kreso AM, Johnson JH, Gratz LD, Bagley ST, Leddy DG. A study of the effects of exhaust gas recirculation on heavy-duty diesel engine emissions. *Int. Fuels Lubr. Meet. Expo., SAE International*; 1998. doi:https://doi.org/10.4271/981422.
- [7] Millo F, Giacominetto PF, Bernardi MG. Analysis of different exhaust gas recirculation architectures for passenger car Diesel engines. *Appl Energy* 2012. doi:10.1016/j.apenergy.2012.02.081.
- [8] Honardar S, Busch H, Schnorbus T, Severin C, Kolbeck AF, Korfer T. Exhaust temperature management for diesel engines assessment of engine concepts and calibration strategies with regard to fuel penalty. SAE Tech. Pap., SAE International; 2011. doi:10.4271/2011-24-0176.
- [9] Piano A, Millo F, Di Nunno D, Gallone A. Numerical analysis on the potential of different variable valve actuation strategies on a light duty diesel engine for improving exhaust system warm up. SAE Tech. Pap., SAE International; 2017. doi:10.4271/2017-24-0024.
- [10] Piano A, Millo F, Di Nunno D, Gallone A. Numerical assessment of the co2 reduction potential of variable valve actuation on a light duty diesel engine. SAE Tech. Pap., SAE International; 2018. doi:10.4271/2018-37-0006.
- [11] Badami M, Mallamo F, Millo F, Rossi EE. Experimental investigation on the effect of multiple injection strategies on emissions, noise and brake specific fuel consumption of an automotive direct injection common-rail diesel engine. *Int J Engine Res* 2003;4:299–314. doi:10.1243/146808703322743903.
- [12] Chen SK. Simultaneous reduction of NO_x and particulate emissions by using multiple injections in a small diesel engine. SAE Tech. Pap., SAE International; 2000. doi:10.4271/2000-01-3084.
- [13] Beatrice C, Napolitano P, Guido C. Injection parameter optimization by DoE of a light-duty diesel engine fed by Bio-ethanol/RME/diesel blend. *Appl Energy* 2014;113:373–84. doi:10.1016/j.apenergy.2013.07.058.
- [14] Zhang Q, Hao Z, Zheng X, Yang W, Mao J. Mechanism and optimization of fuel injection parameters on combustion noise of DI diesel engine. *J Cent*

- South Univ 2016;23:379–93. doi:10.1007/s11771-016-3083-3.
- [15] EC 2017. Commission Regulation (EU) 2017/1151. n.d.
- [16] EC 2017a. Commission Regulation (EU) 2017/1347. n.d.
- [17] Miller J, Franco V. Impact of improved regulation of real-world NO_x emissions from diesel passenger cars in the EU, 2015–2030. ICCT 2016.
- [18] European Court of Auditors. 2019 The EU's Response to the “ Dieselgate ” Scandal 2019.
- [19] EC 2016. Commission Regulation (EU) 2016/427. n.d.
- [20] Standards - EU: Cars and Light Trucks n.d. <https://www.dieselnet.com/standards/eu/ld.php> (accessed January 6, 2019).
- [21] Röpke K, Von Essen C. DoE in engine development. Qual. Reliab. Eng. Int., 2008. doi:10.1002/qre.941.
- [22] Berger B, Rauscher F. Robust gaussian process modelling for engine calibration. IFAC Proc Vol 2012. doi:10.3182/20120215-3-AT-3016.00028.
- [23] Hong S, Wooldridge MS, Im HG, Assanis DN, Pitsch H. Development and application of a comprehensive soot model for 3D CFD reacting flow studies in a diesel engine. Combust Flame 2005. doi:10.1016/j.combustflame.2005.04.007.
- [24] Priesching P, Ramusch G, Ruetz J, Tatschl R. 3D-CFD Modeling of conventional and alternative diesel combustion and pollutant formation - A validation study, SAE Tech. Pap., SAE International; 2007. doi:10.4271/2007-01-1907.
- [25] Reveille B, Kleemann A, Knop V, Habchi C. Potential of narrow angle direct injection diesel engines for clean combustion: 3D CFD analysis, SAE Tech. Pap., SAE International; 2006. doi:10.4271/2006-01-1365.
- [26] Abdul Gafoor CP, Gupta R. Numerical investigation of piston bowl geometry and swirl ratio on emission from diesel engines. Energy Convers Manag 2015. doi:10.1016/j.enconman.2015.06.007.
- [27] GT-SUITE - Engine Performance Application Manual - Version 2018, 2018.
- [28] Montgomery DC. Design and analysis of experiments. John wiley & sons; 2017.
- [29] Mallamo F, Badami M, Millo F. Application of the design of experiments and objective functions for the optimization of multiple injection strategies for low emissions in CR diesel engines. SAE Tech. Pap., SAE International; 2004. doi:10.4271/2004-01-0123.
- [30] d'Ambrosio S, Ferrari A. Potential of double pilot injection strategies optimized with the design of experiments procedure to improve diesel engine emissions and performance. Appl Energy 2015. doi:10.1016/j.apenergy.2015.06.050.
- [31] Singh Y, Sharma A, Tiwari S, Singla A. Optimization of diesel engine performance and emission parameters employing cassia tora methyl esters-response surface methodology approach. Energy 2019. doi:10.1016/j.energy.2018.12.013.
- [32] Traver ML, Atkinson RJ, Atkinson CM. Neural Network-Based diesel engine emissions prediction using in-cylinder combustion pressure. SAE Tech. Pap., SAE International; 2010. doi:10.4271/1999-01-1532.
- [33] Wong KI, Wong PK, Cheung CS, Vong CM. Modeling and optimization of biodiesel engine performance using advanced machine learning methods. Energy 2013. doi:10.1016/j.energy.2013.03.057.
- [34] Park S, Kim Y, Woo S, Lee K. Optimization and calibration strategy using design of experiment for a diesel engine. Appl Therm Eng 2017.

- doi:10.1016/j.applthermaleng.2017.05.171.
- [35] Nikzadfar K, Shamekhi AH. Investigating a new model-based calibration procedure for optimizing the emissions and performance of a turbocharged diesel engine. *Fuel* 2019;242:455–69. doi:10.1016/j.fuel.2019.01.072.
- [36] Martyr AJ, Plint MA. 20 - The pursuit and definition of accuracy: Statistical analysis of test results. In: Martyr AJ, Plint MA, editors. *Engine Test*. (Third Ed. Third Edit, Oxford: Butterworth-Heinemann; 2007, p. 408–22. doi:https://doi.org/10.1016/B978-075068439-2/50023-2.
- [37] Castagné M, Bentolila Y, Chaudoye F, Hallé A, Nicolas F, Sinoquet D. Comparison of engine calibration methods based on design of experiments (DoE). *Oil Gas Sci Technol* 2008. doi:10.2516/ogst:2008029.
- [38] Nishio Y, Murata Y, Yamaya Y, Kikuchi M. Optimal calibration scheme for map-based control of diesel engines. *Sci China Inf Sci* 2018. doi:10.1007/s11432-017-9381-6.
- [39] Millo F, Arya P, Mallamo F. Optimization of automotive diesel engine calibration using genetic algorithm techniques. *Energy* 2018. doi:10.1016/j.energy.2018.06.044.
- [40] Williams CKI, Rasmussen CE. Gaussian processes for regression. *Adv Neural Inf Process Syst* 8 1996;8:514–20.
- [41] Seeger M. Gaussian processes for machine learning. *Int J Neural Syst* 2004;14:69–106. doi:10.1142/S0129065704001899.
- [42] Gregorčič G, Lightbody G. Gaussian process approach for modelling of nonlinear systems. *Eng Appl Artif Intell* 2009;22:522–33. doi:10.1016/j.engappai.2009.01.005.
- [43] Sammut C, Webb GI, editors. *Leave-One-Out Cross-Validation BT - Encyclopedia of Machine Learning*, Boston, MA: Springer US; 2010, p. 600–1. doi:10.1007/978-0-387-30164-8_469.
- [44] Marler RT, J.S. A. Survey of multi-objective optimization methods for engineering. *Struct Multidiscip Optim* 2004;26:369–95. doi:10.1007/s00158-003-0368-6.
- [45] Fletcher R, Powell MJD. A rapidly convergent descent method for minimization. *Comput J* 1963;6:163–8. doi:10.1093/comjnl/6.2.163.
- [46] Sastry K, Goldberg D, Kendall G. Genetic Algorithms. In: Burke EK, Kendall G, editors. *Search Methodol. Introd. Tutorials Optim. Decis. Support Tech.*, Boston, MA: Springer US; 2005, p. 97–125. doi:10.1007/0-387-28356-0_4.
- [47] Goldberg DE. *Genetic Algorithms in Search, Optimization, and Machine Learning*. 1989. doi:10.1007/3-540-44673-7.
- [48] Arya P, Millo F, Mallamo F. A fully automated smooth calibration generation methodology for optimization of latest generation of automotive diesel engines. *Energy* 2019. doi:10.1016/j.energy.2019.04.122.
- [49] Meek DS, Walton DJ. On surface normal and Gaussian curvature approximations given data sampled from a smooth surface. *Comput Aided Geom Des* 2000;17:521–43. doi:10.1016/S0167-8396(00)00006-6.
- [50] Nessler A, Haukap C, Roepke K. Global evaluation of the drivability of calibrated diesel engine maps. *Proc. 2006 IEEE Conf. Comput. Aided Control Syst. Des. CACSD*, 2007. doi:10.1109/CACSD.2006.285530.